Muhammad Farrukh Siddiqui, BSc.

Recrystallization and Grain Growth Behavior of Austenitic Stainless Steel 304L

MASTER'S THESIS

to achieve the university degree of

Master's degree program: Production Science and Management

Submitted to

Graz University of Technology

Supervisor’s

Mohammad Bagher Nasiri

Assoc. Prof. Dipl-Ing. Dr. techn. Norbert Enzinger

IMAT-Institute of Materials Science, Joining and Forming

Graz, May 2021

AFFIDAVIT

I declare that I have authored this thesis independently, that I have not used other than the declared sources/resources, and that I have explicitly indicated all material that has been quoted either literally or by content from the sources used. The text document uploaded to TUGRAZ online is identical to the present master's thesis dissertation.

_____	_____
Date	signature

Abstract

The current thesis focus on investigating the kinetics of reversion transformation of deformation-induced martensite (DIM) into the parent austenite (α′→ε→γ), the recrystallization of austenite grains, and grain growth behaviour of austenitic stainless steel AISI 304L. To stimulate the recrystallization, a deformation is required to apply to the material. Due to cold rolling deformation, strain-induced martensite formed in the metastable austenitic stainless steels (ASSs). The DIM consists of two phases, epsilon (ε) martensite which is a paramagnetic phase and alpha (α′) martensite which is a ferromagnetic phase. Therefore, the Ferritscope as a magnetic detection device has been used to measure the phase fraction of ferromagnetic phases including α′-martensite and δ - ferrite. The light optical microscope (LOM), electron backscatter diffraction (EBSD) and scanning electron microscope (SEM) also used to evaluate the phase fraction of microstructure constituents. To confirm the existing phases in the cold-rolled AISI 304L, the x-ray diffraction (XRD) investigation was conducted on a 25% cold-rolled sample, which confirmed the ε-martensite in the result. The various heat treatments were performed on 25%, 50% and 67% cold-rolled AISI 304L specimens in a temperature range of 600°C to 800°C with different holding time from (90 min to 480 min), in order to study the reversion of DIM and recrystallization phenomena.

According to the results from Ferritscope, LOM and EBSD, the as-received plate contains 3% δ - ferrite in the initial condition due to solidification. The ferromagnetic phase such as α′-martensite start to decrease at 600°C in cold-rolled specimens. However, the LOM and EBSD results of cold-rolled specimens showed that ε-martensite was not changed significantly at a reversion temperature of 600°C. While at 700°C - 180 min of annealing, the recrystallized fine austenite grains formed in the deformed region of 50% cold-rolled and 67% cold-rolled specimen became fully recrystallized. The EBSD results confirmed the completion of the recrystallization in 25% and 50% cold-rolled specimens after 60 minutes of annealing at 800°C. The average grain size of recrystallized specimens was measured around 6μm.

Furthermore, 50% cold-rolled recrystallized at 800°C – 60 min (6µm grain size) and the as-received plate (initial grain size 30µm) were placed for austenite grain growth heat treatments in a temperature range of 900°C to 1200°C with several holding times from 2 min to 120 min. At a temperature of 900°C, the grain growth in recrystallized 50% cold-rolled specimen was noticed as a very slow process. It is indicated that at a temperature of 1000°C, no austenite grain growth was observed in the as-received plate and a slow grain growth process was observed in recrystallized 50% cold-rolled specimen. At a temperature of 1100°C, the austenite grains grew faster in the beginning till 30 min of annealing but with a longer annealing time, the austenite grains stopped growing further with long annealing time. At a heat treatment of 1200°C, grains grew so fast from the beginning of annealing time at 5 min, and abnormal grain growth of some grains was observed with different holding times. The average grain size was measured of as-received plate around 84µm and recrystallized 50% cold-rolled around 81µm after 60 minutes of annealing at 1200°C.

Acknowledgments

I would like to express my deepest gratitude to my thesis first supervisor, Mohammad Bagher Nasiri, for giving me the opportunity and showing his trust to achieve this work. Many thanks for his guidance, advice, and teaching me like an elder brother with tremendous fortitude throughout the experiments and thesis writing.

A very special thanks to my second supervisor Professor Norbert Enzinger, this thesis would not have been succeeded without his support, guidance, and motivation.

I would like to thank, Fatemeh Iranshahi, for the incredible (EBSD) results and electropolishing tips. Also, many thanks, to all the laboratory staff at the IMAT, TU Graz.

Lastly, I would like first to thank my parent and sisters for their support during my studies. And I also thankful to my colleagues especially, Dr Mustafa Tümmer and Graz friends Faisal, Burak, Ali, Mubeen, Jamshaid and Aoun for their unconditional support and motivation.

Table of Contents

List of Tables

List of Abbreviation

ASS: Austenitic stainless steel

AISI: American iron steel institute

DIM: Deformation-induced martensite

FCC: Face centred-cubic structure

BCC: Body centred-cubic structure

HCP: Hexagonal closed packed structure

BCT: Body centred tetragonal structure

TMP: Thermomechanical processing

SFE: Stacking fault energy

HAGB: High angle grain boundary

JMAK: Johnson-Mehl-Avrami-Kolmogorov model

SRX: Static recrystallization

DRX: Dynamic recrystallization

CDRX: Continuous dynamic recrystallization

DDRX: Discontinuous dynamic recrystallization

GDRX: Geometry dynamic recrystallization

COM: Crystallographic orientation map

Rcr: Critical radius

LOM: Light optical microscope

SEM: Scanning electron microscope

EBSD: Electron backscattered diffraction

XRD: X-ray diffraction

HV: Vickers Hardness

1 Introduction

The austenitic stainless steel is also known as chromium, nickel steel, and it is widely used in all types of industrial applications in a corrosive environment. Characteristic areas of use including, chemical, automotive, oil and gas and other process industries like power generation and nuclear plants. Due to their alloying elements, it has a face centre cubic crystal (FCC) microstructure and it is considered to be corrosive resistance and non-magnetic stainless steel [1,2].

1.1 Background

The strength level of austenitic stainless steel (ASS) specifically the yield strength is quite low around 200 MPa in the annealed condition. After solution annealing, and extending the strength level, ASSs are often undergoing cold work [3]. Generally, ASSs show a high strain hardening. Therefore, cold work can be considered as a suitable strengthening method. Renowned steel such as AISI 304L can extend its yield strength up to 1400 MPa with 10% elongation after thermomechanical treatment. Depending on the chemical composition of the steels and the percentage of cold rolling, some strain-induced martensite can be formed during plastic deformation with the sequence of γ→ϵ→α´phase transformation. Generally, this martensite is recognized as `deformation-induced martensite` (DIM) [3,4].

Two types of DIM can be formed in ASSs after cold rolling including hexagonal close-packed (hcp) known as epsilon denoted by a sign (ϵ) and a body centre cubic (bcc) known as alpha denoted by the sign (α´) martensites. Their content always depends on the percentage of cold-rolling deformation and the chemical composition of ASSs [5,6].

Reversion transformation usually occurs according to the chemical composition of ASSs and heating time and temperature. Generally, two types of reversion mechanisms appeared in cold-rolled deformed ASSs including diffusion and shear

type. Diffusion type contains the random nucleation of austenite in the DIM phase, and the orientation of austenite in crystallography is always unsystematic. The shear-type consist of the movement of partial dislocations along the basal plane constitutes the transition mechanism. However, the heavily deformed region of DIM is a good cause of nucleation for new strain-free austenite grains in the subsequent reversion heat treatment [7,8].

Recrystallization is known as the microstructural phenomena through which new strain-free austenite grains formed in the cold-rolled deformed region of ASSs by heat treatment. Recrystallization occurs through the help of stored energy and that energy comes from the cold-working deformation. The new strain-free austenite grains nucleate mainly at the deformed region, such as shear bands and grain boundaries, and the growth of the new grains eats the entire deformed structure [9,10].

Several factors have influenced the recrystallization of ASSs, such as the percentage of cold rolling deformation, initial grain size, the chemical composition of alloys [9,11].

The grain growth starts when recrystallization is completed in the deformed ASSs. It requires the temperature above recrystallization and a long holding time is needed. The force which drives the phenomena of grain growth is the reduction of total grain boundary energy. The grain growth occurs because of the lower free energy of the atom on the convex side, and through a net transmission of atoms from the concave side of curved grain boundaries to the convex side. The influential factors in grain growth are solutes, particles, and heating rate (time and temperature) [9,12].

1.2 Objective

The objective of the present thesis is to investigate the three phenomena in cold-rolled AISI 304L and as received (non-rolled) condition.

- The kinetics of reversion transformation of deformation-induced martensite (DIM).

- The occurrence of recrystallization (temperature and time) phenomena in cold-rolled deformed austenitic stainless steel AISI 304L.
- The grain growth behaviour of recrystallized and the as-received AISI 304L through various heat treatments.

1.3 Procedure

The material was received in the form of the as-received condition (non-rolled plate) and cold-rolled deformed microstructure at room temperature with different percentage of cold rolling of 25%, 50% and 67%. The material was characterized by a variety of measurement techniques including magnetic induction-based device Ferritscope to obtain the value of ferromagnetic phases (δ – Ferrite and α´-martensite) in the initial condition and after heat treatments, the microstructural characterization by Light optical microscope (LOM) to estimate the different phases in the deformed specimens and also grain boundaries of the austenite phase. Scanning electron microscope (SEM) and electron backscatter diffraction (EBSD) to reveal the texture of (DIM) phases, and the recrystallization grains in cold-rolled specimens, X-ray diffraction (XRD) test to detect the existing phases in the cold-rolled deformed specimen, and to identify the mechanical properties of the specimens the Vickers hardness test is conducted. Furthermore, the average grain size of AISI 304L was measured before and after the various heat treatments by the intercept and image processing approach.

The current thesis consists of 7 different chapters. Chapter 1 provides a detailed introduction of the topic and objective of the thesis. Chapter 2 is a literature review that provides the detailed structural changes in austenitic stainless steel after cold rolling, phase transformation and the recrystallization and grain growth phenomena. Chapter 3 and 4 give a brief detail about the measurement methods and the characterization approaches used in the investigation of the material before and after heat treatment. Chapter 5 and 6 consist of the experimental results and conclusion which is followed by the references at the end of chapter 7.

2 Literature Review

2.1 Austenitic stainless steel

The low carbon austenitic series of stainless steels consist of a face-centred cubic (FCC) crystal structure and has a great corrosion resistance up to 900°C both at high and room temperature. The crystallographic structure of austenitic stainless steels (ASSs) contains one atom at every corner of the cube and one in the middle of each face. The FCC structure is formed due to the addition of the alloying elements. The ASSs atoms distribution is shown in Figure 1. Ferritic stainless steel consists of a body-centred cubic (BCC) crystal structure where the atoms are fixed in every corner of the cube and one atom in the middle [2,13].

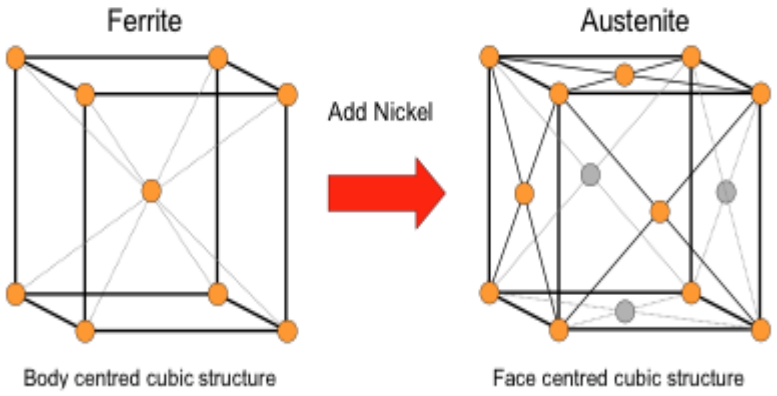

Figure 1. *The microstructure of austenite stainless steel before and after addition of alloying element (Ni) [2].*

Austenitic stainless steels ASSs have different classifications according to the unified numbering system (UNS) including 200 and 300 series. 200 series contain chromium and manganese and 300 series classification contain chromium and nickel [14].

The classification of different standard grades of the 300 series is given in Table 1. The 200 and 300 series have many different compositions and properties, but they also have few common characteristics [14].

The hardness, strength and stress resistance can be enlarged by cold-rolling but not by heat treatment. In the annealed condition, the majority of ASSs are nonmagnetic but through cold working, some may become a little magnetic [14]. The chemical composition for 304L and 316 grades is listed in Table 2. Generally, 304L is considered as a low carbon austenitic chromium-nickel stainless steel with overall corrosion resistance parallel to 304. It is recommended to use in specific harsh environments for the parts which cannot be annealed after welding. [13,14].

Table 1. *Classification of 304L and 316L in different standard grades worldwide[14].*

USA	France	Germany	Germany	Russia	Sweden	UK	European Union	UNS number
AISI	AFNOR	W.N. 17007	DIN 17006	GOST	SIS	BIS	EURO NORM	
304L	Z2CN18-10	1.4306	X2CrNi1811	03KH18N1	2352	304S11	X3CrNi1810	S30403
316L	Z2CND17-13	1.4435	X2CrNiMo1813		2353	316S13	X3CrNiMo17133	S31603

Table 2. *Chemical composition for 304L and 316L [14].*

UNS	Type	C	Mn	P	S	Si	Cr	Ni	Other Elements
S30403	304L	0.03	2	0.045	0.030	1	18	8	N: 0.01
S31603	316L	0.03	2	0.045	0.030	0.75	16-18	10-14	N: 0.01

2.2 Cold work effect on Austenitic stainless steel

Generally, Austenitic stainless steels (ASSs) have excellent corrosion resistance, toughness and weldability. However, the amount of yield strength is fairly little about 200 MPa in the annealed condition. To extend their strength, most of the time ASSs are cold worked after solution annealing. Meanwhile, ASSs have a high strain-hardening coefficient which makes the cold work to be an appropriate strengthening method. Due to the thermomechanical process yield strength increase in ASSs specifically in 304L - type up to 1400 MPa with an elongation of about 10 per cent. Depending on the percentage of cold rolling, and the chemical composition of the ASSs some martensite can be formed and that martensite is known as ‘deformation-induced martensite’ (DIM) [5].

Figure 3 shows the complete overview of the different transformation that happens in the ASSs with different heat treatments. During the cold working of ASSs, stacking faults packs or defected ε - martensite, deformation twins, deformation bands and α´- martensite can be formed, besides severe dislocation. The stacking fault energy (SFE) has a significant role in the deformation structure, growing dislocation, density and distribution of lattice faults and tendency concerning martensite formation. The stabilized alloying elements have a negligible effect on the strain-hardening behaviour of the ASSs. After the cold work of ASSs, two different microstructures can be formed for carrying a high SFE, a cellular dislocation distribution without DIM, and for a low SFE a planar dislocation distribution with the presence of DIM. The bands of deformation can be seen in both. Due to a low degree of deformation stages the volume of ε – martensite is most important in the relation to α´- martensite. If the percentage of α´- martensite raises incessantly with the volume of deformation, the percentage of ε – martensite drives through an extreme and lowers subsequently, and signifying the following order γ→ϵ→α´ [5,15]. There are different types of cold work such as rolling, bending, shearing and drawing [11,16].

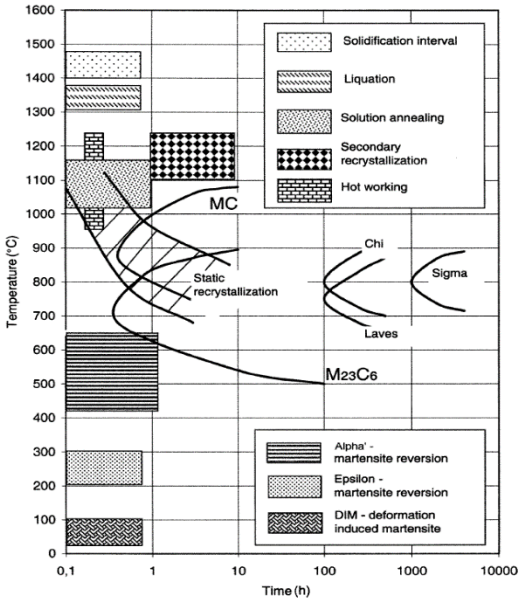

Figure 2. *Phase transformation happens in austenite stainless steel (ASSs) at different temperatures [5].*

2.2.1 Cold rolling

In various cold-work techniques, cold rolling is considered the most common and widely used technique from an industrial point of view. The cold-rolling technique is used for many applications such as car body parts, white goods, construction industry, etc. Figure 3 shows, the thickness reduction of the ASSs plate is moving through two rolling mills. The rolling mill makes several changes in the microstructure of ASSs such as grains size, phase transformation, precipitation and increases the internal stresses [16].

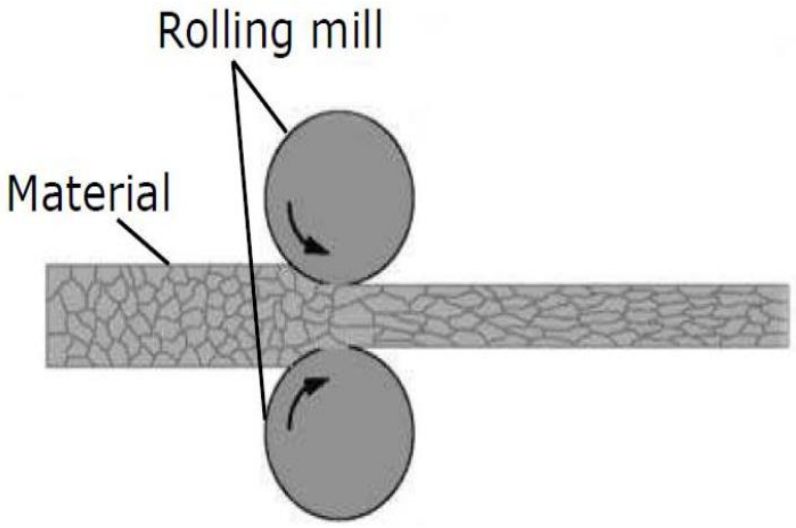

Figure 3. *Cold rolling cross-section[16].*

There are several advantages of the cold-rolling technique such as no influence of oxidation due to the operation carried out at room temperature, the procedure is quite fast and bulk production can be possible, the finished surface is always neat and clean, and availability of thin sheets for various application [16].

2.3 Martensitic stainless steel

“Martensite” was discovered by the German scientist Martens and the terminology is used for the hard micro constituents in quenched steels [17].

Martensitic stainless steels usually have 11 to 18 per cent chromium content but also contain around 1 per cent carbon which increases the hardness and can be used as a cutting tool and, in some cases also contain nickel and molybdenum. The martensitic stainless steels are magnetic by nature and have a decent fatigue property when heat treated. Generally, they do not have decent low-temperature properties and are not recommended to be used ordinarily for cryogenic application because at a lower temperature they become brittle. While improving fatigue resistance and strength by heat treatment, also decreases the toughness and become brittle at a temperature above 400°C. Because of their low ductility and a significant amount of carbon in several grades it is considered inappropriate for welding purpose [8,15,18].

The microstructure of martensitic stainless steels is stronger than the microstructure of austenitic stainless steel, which avoids the dislocation motions [17,19].

Generally, two types of martensite can be formed in stainless steels. The epsilon martensite which is represented by the symbol (ε) and alpha martensite or strain-induced martensite which is represented by (α´) [11,15].

2.3.1 ϵ - martensite

The product ϵ -martensite has a hexagonal closed packed (hcp) crystal structure and paramagnetic nature [6,20]. The texture of ϵ - martensite forms needle-like thin plates that go through the austenite grains and stoped inside the grain boundaries. The microstructure of ϵ -martensite is consistent with a stacking fault and lying on {111}γ plane. The result obtained from the Burgers alignment relationship shows only four different variants of ϵ – martensite [21].

$$\{111\}\gamma \,//\, \{0001\}\,\epsilon$$

$$\langle 110\rangle\gamma \,//\, \langle 2110\rangle\,\epsilon$$

The well-known mechanism for the creation of ϵ - martensite is the co-relate motion of $\frac{a}{6}$<112> Shockley partial dislocations. The resemblance between the microstructure of ϵ - plane and deformation twin shown in Figure 4. Although a plane of ϵ - martensite requires a stacking fault on every next plane and twin can be defined as a stacking fault on each head to head <111> γ plane the formation of ϵ - martensite has a similar mechanism to the creation of twins [21,22].

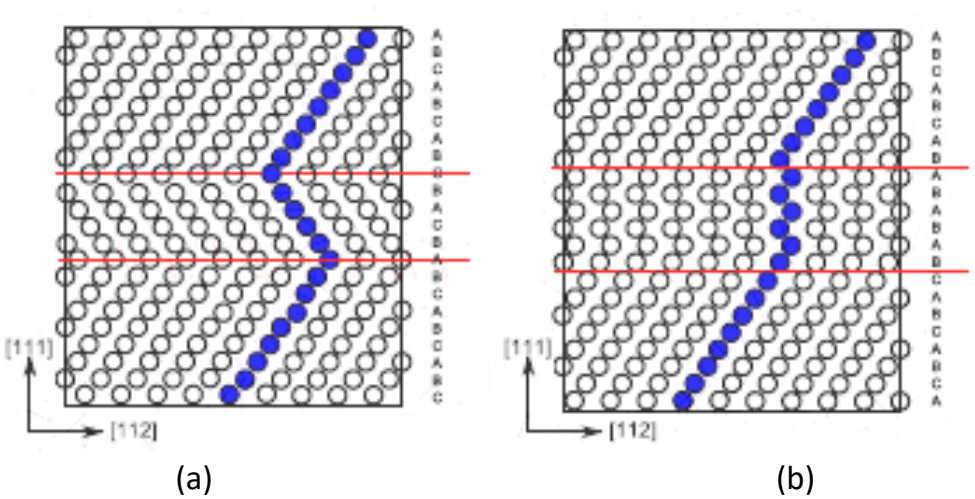

(a) (b)

Figure 4. *The plane of a twin (a) and the thin plane of ε – martensite (b) [21].*

2.3.2 α´- martensite

α´- martensite has a body centre cubic crystal structure (BCC) and has ferromagnetic nature. In some cases, α´- martensite has a body-centred tetragonal (BCT) structure but in stainless steels because of a fairly low amount of interstitials, it is generally mentioned as BCC rather than BCT [23]. Nucleation of α´- martensite occurs from ϵ-martensite at intersections of shear bands, because of the impact of stacking fault energy (SFE) of the austenite phase. The α´- martensite is growing by successive nucleation and coalescence of new nuclei, therefore the intersection of new shear bands will be formed as a function of the new nuclei [1,20].

The chemical content of austenitic stainless steel (ASSs), the course that encourages the phase transformation plays an important part in the martensitic transformation, and the SFE also depend on the composition of ASSs [1,20,22].

The few research of reversion of deformation-induced martensite (DIM) phases ε and α´- martensite into the ASSs were carried out from the point of view of controlling microstructure and improving mechanical properties. The significant improvement in the mechanical properties gives rise to substantial curiosity in the development of ultrafine-grain materials. During heat treatment, the plastically deformed ASSs undergo recovery and recrystallization in contrast, the DIM phases reverse back to the parent austenite [24].

2.4 Reversion transformation of deformation-induced Martensite

The reversion transformation of deformation-induced martensite (DIM) in austenitic stainless steels (ASSs) is less studied than its formation [7,15]. The reversion of DIM in the ASSs is obtained at a considerably lower temperature rather than the recrystallization temperature. The reversion can happen in two ways the shear-type mechanism and diffusional controlled mechanism. The diffusional reversion involves random nucleation of austenite in DIM or at the lath boundaries and the orientation of austenite in the crystallography is always unsystematic. Therefore, the nucleated grains grow in the form of equiaxed grains. In the shear reversion mechanism, the diffusionless transformation happens and the DIM phase returns to the austenite phase. In the case of lowering the martensitic shear reversion temperature by increasing the Gibbs free energy, the transformation between face centre cubic (FCC) and body centre cubic (BCC) structure is impacted by the increase of alloying element nickel and chromium ratio. Such steels undergo the martensitic reversion in a low-temperature range when the ratio of the alloying elements is sustained as high [8,9].

Thermodynamically, a minimum driving force is needed for the shear mechanism to be functional and the lowest possible temperature is above 600°C for the ASSs. The morphology of newly formed austenite grains relates to the parent DIM and it holds a high dislocation density, and the defects recover to form subgrains due to long annealing. Shear type reversion always occurs within a small range of temperature, while diffusion-type reversion always occurs above the temperature range of ∼200 °C. The estimation of the critical driving force for shear-type reversion is about 500 J/mol. The reversion mechanism is followed by recrystallization and it results in refined grain microstructure ASSs [8,9,25,26].

Generally, two factors are more essential for the reversion transformation of DIM, the temperature range and chemical composition of austenitic stainless steel ASSs [9,26].

2.5 Recovery

Recovery is defined as the changes in a deformed structure which start before recrystallization and moderately re-establish the properties to their standards before deformation. It is understood that recovery is essential because of the variation in the dislocation structure of the materials. Recovery may occur not only in plastically deformed but in any crystal into which a non-equilibrium and high absorption of point defects has been presented, for example, materials that have been rapidly cooled or irradiated from high temperatures. Dislocation recovery is a series of the microstructural transformation of actions which are shown in Figure 5, usually form during annealing of specific cases and will rely on several limitations such as material, strain, deformation and annealing temperature. In several cases, the recovery can appear during deformation as a dynamic recovery [27].

(a) Dislocation masses (b) Formation of cell (c) Annihilation of dislocation inside the cell

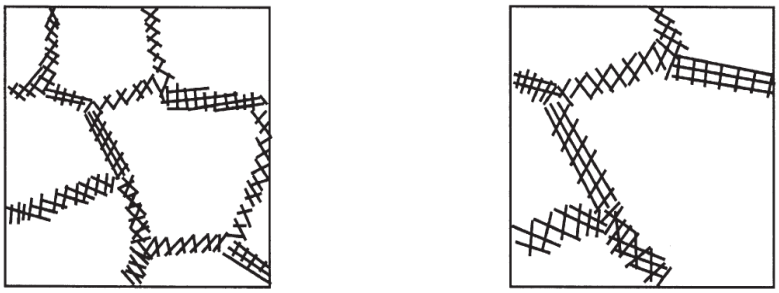

(d) Formation of subgrain (c) Sub grain growth

Figure 5. *Several phases in the recovery of plastically deformed materials [27].*

Recovery and recrystallization are sequential processes and controlled through the stored energy of the deformed region. When the recrystallization has started and the deformed microstructure has been disbursed, then no additional recovery can occur. The recovery process performs a significant role in recrystallization and sometimes it is difficult to separate both processes [27,28].

2.6 Recrystallization

Recrystallization participates in the creation of new strain-free austenite grains in deformed portions of the materials and led to change the microstructure to a normal condition from the plastically deformed condition [27].

Recrystallization of the deformed microstructure is called primary recrystallization. The process of non-homogeneous grain growth that may arise in fully recrystallized material is called secondary recrystallization [27].

In general, the term recrystallization refers to the primary recrystallization. It is easy to divide primary recrystallization into two sections, nucleation is the first arrival of recrystallized grains in the deformed region and growth of new grain replaces the deformed region of the materials. The phase transformation and kinetics of recrystallization are similar which occurs by nucleation and growth [15,27,29].

2.6.1 Nucleation

Nucleation may be defined as a crystallite of low internal energy growing into deformed or recovered material from which it is separated by a high angle grain boundary (HAGB). During recrystallization, if the number of nuclei per unit volume (N) remains constant and it would be an important parameter. In other words, the nucleation rate $N = \frac{dN}{\mathrm{dt}}$ also needs to be measured. However, nucleation during recrystallization is an intricate course, the rate of nucleation is not anticipated as an easy parameter The rate of nucleation is not persistent in every case during recrystallization [27].

2.6.2 Growth

The growth of recrystallized grains is more eagerly examined rather than their nucleation. It is normally recognized that the velocity (V) of a high angle grain boundary (HAGB), which is also the growth rate of the grains (G) is given in equation (1).

$$V = G = MP \qquad 1$$

where (M) is denoted by the mobility of boundary and (P) denoted by the boundary net pressure [27,30].

2.7 Static Recrystallization

The kinetics of static recrystallization in deformed metals and alloys have been conventionally analysed by using the standard relationship by Johnson-Mehl-Avrami-Kolmogorov (JMAK) model also known as the Avrami equation. The JMAK equation (2) is given below.

$$F = 1 - exp\,[-B \cdot t^{k}] \qquad 2$$

where (F) is denoted by the volume fraction recrystallized, (B and k) are denoted by the model-rely constant, and (t) is denoted by the time. The kinetics of recrystallization are typically related with the JMAK model by plotting log (-ln (1 - F)) against log (t) produces a slop of straight line equal to the (k). The JMAK model relies on some expectations such as unsystematic and normal nucleation, persistent and smooth growth rate, uniform impingement and cycloidal grain outlines. The constant of the JMAK model depends on the nucleation type i.e, continuous nucleation, site - saturated nucleation in which the initial nuclei have a secured digit and nucleation rate is zero at t > 0, or nucleation rate uninterruptedly fluctuating. The constant (k) has value (3) for a site - saturated nucleation along with three-dimensional (3D) growth and (2) for two-dimensional (2D) growth. The value of constant nucleation rate (k) is 3 for (2D) growth and 4 for (3D) growth. The extended JMAK model contains heterogeneous site-saturated and the constant rate of nucleation at grain boundaries, corner and edges, the value 1 for k for boundary nucleation, 2 for a corner, and 3 for edges are shown in Table 3 [31,32].

Table 3. *The constant of the JMAK model depends on the nucleation types [27].*

Growth Dimension	Site Saturation	Constant Nucleation
1D	1	2
2D	2	3
3D	3	4

For several aspects of static recrystallization, many researchers have been investigating JMAK deviations theoretically and experimentally, specifically the nucleation and growth process by time or space dependencies [31].

2.8 Dynamic Recrystallization

Dynamic recrystallization (DRX) appears during straining, and to be considered limited to low stacking fault energy materials including austenitic stainless steel (ASSs). The major factor may influence substantial consequence on dynamic recrystallization DRX, such as stacking fault energy (SFE), the thermomechanical processing (TMP), the grain size in the initial condition, the chemical composition of steels, and second phase particles [24,33].

In simple words, DRX is defined as 'The static recrystallization (SRX) denotes the recrystallization process throughout annealing which happens during deformation at higher temperatures is called dynamic recrystallization DRX' [33,34].

Throughout the deformation prior grain boundaries extending to the deformation path, grain boundary edges or corners become visible and then the nucleation of new DRX grains occurs at the edge or corner side of grain boundaries (i.e. bulging). At critical strain ϵc, the nucleation of DRX grain may start, by increasing the percentage of deformation the creation of necklace structure and the DRX microstructure continues further. The effect of initial grain size has completely vanished but the deformation conditions, temperature and strain frequency have effects on the DRX necklace structure. The DRX contains partly a high dislocation density as shown in Figure 6 [33,35].

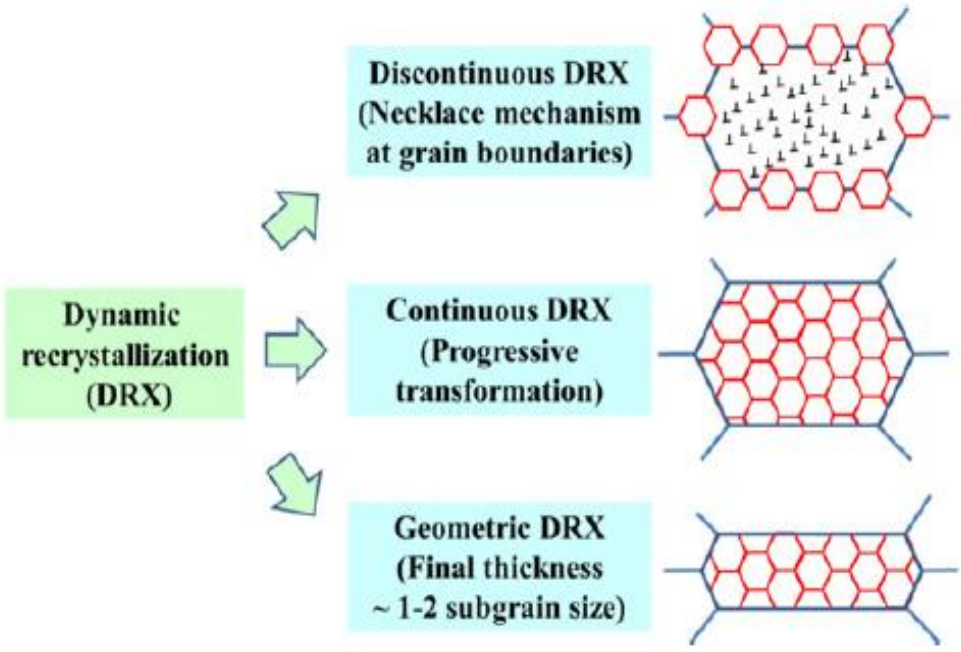

Figure 6. *Three different types of dynamic recrystallization occur in metals and alloys [33]*

Continuous dynamic recrystallization (CDRX) is the process of formation of new grain boundaries by misorientation of adjacent subgrain. CDRX occurs in the large grain boundary velocity, the subgrain boundaries are removed by moving boundaries before they transform into large-angle grain boundaries. Discontinuous dynamic recrystallization (DDRX) is taking place by nucleation and growth of new grains eating rapidly the surrounding strain hardened matrix. The major differences between DDRX and CDRX can be described as follows.

- At large strains, CDRX dominant in strong crystallographic texture whereas the formation of texture delayed by DDRX.
- The temperature relies upon the flow stress is generally reported to be larger for DDRX [36].

Geometry dynamic recrystallization (GDRX) is defined as the generation of equiaxed grains during hot deformation by the relocation of HAGBs to contour serrations, thinning of the grain thickness, and impingement of serrated HAGBs when addressing 1-2 subgrain size distance [33].

2.9 Grain Growth

The surface energy of the grain boundaries is the driving force of grain growth and it occurs at elevated temperatures. The total number of grains decreases when larger grains start eating smaller grains. Some grains start to shrink when the overall surface energy is lower and their total area reduces. The mean value of grain size increases when grains are constantly growing over time. To calculate the grain size of the material the grain diameter have been used. The law of Ideal grain growth associates with grain diameter average to initial grain size and time which is given by equation (3).

$$D^2 + Do^2 = \mathrm{Kt} \qquad 3$$

Where D is denoted by the average grain diameter, D_0 is denoted by the initial grain size, constant of proportionality represented by K that associates with temperature and activation energy for grain growth and holding time denoted by t [38].

The following factors are affecting grain growth.

2.9.1 Rate of heating

The rate of heating of the austenitic stainless steel (ASSs) has been intended to have a significant impact on grain growth kinetics. The result of a slower heating rate has revealed a larger grain size D_0. During the heating process, the difference in initial grain size can be described by grain growth. The grains are continually growing when the specimen is heated from its austenite transition temperature to the target temperature. The slower heating rate specimen takes a longer time to reach the target temperature as compared to the fast heating rate specimen [37,40].

2.9.2 Zener pinning

In the existence of a second phase particle that pins in place of grain boundaries, the grain growth can be reserved. The Zener forces are the holding forces applied to grain boundaries. A critical radius *(R_{cr})* of grain is where the driving force is parallel to the

pinning force employed by second phase particles on grain boundaries is given in equation (4). This equation also called the Zener Equation.

$$Rcr = \mathrm{A} * \frac{\mathrm{r}}{f} \qquad 4$$

Where A is denoted by a constant, r is denoted by the second phase particle mean radius, and f represents the volume fraction of the second phase particles which may hinder the grain growth comprise a very small oxide, sulphide, and carbide particles. At elevated temperature where the particles are disappearing or dissolve Zener, pining can not be detected, but at lower temperatures where second phase particles exist Zener, pinning can be observed [37,41].

3 Material Characterization

In this chapter, the kinetics of reversion transformation of deformation-induced martensite (DIM), the recrystallization and growth of austenite grains are analysed. The existing phases in the cold-rolled deformed specimen of austenitic stainless steel AISI 304L such as deformation-induced martensite (DIM) phases (α´ and ε) and δ - ferrite in the as-received plate were estimated before and after various heat treatments. The following measurement techniques have been used in this study such as Ferritscope, Light optical microscope (LOM), Scanning electron microscope (SEM), Electron backscatter diffraction (EBSD), X-ray diffraction (XRD) and Vickers hardness test.

3.1 Ferritscope FMP30

The magnetic detection device Ferritscope FMP30 by Fischer works based on the magnetic induction method. The device generates a magnetic field through a coil, which relates to the magnetic content of the materials. The change of the magnetic field tempts a voltage proportional to the ferrite content in a second coil then, this voltage is assessed as shown in Figure 7.

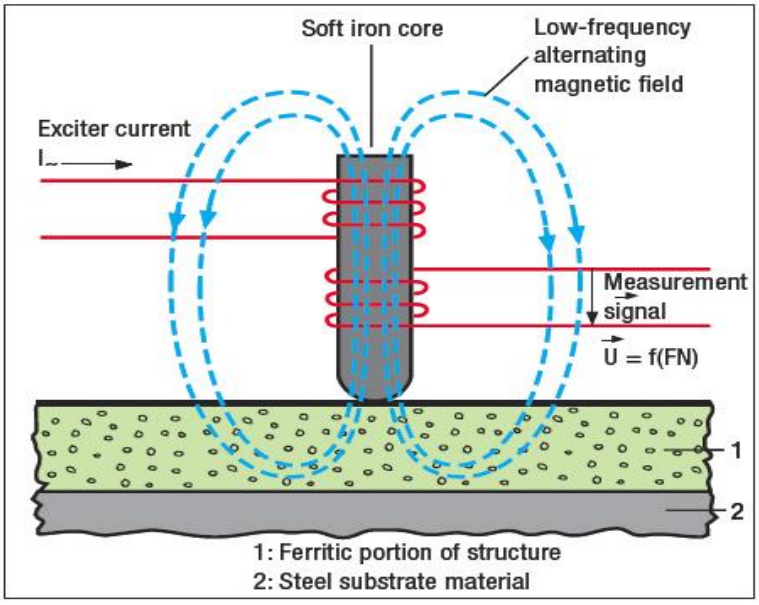

Figure 7. *The basic mechanism of Ferritescope FMP30 [42].*

All magnetic contents are recognized by this device easily such as delta - ferrite, and deformation-induced α´- martensite. To obtain the value of magnetic phases of the material, the device has to be calibrated according to international standards. The Fisher calibration standards set both Ferrite Number (FN) and Ferrite% (F%). In order to maintain the accuracy in the final result at least 30 to 50 readings have to be taken. In this study, 60 readings were taken of each specimen from different point areas [42,43].

3.2 Light Optical Microscope (LOM)

A Zeiss conventional light optical microscope (LOM) was employed to take micrographs of the etched specimens and higher magnifications up to 500x were used to analyse the overall interesting phases of the as-received, deformed and heat-treated specimen where various substructures of different phases such as austenite, martensite and δ - ferrite could be highlighted. In image processing, the phase fraction is measured by using the high magnification LOM images with special software ImageJ. It is considered one of the most reliable techniques. Nevertheless, the final result depends on the quality of the LOM images and operator skills. The images should be neat and clean without any scratches and not be over etched.

3.3 Scanning Electron Microscope (SEM)

The cold-rolled deformed and as-received microstructure of AISI 304L before and after heat treatment were investigated by using a Zeiss Sigma field emission scanning electron microscope (SEM). The accelerating voltage of 20 kV and 10 kV was applied to reveal the texture of the austenite and deformation-induced martensite (DIM) phase. Due to the high amount of misorientation within the grain boundaries of cold-rolled deformed and partially recrystallized specimens, the SEM micrograph has poor contrast. Therefore, electron backscatter diffraction (EBSD) mapping was used to reveal the grain texture.

3.4 Electron Backscatter Diffraction (EBSD)

The electron backscatter diffraction (EBSD) technique was applied to obtain information about different phases and crystallographic orientation of cold-rolled deformed AISI 304L before and after heat treatment. The EBSD technique can be used to assess plastic deformation material because the percentage of a deformed region can be proposed through crystal reorientations of grains, and also the plastic strain has an inline relationship with grains average misorientation (GAM) [44].

3.5 X-Ray Diffraction (XRD)

The x-ray diffraction (XRD) analysis was performed with SIEMENs D5005, using Cu-Anode 40kV, 40mA. A scanning speed of 0.10 s^{-1} for sample, 25% cold-rolled in the initial condition was carried out. The scattered signal from the sample is recorded and graphed. The peaks that appear on the graph depend on the atomic structure of the material inspected. The texture present in the sheet materials after plastic deformation can interrupt the accuracy of the XRD technique. By averaging intensities of different diffraction peaks, the impact of texture can be minimized [43].

3.6 Vickers Hardness Measurement

The hardness offers a significant indication of the mechanical properties of materials that is considerable in quality, design, alloy development, and material selection. In the present study, the Vickers hardness HV10 static indentation tests were conducted according to Vickers at the borders and the centre of each mounted sample. A diamond made pyramidal indenter was holding for 15s with a load of 10 kg (HV10) into the investigated material AISI 304L before and after heat treatments.

4 Experimental Work

4.1 Samples preparation

The material of investigation is well known and widely used austenitic stainless steel grade AISI 304L (EN 1.4301). The plates underwent a cold rolling process in the Vostalpine to apply different cold-rolling deformation such as 25%, 50% and 67% which are mentioned in Table 4. The chemical composition of the material AISI 304L is given by the provider Kloeckner metals Austria Gmbh & CO KG is listed in

Table *5*.

Table 4. *As-received and cold-rolling deformation rate of austenitic stainless steel AISI 304L.*

	As-received	Cold Rolled		
AISI 304L	Non-rolled	25%	50%	67%

Table 5. *The chemical composition of austenitic stainless steel AISI 304**L** is provided by Kloeckner metals Austria Gmbh & CO KG.*

Alloy	Chemical composition(wt.%)								
	C	Mn	Si	Ni	Cr	N	S	P	Fe
AISI 304l	0.08	1.99	1.34	8.01	19.04	0.1	0.02	0.03	Balance

The calibrated device Ferritscope FMP30 was employed in a 3 - axis direction such as Normal Plane, Rolling Plane and Transverse plane in order to to obtain the exact mean value of magnetic phases of each cold-rolled plate of AISI 304L before and after heat treatments. Around 60 readings were taken overall for each sample and 20 readings for each direction from different point areas with the help of the Ferritescope probe. Every plate of cold-rolled and as-received specimens categorised in block size 10 mm x 60 mm x 100 mm as shown in Figure 8. later on, the randomly selected blocks of the specimens were cut into small pieces.

The microstructure of AISI 304L was investigated before and after various heat treatments by conventional light optical microscope (LOM), scanning electron microscope (SEM), electron backscatter diffraction (EBSD) and X-ray diffraction (XRD).

The specimens underwent metallography procedure, the specimens were first mounted by CITOPRESS and then, the specimens were ground by 80 to 4000 grit sandpapers and went to the mechanical polishing up to 1 µm by Struer. Immediately, the specimen immersed in the water and stayed a few minutes in ethanol to acquire the clear surface texture. In some cases, electrolytic polishing using Struer Lectropol in a mixture of electrolyte A2 I at 22°C for 12 seconds and a potential difference of 40V.

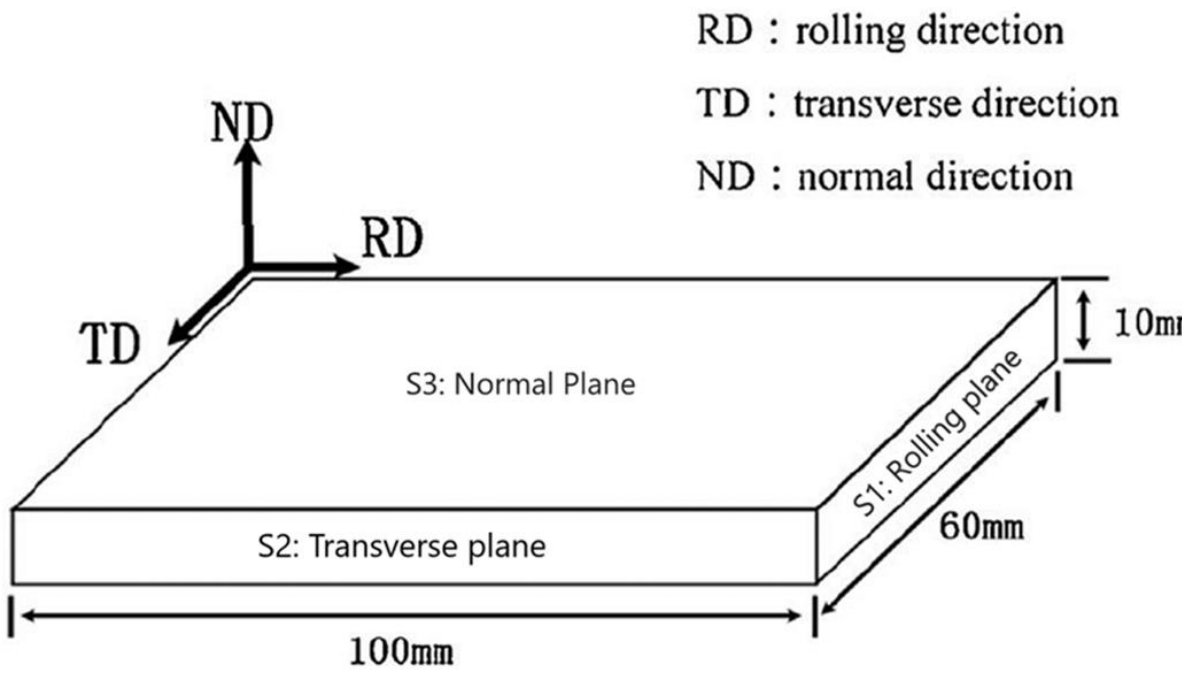

Figure 8. *The block size of AISI 304L.*

However, austenitic stainless steel 304L is generally easy to polish but etching considers being the most difficult process. The ability of AISI 304L such as corrosion resistance makes the choice of etchant tougher than carbon and other alloys of steels.

A few etchants have been used during the investigation of the cold-rolled deformed microstructure of AISI 304L and as-received condition before and after heat treatment listed in Table 6. The Aqueous nitric acid electrolyte etchant was used for highlighting the austenite grain boundaries for all the specimen, and to obtain a better result the etching time was set around 40 seconds, 1V potential difference, 32°C temperature and 18 flow rate were applied in each case. After applying the etchant on the surface of the sample, the samples immediately immersed in a water and ethanol bath. Beraha tint etchant was used to reveal the δ – ferrite and deformation-induced martensite (DIM) content in all the specimens, Beraha tint is a colour etchant and shows the result by different colour contrast. In the procedure of Beraha tint etching, the specimen immersed in the Beraha tint solution just for a maximum of 5 to 10 seconds and needs an appropriate wash in the water and ethanol to obtain good results. Beraha tint etchant remains active just for an hour after that it should be discarded by following the proper safety measures.

Table 6. *Names and chemical composition of etchants were used during the investigation of the AISI 304L microstructure [23].*

Etchants	**Composition**
Aqueous nitric acid electrolytic etch	60 mL HNO_3 and 40 mL H_2O
Beraha's tint etch	1 part HCl, 2 parts H_2O, 1 g $K_2S_2O_5$ per 100 mL of solution

4.2 Heat treatment

The cold-rolled specimens underwent various heat treatments process at 600°C to 800°C with different holding times from (30 min to 480 min) for reversion transformation of deformation-induced martensite (DIM). The temperature range of 900°C to 1200°C with different holding times from (2 min to 120 min) was used for the grain growth of recrystallized austenite grains and as-received plate (non-rolled).

The list of various heat treatments is given in Table 7. The furnace was set to heat at the required temperature, and once the furnace reaches the required temperature the specimens are placed into the furnace immediately. The temperature dropped between 15 to 25°C due to the placement of the specimens and then the furnace took around 2 to 5 minutes to reach the target temperature again.

Table 7. *A table of various heat treatments was applied for reversion transformation of (DIM), recrystallization, and grain growth behaviour of AISI 304L.*

Samples AISI 304L	**Temperature (°C)**	**Time (minutes)**													
		2	**5**	**7**	**10**	**15**	**30**	**45**	**60**	**90**	**120**	**180**	**240**	**360**	**480**
25%, 50%, 67 % cold-rolled	600									x					x
	700											x	x	x	
	800						x		x	x					
. 50% cold-rolled recrystallized at 800°C – 60 min (6µm). . As-received plate (30µm).	900		x		x		x		x	x	x				
	1000	x	x	x	x		x		x						
	1100	x	x	x	x		x		x						
	1200		x		x	x	x	x	x						

5 Results and Discussion

5.1 As-received and cold-rolled AISI 304L in the initial condition

Figure 9(a) shows the microstructure of AISI 304L in as-received condition by using the light optical microscope (LOM). The microstructure of the as-received condition contains up to 3% δ - ferrite due to solidification. The Ferritscope and image processing phase fraction results confirmed the amount of δ - ferrite content in the as-received plate of AISI 304L.

Beraha tint etchant was used to reveal the microstructure of the as-received plate by colour contrast, the dark blue colour represents the amount of δ - ferrite and the rest represent the amount of homogenous γ - austenite grains.

Figure 9(b) shows the microstructure of 25% cold-rolled deformed AISI 304L. According to previous studies due to the cold working effect, the austenite phase transformed to deformation-induced martensite (DIM) phase, and two martensites (ϵ and α´) formed in the microstructure of AISI 304L. Beraha tint etchant was used to reveal the amount of DIM and δ - ferrite content for all the specimens.

The etchant highlighted the DIM content with black colour and austenite phase with white colour. The LOM shows the texture of DIM (ϵ), the thin parallel needles like shape that go through the parent austenite grain and stopped inside the grain boundaries.

The amount of DIM increased due to the increase in the percentage of cold rolling thickness reduction. According to the LOM results, the amount of DIM has high values in the transverse plane (rolling direction) as compared to the other two directions, the LOM results of 50% and 67% cold-rolled AISI 304L shows in Figure 9(c) and (d).

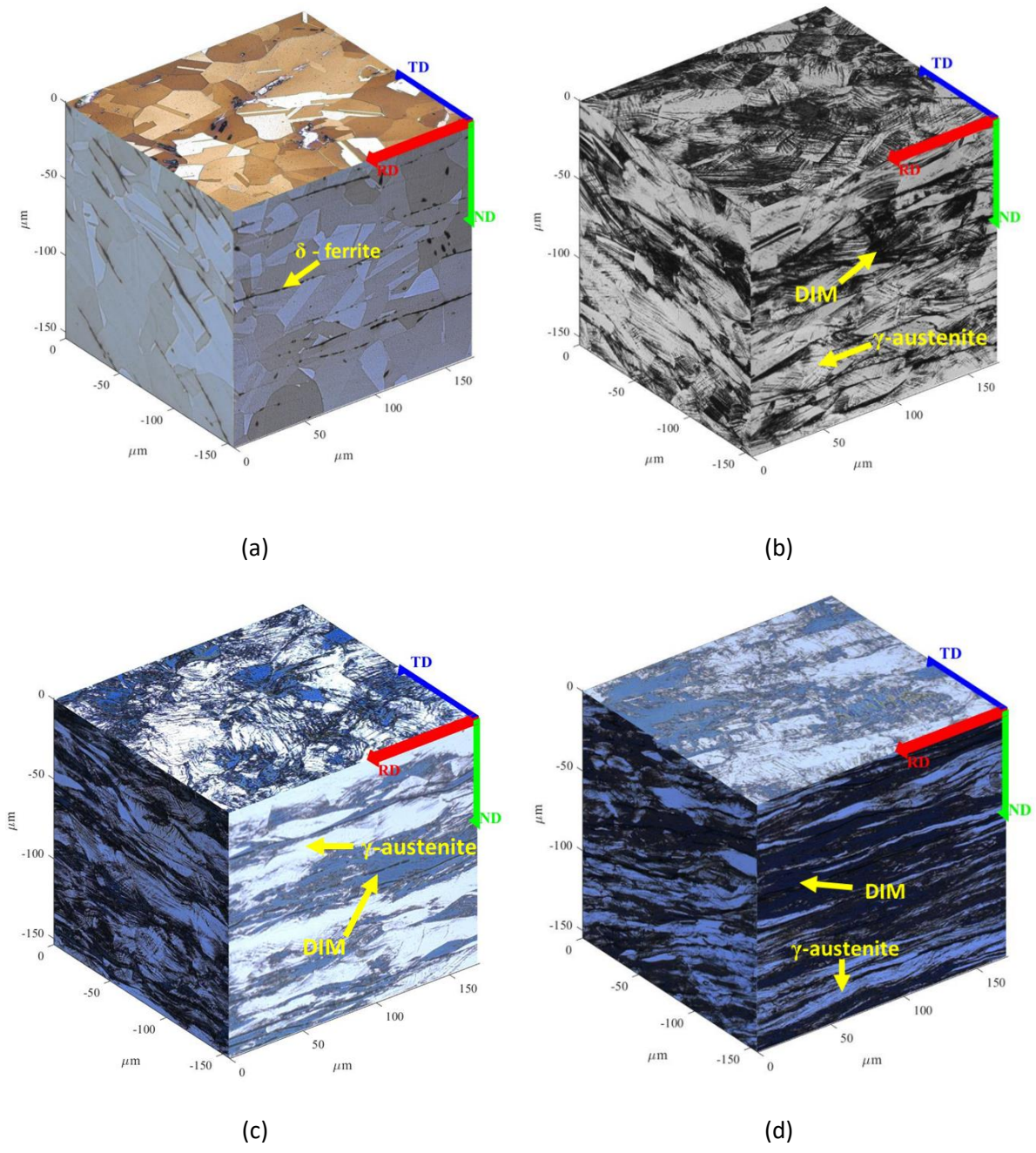

Figure 9. *The LOM images of four different specimens in the initial condition from 3 – axis directions. (a) the as-received plate. (b) 25% cold-rolled. (c) 50% cold-rolled, and (d) 67% cold-rolled.*

The electron backscatter diffraction (EBSD) result confirmed the amount of δ – ferrite in the as-received plate of AISI 304L in the initial condition from the rolling direction shown in Figure 10(a). The EBSD result also shows the austenite grain boundaries with a twin in some areas of the specimen.

The EBSD result of 25% cold-rolled AISI 304L gave the evidence of DIM ε and α´ phases in the transverse plane (TP) shown in Figure 10(b). The EBSD map also shows the amount of δ – ferrite and parent γ – austenite phase in the 25% cold-rolled specimen in the initial condition.

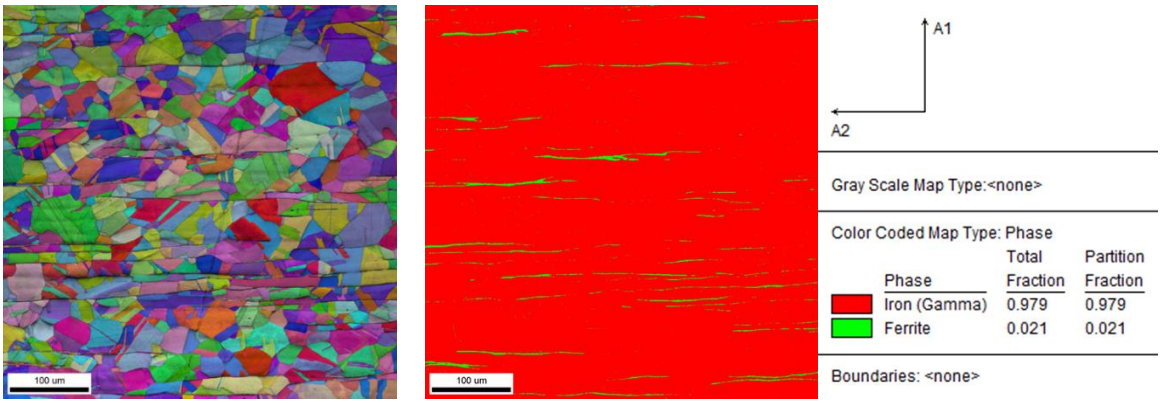

(a)

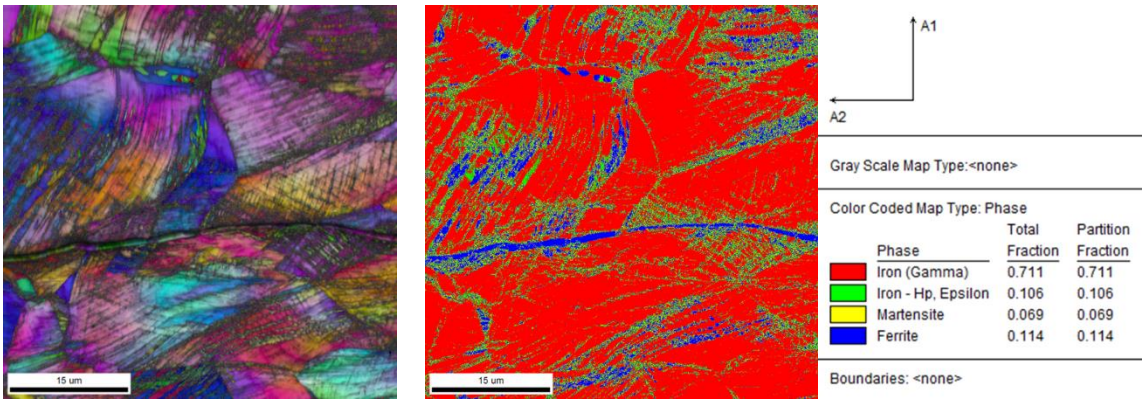

(b)

Figure 10. *(a) the EBSD results of the as-received condition contain the amount δ – ferrite (b) EBSD result of 25% cold-rolled confirmed the amount of ε – martensite in the transverse plane (TP) also highlighted the other phases in the cold-rolled deformed AISI 304L.*

The DIM phases are not distinguishable by LOM result, thus, the specimen 25% cold-rolled AISI 304L is placed for x-ray diffraction (XRD) measurement analysis to obtain the actual amount of existing phases in the initial condition. The XRD result of 25% cold-rolled shows some peak of ε - martensite in the deformed region see in Figure 11, the XRD result also highlighted the peak of α´ – martensite, δ – ferrite and the parent γ – austenite phases in the result.

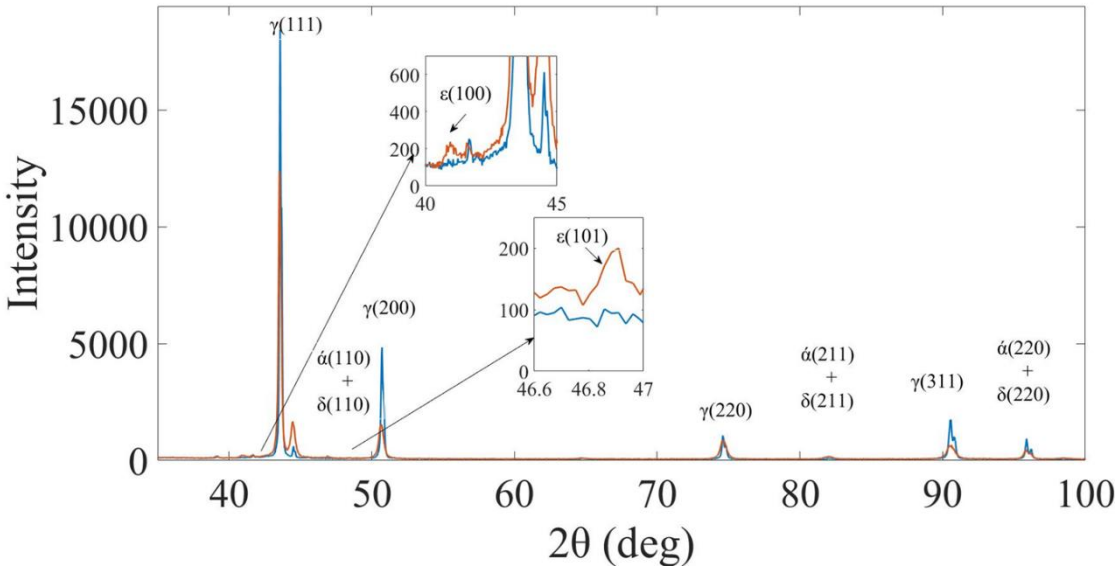

Figure 11. *The (XRD) test of 25% cold-rolled AISI 304L in the initial condition and shows a peak of ε - martensite.*

It is not possible to differentiate the two phases of DIM (ϵ and α´) through image processing phase fraction of microstructure constituents by using LOM images. Therefore, the magnetic induction device Ferritscope was employed to analyse the magnetic phases δ – ferrite and α´- martensite in the cold-rolled deformed AISI 304L. Figure 12, shows the comparison results that are obtained from the Ferritscope and image processing phase fraction by using LOM images. The results show the as-received condition contains around 3% δ - ferrite in the initial condition. The image processing phase fraction of microstructure constituents by ImageJ program shows the collective result of DIM phases (ϵ and α´) and also δ – ferrite in cold-rolled deformed AISI 304L. The calibrated device Ferritscope confirmed the amount of α´-martensite and δ – ferrite contents in the cold-rolled deformed specimens. When the percentage of cold rolling increases the volume of magnetic phases also increases.

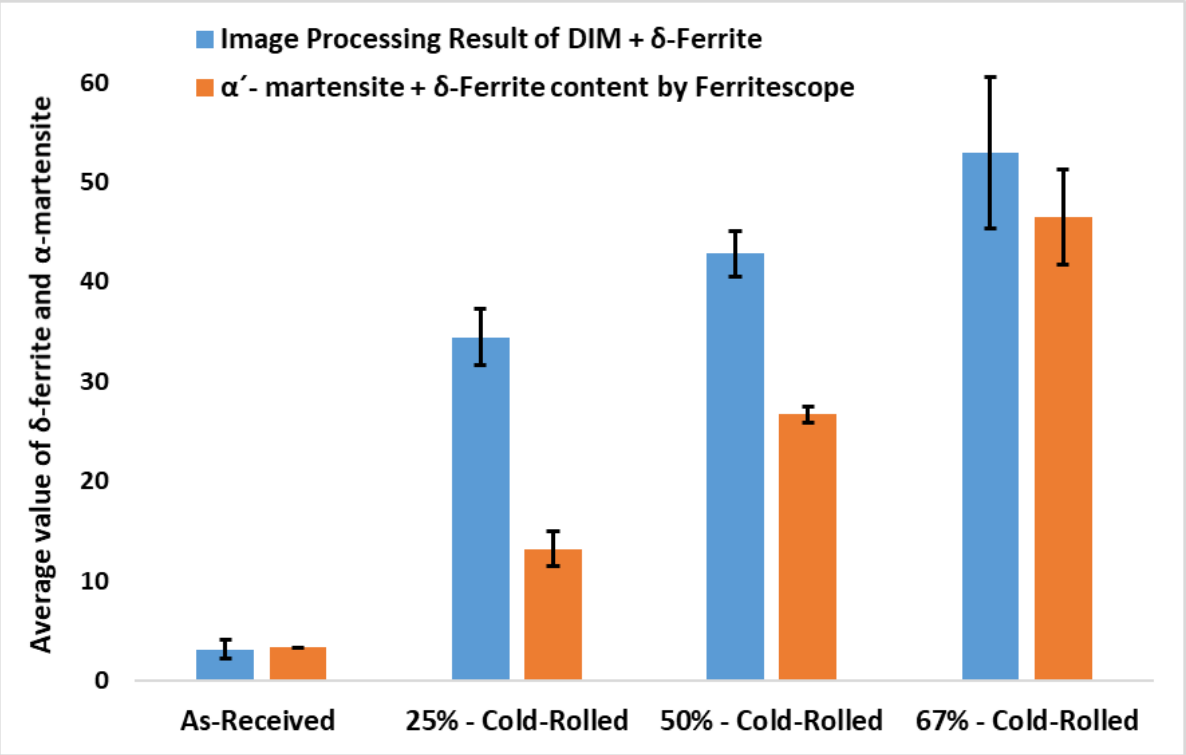

Figure 12. *The graph shows a comparison result of the image processing phase fraction of DIM + δ - ferrite by ImageJ program, and the average value of α´- martensite content + δ - ferrite was obtained by calibrated device Ferritscope. The as-received plate only contains δ - ferrite.*

5.2 The average grain size of AISI 304L in the initial condition

To measure the average grain size of the as-received plate and cold-rolled specimens in the initial condition the most common technique linear intercept method was used. While using the intercept method the scale bar of the software ImageJ should be set according to the scale size of the light optical image. To maintain the accuracy in the result, the randomly selected line must be drawn as long as it can produce 50 to 100 intersection points at the micrograph. At least 5 random lines have to be drawn to obtain the satisfying average grain size results. The formula of the intercept method to calculate the average grain size is given below [37].

$$Average\ Grain\ Size\ = \frac{\text{Randomly drawn distance line}}{\text{Number of intersected grains}}$$

Aqueous nitric acid electrolyte etchant was used to reveal the grain boundaries of the as-received and cold-rolled specimens of AISI 304L. Figure 13, shows the detail of the average grain size of the as-received and cold-rolled specimens by the linear intercept method.

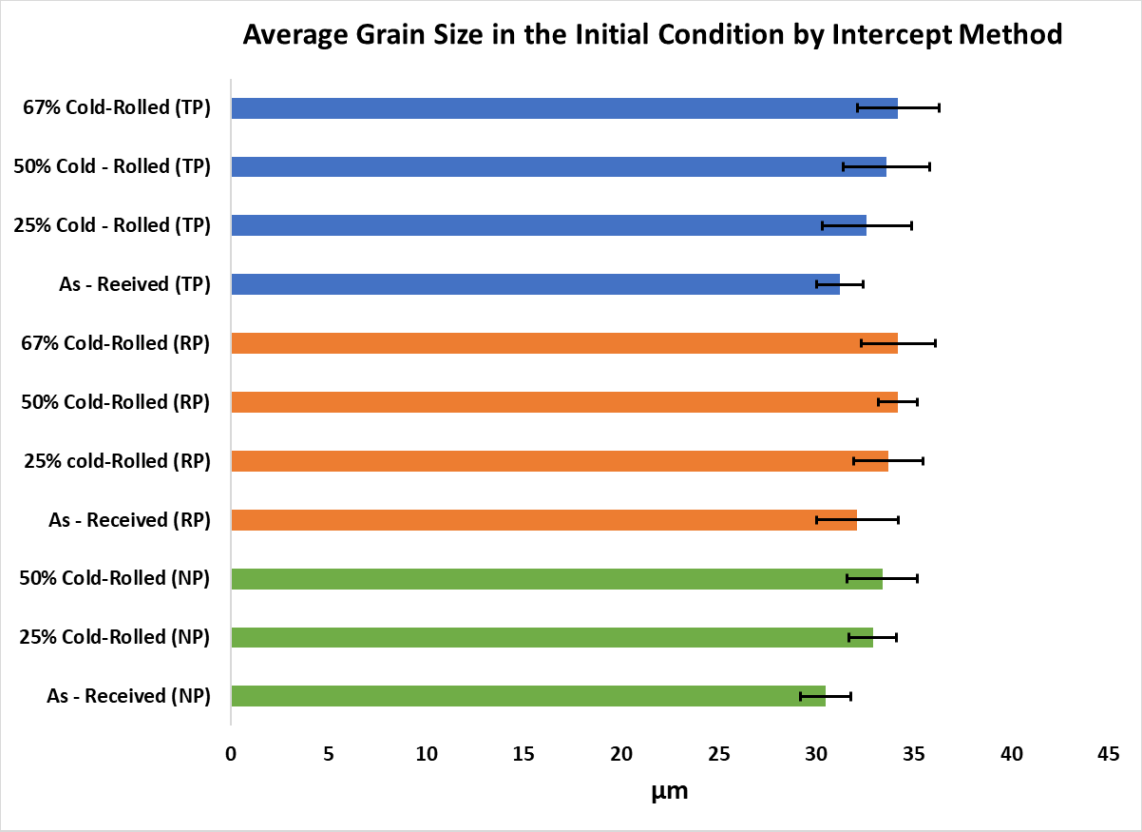

Figure 13. *Shows the result of the average grain size of the as-received plate and cold-rolled AISI 304L in the initial condition. The average grain size was measured by the intercept method.*

Figure 14(a), (b), (c), and (d) are the randomly selected LOM images that were used to measure the average grain size from different planes of the as-received condition and 25%, 50%, 67% cold rolling deformation of AISI 304L.

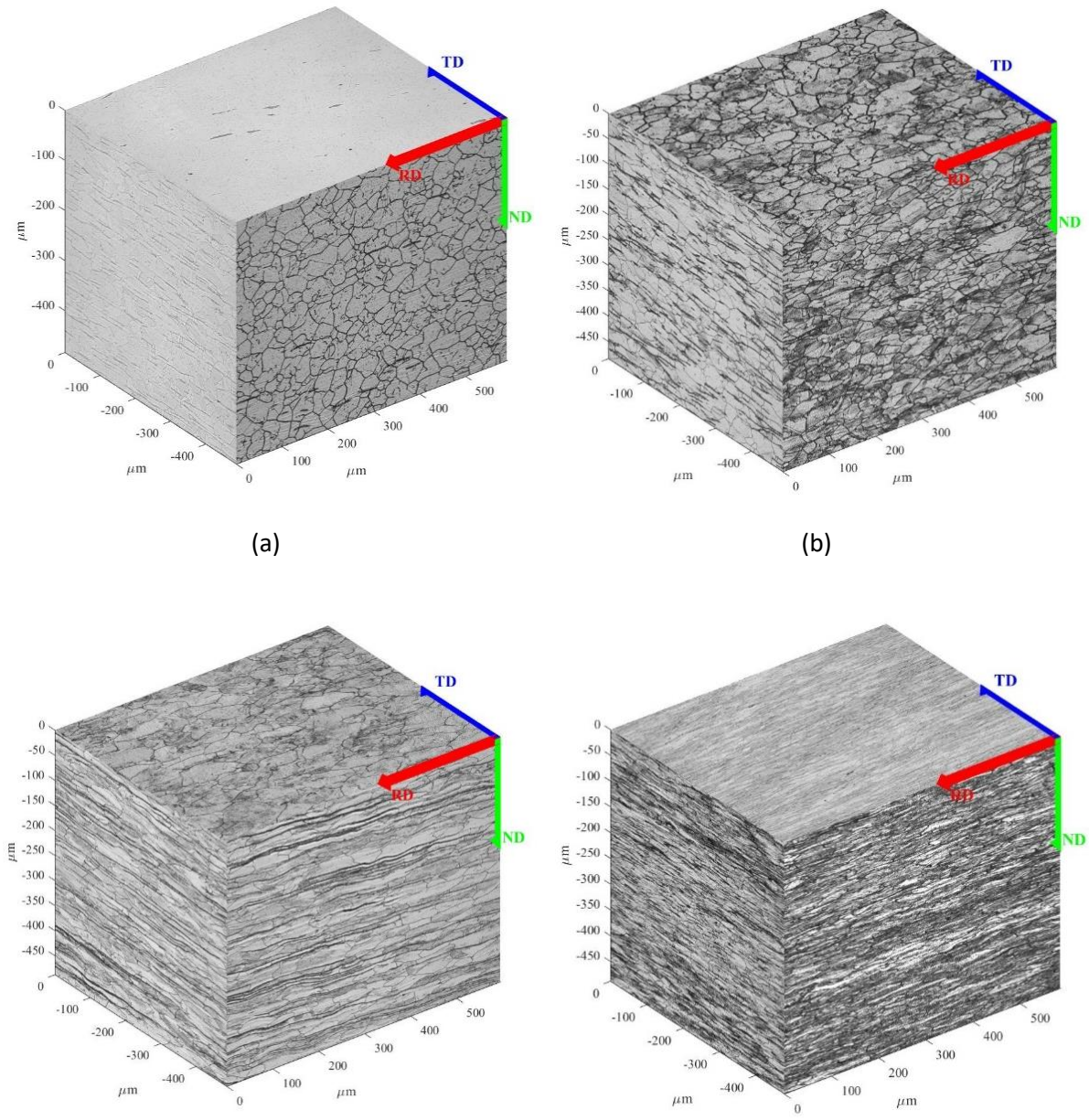

Figure 14. *Randomly selected LOM images were used to measure the average grain size in the initial condition. Figure (a) As-received plate, figure (b) 25% cold-rolled, figure (c) 50% cold-rolled, and figure (d) 67% cold-rolled AISI 304L.*

5.3 Reversion treatment of deformation-induced Martensite

Padilha and co-authors [5] reported that the reversion of α´- martensite starts in the temperature range of 600°C to 750°C with long annealing time and they also mentioned the Singh's work in their study, the α´- martensite remain stable between

200°C to 400°C. Antti and co-authors [7] studied the reversion of strain-induced martensite in austenitic stainless steel (ASSs) 304L begins at a temperature of 650°C and completely fine grain structure obtained at 900°C after 30 minutes of annealing. Meysam and co-author [45] investigated the kinetic of reversion transformation of deformation-induced martensite (DIM) at a temperature of (750°C) with 70% cold-rolled thickness reduction of AISI 304L, they stated the reversion of DIM at (750°C) was observed a fast process with a function of time and recrystallized grain structure formed with a longer annealing time.

5.3.1 Reversion treatment results of the present study

In order to investigate the kinetics of reversion transformation of deformation-induced martensite (DIM) into the parent austenite phase, the austenitic stainless steel AISI 304L with different cold-rolling deformation was placed for reversion treatments with the temperature range of (600°C to 800°C) with different time frames. The deformed region of AISI 304L underwent recovery and recrystallisation during the heat treatment and at the same time, DIM transforms into the parent austenite phase. The reversion process of DIM in austenitic stainless steel AISI 304L leads to the grain refinement and very tiny fine austenite grains are obtained. The following annealing reversion treatments have been applied to the specimens of 25%, 50%, 67% cold-rolled deformed AISI 304L see in Table 8.

Table 8. *The heat treatment plan for reversion treatment of deformation-induced martensite (DIM), and recrystallization.*

Samples Cold-rolled AISI 304L	**Temperature (°C)**	**Time (minutes)**							**Cooling**
		30	**60**	**90**	**180**	**240**	**360**	**480**	
25%, 50%, 67%	600			x			x		Ambient
	700				x	x		x	
	800	x	x	x					

The reversion of DIM at a temperature of 600°C was observed as a slow process, the light optical microscope (LOM) images and Ferritscpe shows the evidence of reversion of DIM into the austenite phase after different reversion annealing.

According to the LOM and Ferritscope result, the α´- martensite reversed back to the austenite phase in the temperature range of (600 to 700°C) and at the same time and temperature, ϵ - martensite remain stable. The LOM result shows the amount of stable ϵ - martensite at a temperature of (700 – 180 min). The reversion of ϵ - martensite was observed by LOM result at a temperature of (700°C - 240 minutes). Therefore, newly recrystallized austenite grains were formed in the heavily deformed region of AISI 304L.

The calibrated device Ferritscope shows the reversion of α´- martensite and magnetic content δ - ferrite in Figure 15 after different reversion treatments.

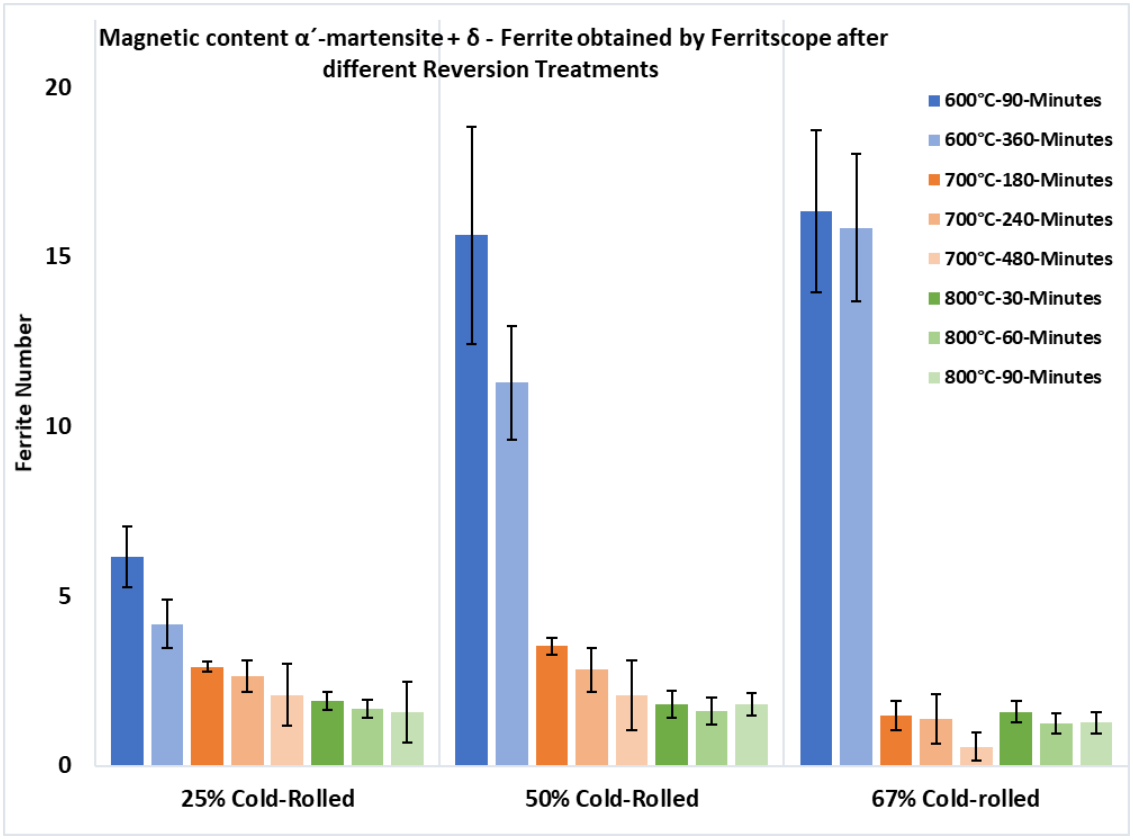

Figure 15. *Shows the amount of actual α´-martensite and magnetic content δ - ferrite obtained by calibrated device Ferritescope after different reversion treatments of deformation-induced martensite (DIM).*

The Ferritscope result of cold-rolled samples in the initial condition before heat treatment, as mentioned above in Figure 12.

The LOM images Figure 16 reversion treated at 600°C, Figure 17 reversion treated at 700°C and Figure 18 reversion treated at 800°C shows the visual evidence of reversion of DIM at different temperatures and time frames. The LOM and Ferritscope results of 25% cold-rolled sample from different directions at a reversion treatment of 600°C - 90 min shows the amount of α´- martensite start to reverse back to the parent austenite phase see in Figure 16(a) and the ϵ - martensite remain stable at this temperature and time. The Ferritscope and LOM results gave strong evidence of the complete reversion of α´-martensite to parent austenite at a temperature of 700°C - 180 min, and some amount of δ – ferrite can be seen in Figure 17(a) and (b). Whereas the ϵ -martensite starts to reverse back to the parent austenite phase at a temperature of 700°C - 480 min and completely reversed back to the parent austenite phase at a temperature of 800°C - 60 min as shown in Figure 18(a). Figure 15, shows the reversion of α´- martensite in 25% cold-rolled specimen starts at 600°C - 90 min and in that temperature, the reversion of α´-martensite was observed as a slow process and the complete reversion of α´ - martensite in 25% cold-rolled specimen occurred at a temperature of 700°C - 180 min.

The results of 50% colled-rolled from different directions at different reversion treatments shown in Figure 16, Figure 17 and Figure 18. According to Ferritscope result see in Figure 15 and LOM results, it can be seen the amount of α´-martensite completely reversed back to parent austenite at a temperature of 700°C - 180 min see in Figure 17(c) and (d). The LOM result also shows some amount of δ - ferrite in the microstructure of 50% cold-rolled at different reversion temperatures shown in Figure 17(c). The LOM result gives strong evidence of complete reversion of ϵ - martensite to the parent austenite phase at a temperature of 800°C - 60 min is shown in Figure 18(b). At a temperature of 700°C for a longer time, the reversion of DIM was observed as a fast process with the help of LOM and Ferritscope results.

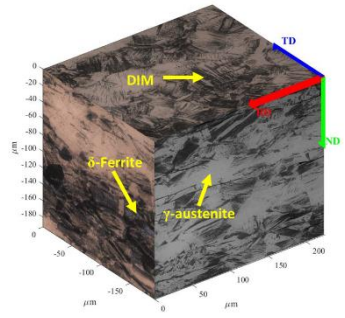

16 (a). LOM image of 25% cold-rolled AISI 304L from three directions after reversion treatment at 600°C – 90 min.

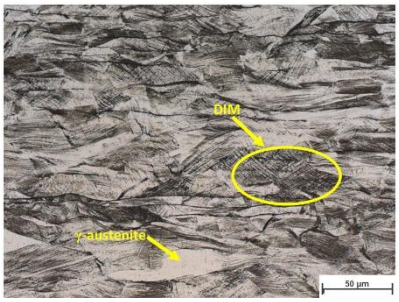

16 (b). LOM image of 25% cold-rolled from the transverse plane heat-treated at 600°C-360 min. Shows some amount of DIM (α´- martensite) reversed back to austenite but ε - martensite stayed stable.

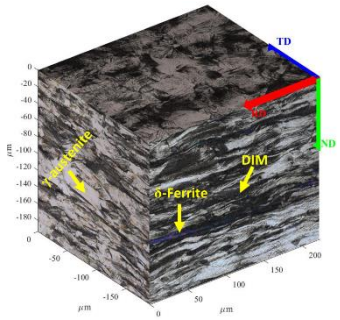

16 (c). LOM image of 50% cold-rolled from three directions after reversion treatment at 600°C – 90 min. Does not show any evidence of reversion of DIM, and some amount of δ - ferrite presence in the microstructure.

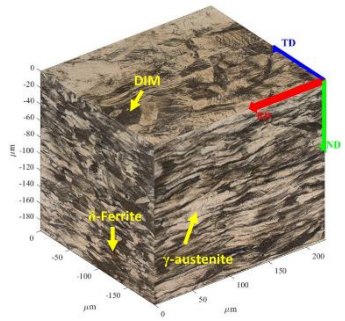

16 (d). LOM image of 50% cold-rolled from three directions after reversion treatment at 600°C – 360 min. The amount of DIM (α´- martensite) reversed back to austenite but ε - martensite stayed stable.

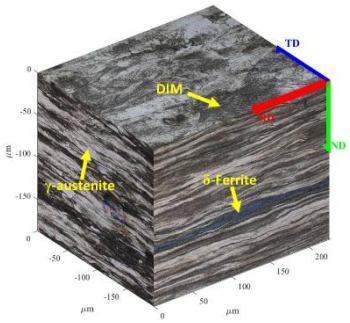

16 (e). LOM image of 67% cold-rolled from three directions after reversion treatment at 600°C – 90min. Does not show any evidence of reversion of DIM. Some amount of δ - ferrite can be observed.

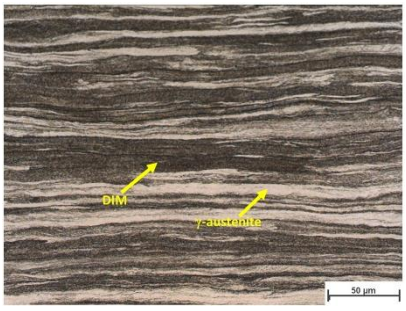

16 (f). LOM image of 67% cold-rolled from the transverse plane reversion treated at 600°C – 360 min, the DIM stayed stable.

Figure 16. *The cold-rolled AISI 304L reversion treated at 600°C.*

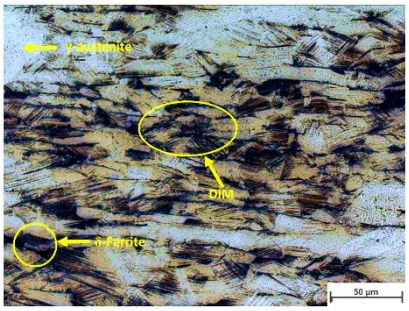

17 (a). LOM image of 25% cold-rolled AISI 304L rolling plane reversion-treated at 700°C – 180 min. The amount of DIM (α´) reversed back to austenite and ε - martensite remain stable.

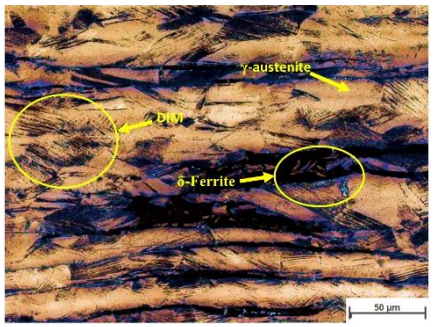

17 (b). LOM image of 25% cold-rolled transverse plane reversion-treated at 700°C – 180 min. A significant amount of δ – ferrite can be observed.

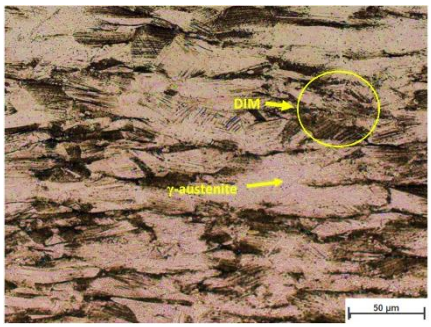

17 (c). LOM image of 50% cold-rolled rolling plane reversion treated at 700°C – 180 min. The amount of DIM (α´) reversed back to austenite and some ε - martensite remain stable.

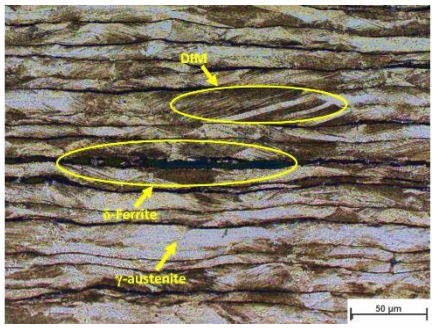

17 (d). LOM image of 50% cold-rolled transverse plane reversion treated at 700°C – 180 min. Some amount of δ-ferrite can be seen in the microstructure.

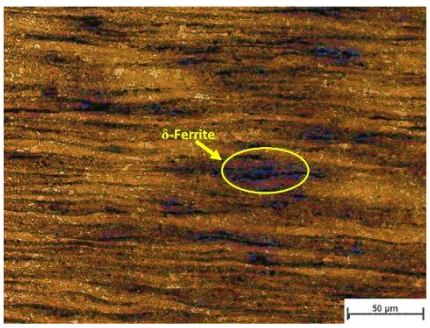

17 (e). LOM image of 67% cold-rolled rolling plane reversion treated at 700°C – 180 min. All DIM reversed back to parent austenite. Some amount of δ-ferrite can be seen in the microstructure.

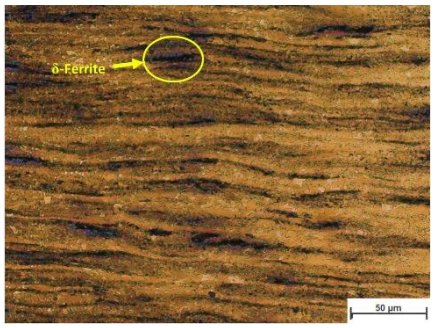

17 (f). LOM image of 67% cold-rolled transverse plane reversion treated at 700°C – 180 min. Some amount of δ-ferrite can be seen in the microstructure.

Figure 17. *The cold-rolled AISI 304L reversion treated at 700°C.*

The results of 67% cold-rolled from different directions after various reversion treatment, at 600°C - after 90 min Figure 16(e) and (f) shows a significant amount of DIM content in all three directions, and also the Beraha tint etchant highlighted the amount of δ - ferrite with dark blue colour lines in the rolling direction. According to Ferritscope result Figure 15 and LOM results, all DIM reversed back to parent austenite at a temperature of 700°C after 180 minutes of heat treatment which can be seen in Figure 17(e) and (f). At the same temperature and time, the LOM results also show some amount of δ – ferrite in the microstructure.

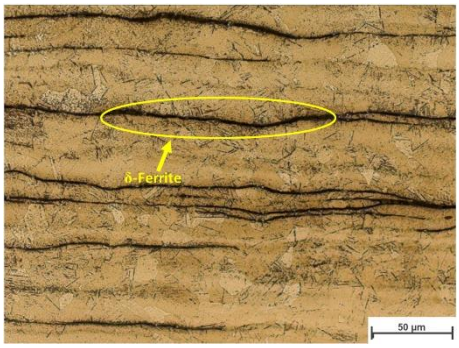

18 (a). LOM image of 25% cold-rolled AISI 304L transverse plane reversion treated at 800°C – 60 min. The stable ε - martensite reversed back to austenite.

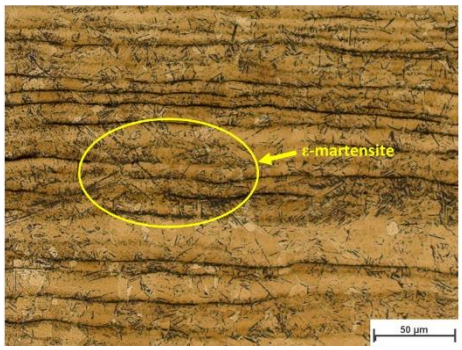

18 (b). LOM image of 50% cold-rolled rolling direction reversion treated at 800°C – 60 min. All ε - martensite reversed back to the austenite phase.

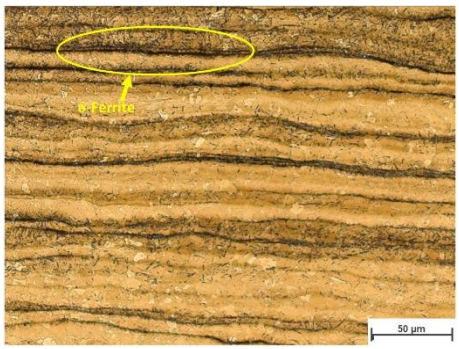

18 (c). LOM image of 67% cold-rolled transverse plane after reversion treated at 800°C – 60 min. Some amount of δ-ferrite can be seen.

Figure 18. *The cold-rolled AISI 304L reversion treated at 800°C.*

The LOM result highlighted the amount of δ - ferrite in the microstructure of 67% cold-rolled (Transverse plane) at different reversion treatments as shown in Figure 17(e),

(f), and Figure 18(c). At a reversion temperature of 700°C after 180 min of annealing, very tiny newly recrystallized austenite grains are formed in the microstructure of 67% cold-rolled AISI 304L. At 700°C, the reversion of DIM was observed as a fast process in 67% cold-rolled AISI 304L. The device Ferritscope also detects the δ - ferrite content in the microstructure after different reversion treatments.

5.4 Recrystallization

During reversion transformation of deformation-induced martensite (DIM) into the parent austenite phase, the austenitic stainless steel AISI 304L undergo recovery and recrystallization phenomena. In primary recrystallization phenomena, the newly austenite grains are nucleated in the deformed region of the AISI 304L and that newly nucleated grains can grow further. The kinetics of primary recrystallization is expressed by the Avrami equation (see equation 2 on page 13), the fraction of newly recrystallized grains as a function of heating time, and the constant of the Avrami equation k as a function of material deformation percentage. When the percentage of cold rolling deformation is high the recrystallization occurs early. The stored energy in the grain boundaries after cold rolling deformation is the driving force for the primary recrystallization phenomena. Mostly, at a lower temperature of annealing and with less amount of deformation the result may only be recovery, whereas recrystallization requires a higher temperature [46][47].

In the present study, the recrystallization (temperature and time) of newly austenite grains in the deformed region of AISI 304L with 25%, 50% and 67% cold rolling deformation through different heat treatments have been examined. The grain size distribution was measured by the linear intercept method after every heat treatment at (600°C to 800°C) temperature range from different planes of cold-rolled specimens. The aqueous nitric acid electrolyte etchant was used to reveal the grain boundaries.

At 600°C after 90 min of heat-treatment, the specimens still show a significant amount of DIM texture inside the parent austenite grains, and no evidence was found for recrystallized austenite grains at this temperature and time.

By Heat treatment at 700°C for 180 min, the 25% cold-rolled deformed shows no evidence of recrystallized austenite grains.

However, 50% cold-rolled specimen shows newly recrystallized austenite grains in the deformed region as shown in Figure 19(a) and (b), and in the transverse plane (Rolling direction) high amount of recrystallized austenite grains can be observed in the deformed region. The microstructure of 50% cold-rolled after different heat treatments can be differentiated in three regions, the etchant highlighted the DIM region separately, newly recrystallized austenite grains in the deformed region, and the parent austenite grains size up to 30µm. Also, the etchant revealed some amount of stable ϵ -martensite texture in the microstructure.

At 700°C - 180 min of heat treatment, the 67% cold-rolled specimen shows completely recrystallized austenite grains as shown in Figure 19(c) and (d).

The newly nucleated austenite grains grew further with a longer annealing time. The recrystallization in 67% cold-rolled deformed specimen was observed fast process. Due to the high degree of cold rolling reduction, the stored energy in grain boundaries and annealing temperature and time leads to the recrystallization phenomena according to the pattern of the Avrami model.

The grain size of newly formed grains was measured approximately up to 2µm in 67% cold-rolled specimen after heat treatment at 700°C after 180 min. The aqueous nitric acid electrolyte etchant does not show any evidence of DIM content but δ - ferrite can be seen after heat treatment at 700°C- 180 min.

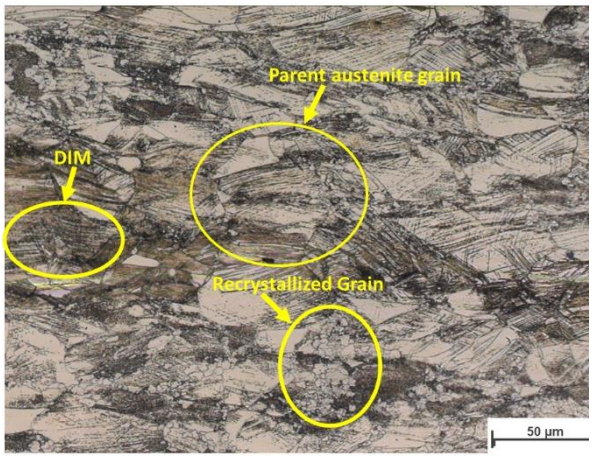

19 (a). 50% cold-rolled (Rolling plane) heat-treated at 700°C- 180 min. Some recrystallized austenite grains formed in the deformed region.

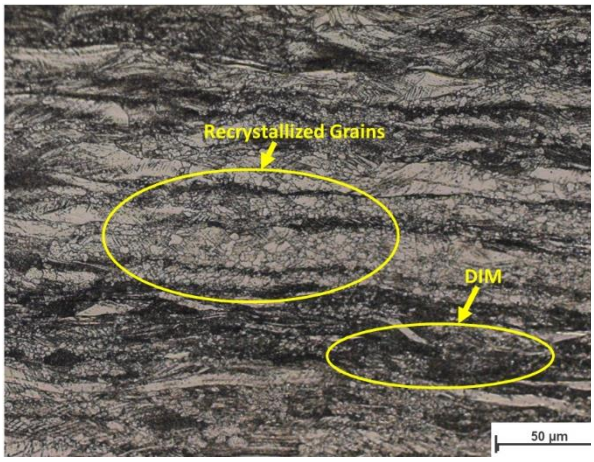

19 (b). 50% cold-rolled (Transverse plane) heat-treated at 700°C- 180 min. A large amount of recrystallized austenite grains formed in the deformed region.

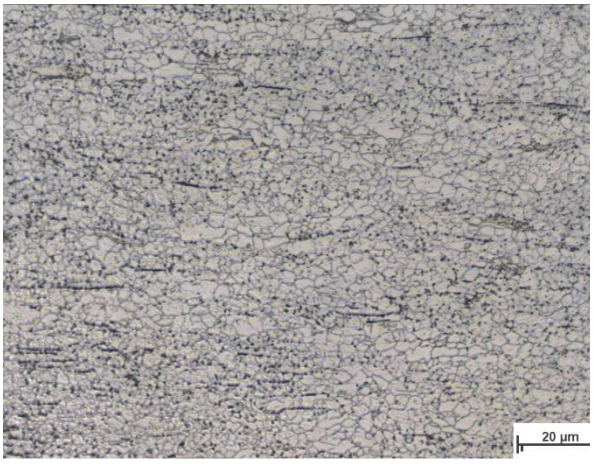

19 (c). 67% cold-rolled (Rolling plane) heat-treated at 700°C- 180 min, a fully recrystallized austenite grains structure formed.

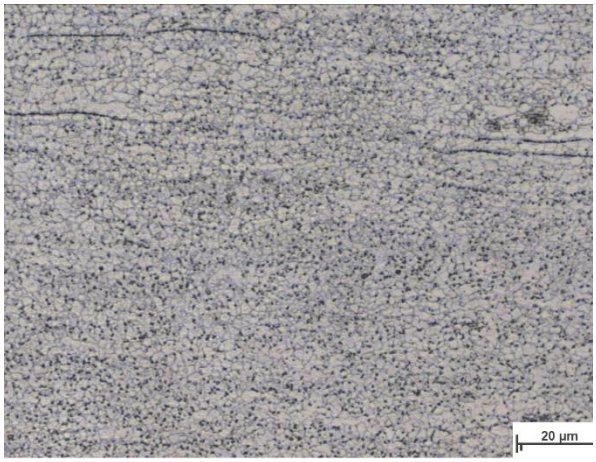

19 (d). 67% cold-rolled (Transverse plane) heat-treated at 700°C- 180 min, a fully recrystallized austenite grains structure formed.

At reversion treatment of 700°C - 240 min, no evidence of recrystallization detected in 25% cold-rolled deformed specimen (Transverse Plane). The etchant revealed the parent austenite grains and some amount of stable ϵ - martensite texture. The 50% cold-rolled deformed specimen from the (Transverse Plane) half of the deformed region underwent recrystallization as shown in Figure 19(e), some previously recrystallized austenite grains follows grain growth phenomena at this temperature and time. The 67% cold-rolled specimen undergoes grain growth phenomena, the grains are growing by increasing the annealing time but at a temperature of 700°C -

240 min of heat treatment, the grain growth was observed a very slow process and some amount of δ - ferrite can be seen in Figure 19(f).

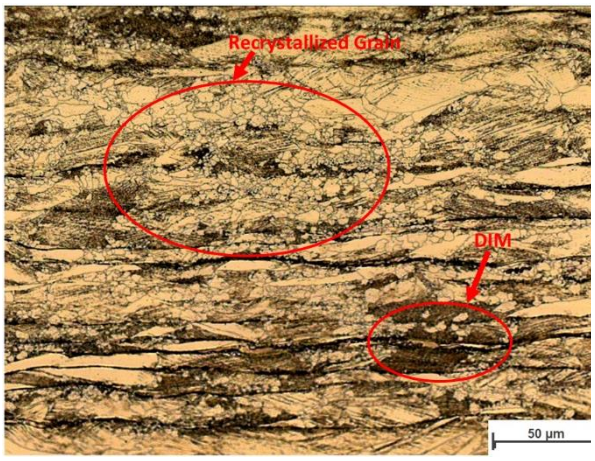

19 (e). 50% cold-rolled AISI 304L (Transverse plane) heat-treated at 700°C- 240 min, half of the specimen became recrystallized.

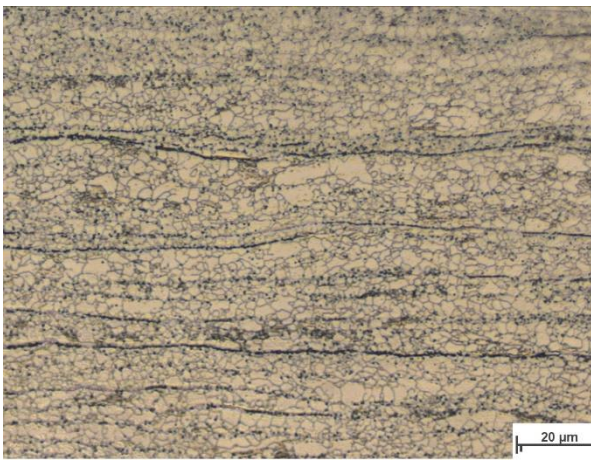

19 (f). 67% cold-rolled AISI 304L (Transverse plane) heat-treated at 700°C- 240 min. Shows fully homogeneous recrystallized austenite grains structure, and the grain growth phenomena were observed in 67% cold rolling reduction.

Figure 19. *The recrystallization result of 25%, 50%, and 67% cold-rolled AISI 304L at heat treatment of 700°C with different time frames.*

The specimens 25%, 50% and 67% cold-rolled were placed in a furnace for further heat treatments at 800°C temperature with three different time frames (30, 60 and 90 minutes). The specimens were investigated from the transverse plane. At a temperature of 800°C - 30 min, the 25% cold-rolled deformed specimen became partially recrystallized; few newly recrystallized austenite grains were formed in the heavily deformed region as shown in Figure 20(a). The average grain size is less than 3µm, and the LOM image also shows some amount ϵ -martensite texture. After increasing the annealing time to (60 min) shown in Figure 20(b), the completely recrystallized homogeneous grain structure was obtained and some amount of δ - ferrite can be seen in the microstructure. The grain growth of newly recrystallized austenite grains was observed at a temperature of 800°C for a 90 min annealing time.

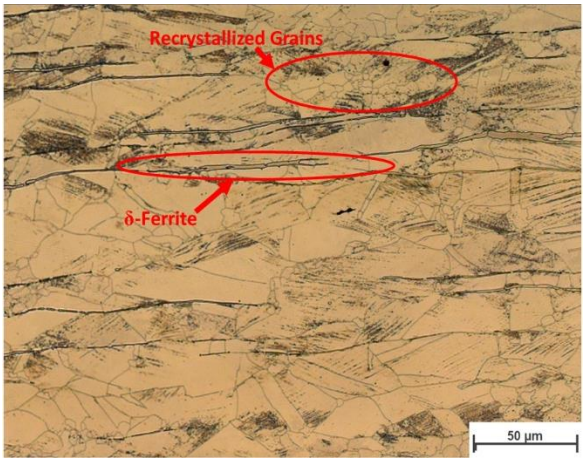

20 (a). LOM image of 25% cold-rolled AISI 304L (Transverse Plane) heat-treated at 800°C-30 min. Few newly nucleated austenite grains and δ-ferrite can be seen in the microstructure.

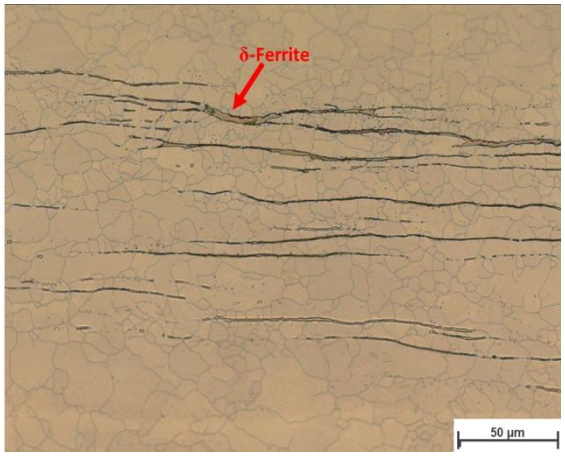

20 (b). LOM image of 25% cold-rolled AISI 304L (Transverse Plane) heat-treated at 800°C-60 min. The Completely homogeneous recrystallized austenite grains structure formed and also δ – ferrite can be seen.

The 50% cold-rolled deformed specimen at 800°C - 30 min of heat treatment became fully recrystallized. The recrystallization phenomena occurred a little bit faster in 50% deformed specimen in comparison with 25% deformed. By increasing the time of annealing at 800°C - 60 min, the LOM Figure 20(c) shows some grain growth of newly recrystallized austenite grains but at 800°C - 90 min of heat treatment shows no evidence of grain growth and the grains size remain same at this annealing time.

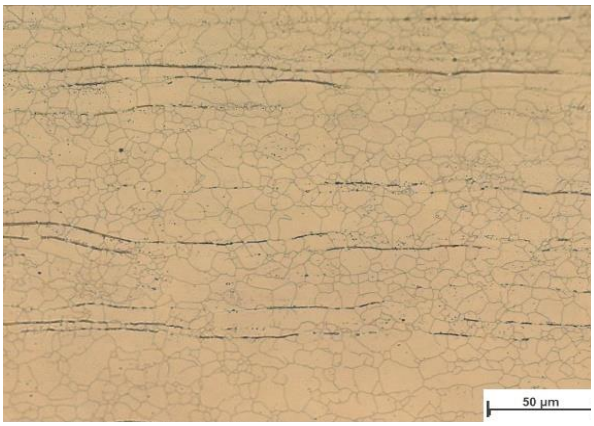

20 (c). LOM image of 50% cold-rolled AISI 304L (Transverse Plane) heat-treated at 800°C-60 min. The Completely recrystallized austenite grains structure formed.

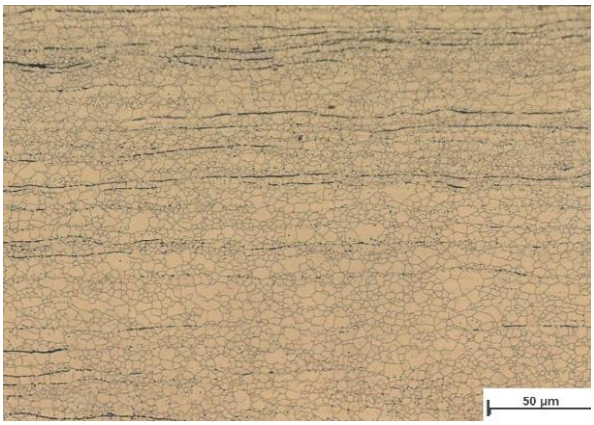

20 (d). (LOM) image of 67% cold-rolled AISI 304L (Transverse Plane) heat-treated at 800°C-60 min. The homogeneous austenite grains structure can be seen.

Figure 20. *The recrystallization result of 25%, 50%, and 67% cold-rolled AISI 304L at heat treatment of 800°C with different time frames.*

The 67% cold-rolled specimen after heat-treated at 800°C - 60 min shows some grain growth see in Figure 20(d), after increasing the annealing time to 90 min the grains remain stable in size.

The electron backscatter diffraction (EBSD) result of 50% cold-rolled AISI 304L from transverse plane confirmed the formation of newly recrystallized austenite grains in the deformed region at a heat treatment temperature of 700°C – 180 min. The EBSD map also differentiated the other phases in the result such as ε, α´- martensite, δ – ferrite and parent γ – austenite phase as shown in Figure 21(a). By the increase of annealing time at 700°C – 240 min the 50% cold-rolled AISI 304L moderately became recrystallized as shown in Figure 21(b). The EBSD result of 67% cold-rolled AISI 304L after heat treatment at 700°C – 240 min, shows recrystallized austenite grain structure see in Figure 21(c). The recrystallization occurs very fast in 67% cold-rolled. The average grain size of the newly recrystallized grain size was measured approximately around 3µm in the transverse plane (TP).

The EBSD result of 25% cold-rolled AISI 304L at a temperature of 800°C – 30min shows some partially recrystallized austenite grains and the number of different phases in the deformed region such as ε – martensite, δ – ferrite and parent γ – austenite phase as shown in Figure 21(d), with a long annealing time to 60 min the recrystallization was observed very fast in 25% cold-rolled specimen can be seen in Figure 21(e).

The LOM and EBSD mapping revealed the recrystallized austenite grain structure in 50% cold-rolled AISI 304L at a temperature of 800°C – 60 min see in Figure 21(f). The average grain size of fully recrystallized 50% cold-rolled austenite grains was measured around 6µm.

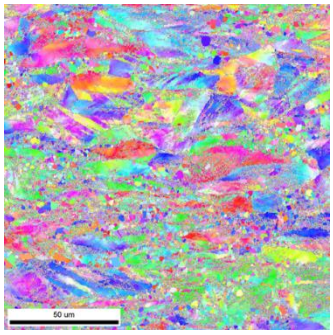

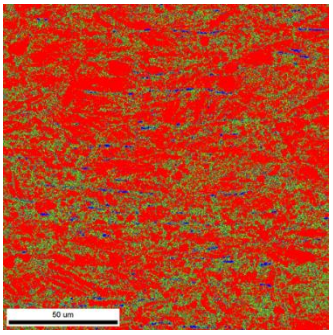

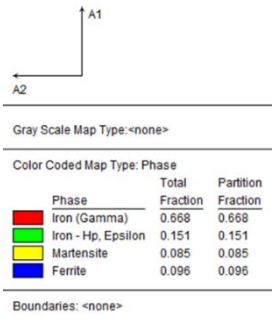

21 (a). The EBSD result of 50% cold-rolled AISI 304L (Transverse Plane) after heat-treated at (700°C – 180 min), some newly recrystallized austenite grains formed in the deformed region.

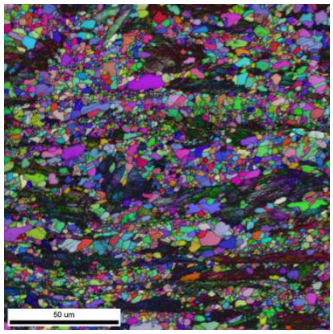

21 (b). The EBSD result of 50% cold-rolled AISI 304L (TP) after heat treatment at 700°C – 240 min.

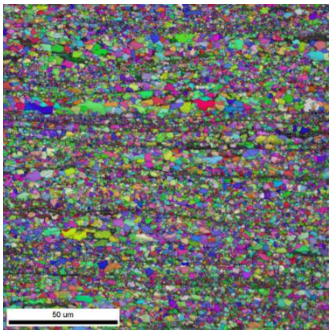

21 (c). The EBSD result of 67% cold-rolled (TP) after heat treatment at 700°C – 240 min, became fully recrystallized.

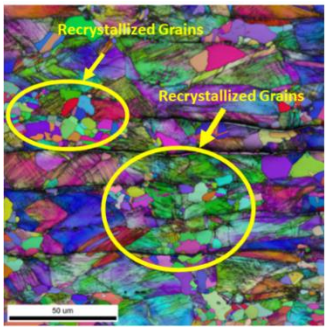

21 (d). The EBSD result of 25% cold-rolled (TP) after heat treatment at (800°C – 30 min), some recrystallized austenite grain formed in the deformed region.

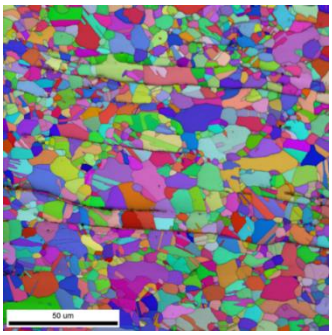

21 (e). The EBSD result of 25% cold-rolled (TP) after heat treatment at 800°C – 60 min, became fully recrystallized.

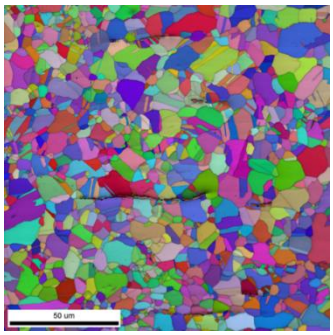

21 (f). The EBSD result of 50% cold-rolled AISI 304L (TP) after heat treatment at 800°C – 60 min, completely homogeneous recrystallized austenite grain structure obtained.

Figure 21. *The EBSD results of recrystallization (Temperature and Time) in 25%, 50% and 67% cold-rolled AISI 304L shown in figure (a to f) after various heat treatments.*

The average grain size of newly recrystallized austenite grains was measured at different heat treatment temperature and time as shown in Figure 22. The average grain size of 25% and 50% specimens at an annealing temperature of 600°C remain the same from the initial condition, the average grain size was measured between 30 to 35µm.

At 700°C – 180 min of heat treatment, the recrystallized austenite grains were formed in 50% cold-rolled (Transverse Plane) with an average grain size of 3µm, and in 67% cold-rolled specimen the recrystallized austenite grains were formed in both rolling and transverse plane direction with an average grain size of around 3µm.

The completely recrystallized grain structure occurred in 25% cold-rolled specimen after heat treatment at 800°C - 60 min, the average grain size was measured at approximately around 6µm in the transverse plane (Rolling Direction).

The grain growth was observed in 67% cold-rolled specimen by increasing the annealing time at 800°C – 90 min of heat treatment but a very slow process was observed.

In a 50% cold-rolled specimen the completely recrystallized austenite grain structure was formed at a temperature of 800°C – 30 min with an average grain size of around 6µm, and the homogeneous grain growth was observed a moderate process in 50% cold-rolled specimen with long annealing time. The average grain size was increased up to 2µm at an annealing temperature of 800°C – 90 min.

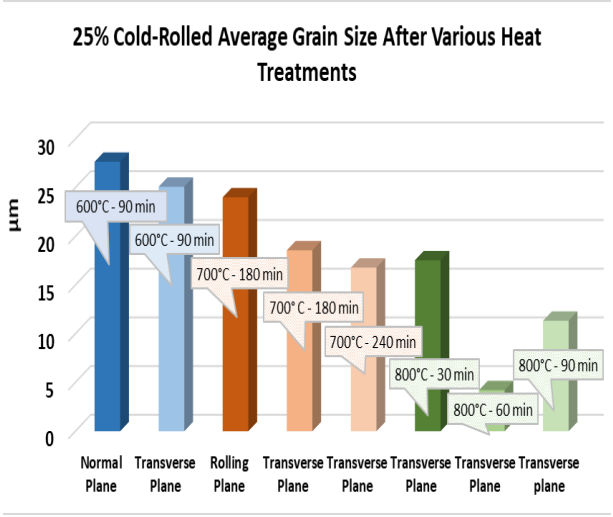

Subfigure (a). Shows the average grain size of 25% cold-rolled after various heat treatments. At 800°C – 60 min, the grain structure became fully recrystallized.

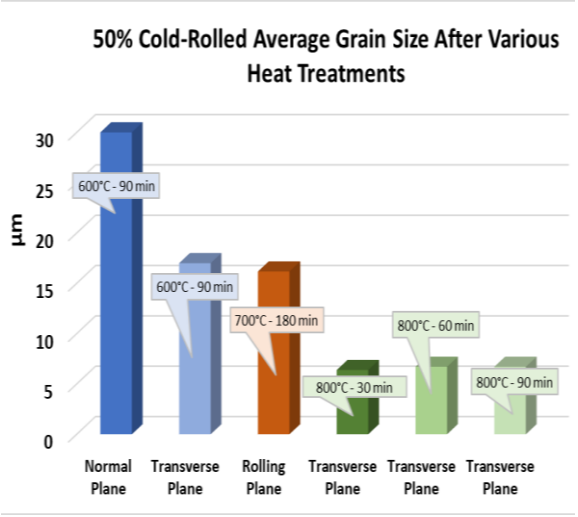

Subfigure (b). Shows the average grain size of 50% cold-rolled after various heat treatments. At 800°C – 60 min, the grain structure became fully recrystallized.

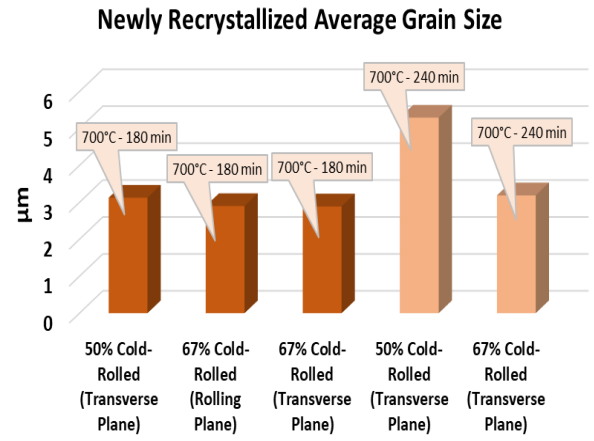

Subfigure (c). Shows the average grain size of newly recrystallized grains in the deformed region of 50% and 67% cold-rolled specimen after various heat treatments.

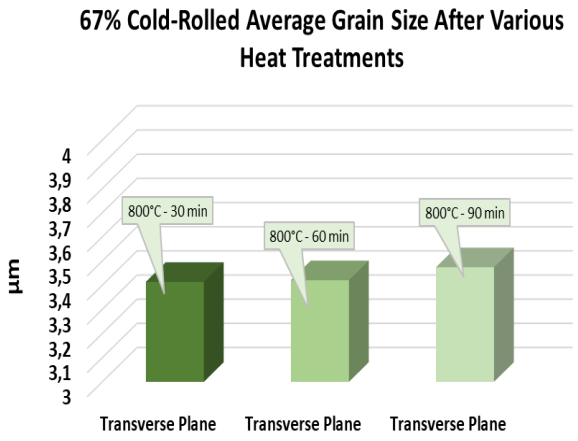

Subfigure (d). Shows the average grain size of the fully recrystallized grain structure of 67% cold-rolled specimen after various heat treatments.

Figure 22. *(a) the average grain size of 25%, (b) the average grain size of 50% and (d) 67% cold-rolled specimens after various heat treatments. The average grain size of newly recrystallized austenite grains was measured by the linear intercept method listed in subgrain (c).*

5.5 Grain Growth

5.5.1 Introduction

Generally, grain growth is defined as an increase in the average grain size in a crystal structure. The phenomenon of grain growth affects the mechanical properties of austenitic stainless steel and also revealed the behaviour of grain boundaries after heat treatment [38]. Rodrigo Pinto and co-authors [48] investigated the grain size evolution of austenitic stainless steel 304 (as-received condition) at a temperature of 1100°C with different holding times (15 to 180 min). They reported the grain growth took place slowly at a time of 15 min to 180 min, and the average grain size was measured after 60 minutes of annealing by linear intercept method around 100 ±19µm and after 180 minutes of annealing, it was measured around 120µm±24µm. They have also reported some abnormal grain growth in the specimens annealed at (1100°C – 30 min). Shirdel and co-authors [49] studied the grain growth behaviour of 304L at a wide range of temperature from (800°C to 1200°C), the average grain size of the as-received sample in the initial condition was measured by the linear intercept method around 20µm. At an annealing temperature of 800°C, they have not found any evidence of grain growth but at 900°C with a longer annealing time of 4 hours, significant grain growth was detected due to the synergic effect of heating time and temperature. The grain growth temperature at 1000°C with 4 hours annealing time and 1150°C heating temperature with 2 hours annealing time, equally distributed grain size was reported in their study. At a temperature of 1200°C, the abnormal grain growth was detected after 4 hours of annealing and the size of the larger grain was 300 times bigger than in the initial condition. Tikhonova and co-authors [50] examined the grain growth of recrystallized austenitic stainless steel 304-type with an average grain size of 7µm from a temperature of (800°C) with time frames 30 to 120 minutes. At 30 minutes of annealing, the grain size increases up to 0.78 µm and by the increase of annealing time to 2 hours, the grain size increases further around 1.06µm. Gavard and co-authors [51] studied the grain growth phenomena of 40% cold-rolled austenitic stainless steel type

304L annealed at 1150°C for 20 minutes with water quenched. They have reported the average grain size around 80µm at a temperature of 1200°C with 60 minutes annealing time.

In the present study, to better analyse the grain growth behaviour of AISI 304L after various grain growth heat treatments, two specimens fully recrystallized 800°C – 60 min 50% cold-rolled average grain size 6µm and as-received plate with an average grain size of 30µm in the initial condition were chosen. The heat treatment plan for grain growth of recrystallized 50% cold-rolled and as-received plate listed below in Table 9.

Table 9. *The heat treatment plane for grain growth.*

Samples	**Temperature (°C)**	**Time (minutes)**									
		2	**5**	**7**	**10**	**15**	**30**	**45**	**60**	**90**	**120**
As-received condition (30µm)	1200		x		x	x	x	x	x		
	1100	x	x	x	x		x		x		
	1000	x	x	x	x		x		x		
50% colled-rolled and recrystallized at 800°C – 60 minutes (6µm)	1200		x		x	x	x	x	x		
	1100	x	x	x	x		x		x		
	1000	x	x	x	x		x		x		
	900		x		x		x		x	x	x

The average recrystallized grain size of 50% cold-rolled heat-treated at 800°C – 60 min was measured by the linear intercept method around 6 µm and the average grain size of the as-received plate in initial condition was measured around 30µm. Two methods; the traditional one linear intercept and the newly developed image processing model have been used to measure the average austenite grain size.

The randomly selected light optical microscope (LOM) images of various heat treatment were used to analyse the grain growth. The austenite grain size was measured and evaluated using the average grain size measurement by the linear intercept method through software ImageJ. To obtain an average grain size distribution and maintained the accuracy in the result, a minimum of 200 austenite grains were measured for each specimen.

5.5.2 Grain size distribution by Image Processing Program

To measure and evaluate the grain size the MatLab facilities used to convert the light optical microscope (LOM) images into artificial crystallographic orientation map (COM) data, an image processing routine was programmed by supervisor M. Nasiri.

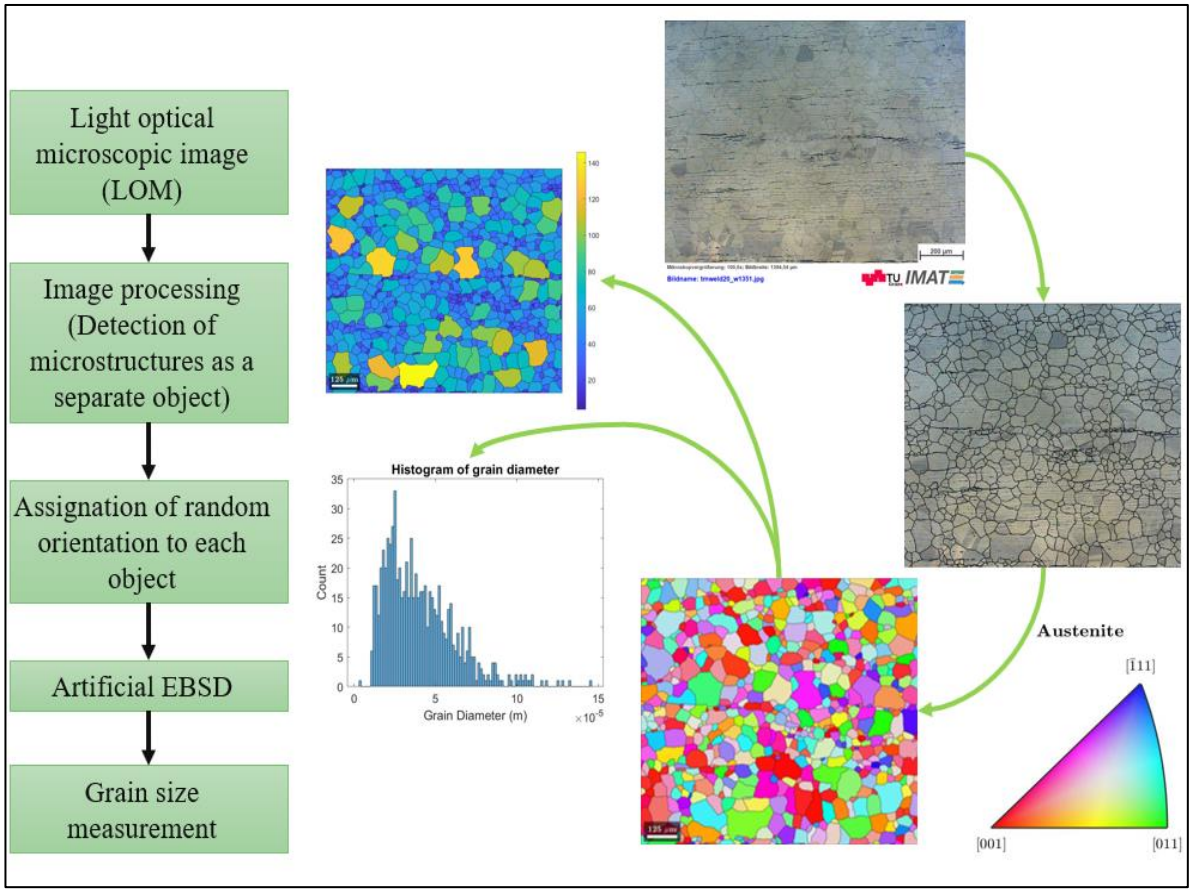

Figure 23. *Flowchart and procedure of grain size measurement by Image processing model developed by supervisor M. Nasiri.*

As shown in Figure 23, the grain boundaries in the LOM image are detected after filtering and sharpening then the grains are constructed by tracing the grain boundaries. The routine identifies each grain as an individual object and assigns a random orientation to each object and produces an artificial COM data file. Using the MatLab scripts. The size of each grain is calculated and those data can be exported as an Excel or MatLab file.

Figure 24(a) shows the initial microstructure of as-received AISI 304L and is the same picture after image processing. The last picture of the right-hand side shows the grain diameter distribution.

Figure 24(b) shows the initial microstructure of AISI 304L after cold rolling with 50% deformation and recrystallization heat treatment for 800°C - 60 min. Depicts the LOM picture after image processing and the last picture of the right-hand side shows the grain diameter distribution.

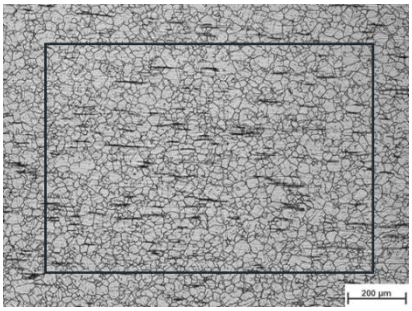

24 (a). The microstructure of the as-received specimen in the initial condition.

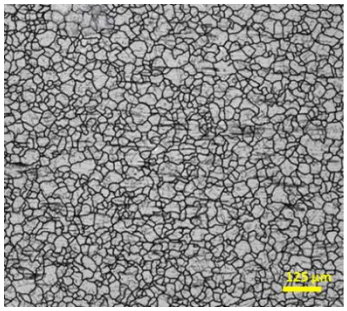

The same picture after image processing.

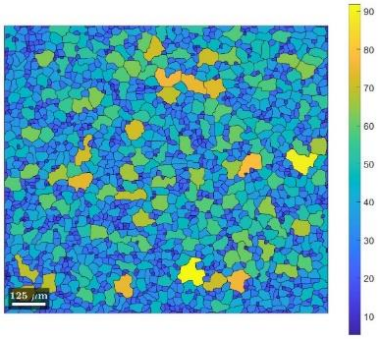

Shows the grain diameter distribution.

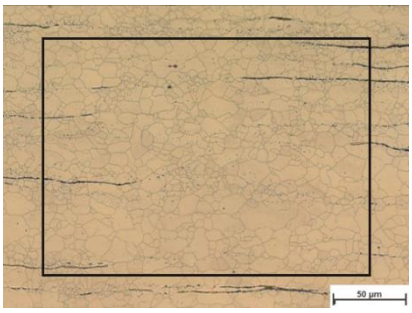

24 (b). LOM image of recrystallized 50% cold rolling reduction.

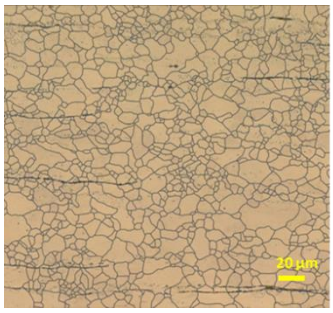

Processed LOM image of recrystallized 50% cold-rolled.

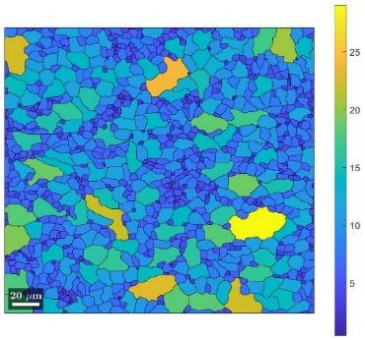

Grain diameter distribution by artificial EBSD map.

Figure 24. *The LOM and image processing program results of the as-received plate (a) and recrystallized 50% cold-rolled figures (b), Processed LOM image figures, and the last picture of the right-hand side shows the Grain diameter distribution figures.*

5.5.3 Average Grain size measurement

The average austenite grain size is increasing as a function of annealing temperature and time. To determine the average grain size of different heat treatments, the recrystallized 50% cold-rolled (average grain size 6µm) was placed for an annealing temperature at 900°C with different holding times, the average grain size grew with increasing the annealing time, the normal grain growth was observed but it was a very slow process. The total average grain size was measured 21µm at a temperature of 900°C for 120 minutes. The as-received and recrystallized 50% cold-rolled specimens were placed for further grain growth heat treatment at 1000°C with different holding times, normal austenite grain growth was observed in both specimen as shown in Figure 25(a) and (b). The average grain size of the as-received specimen remains stable and it was measured 30µm by the linear intercept method and by the image processing program was measured around 28µm as shown in Figure 25(a). The histogram shows the distribution of grain size of each temperature and time in micrometre (µm). Meanwhile, the average grain size of recrystallized 50% cold-rolled specimen was measured around 28µm by the linear intercept method and 34µm by the image processing model can be seen in Figure 25(b).

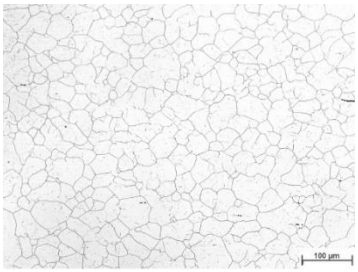

25 (a). LOM image of the as-received plate heat-treated at 1000°C – 60 min, the average austenite grain size was measured 30µm.

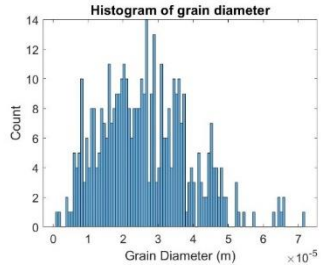

The histogram shows the distribution of grain size of the as-received plate AISI 304L.

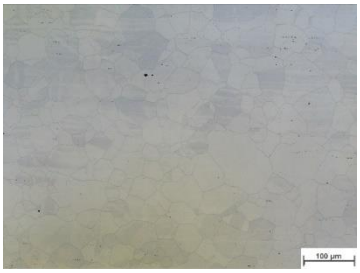

25 (b). LOM image of recrystallized 50% cold-rolled heat-treated at 1000°C – 60 min, the average grain size was measured 28µm.

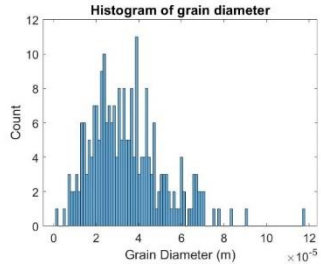

The histogram shows the distribution grain size of recrystallized 50% cold-rolled AISI 304L.

Grain growth heat treatment temperature of 1100°C, the normal grain growth was observed in the as-received and also in recrystallized 50% cold-rolled specimens as shown in Figure 25(c) and (d).

The average austenite grain size was increased in as-received plate after 60 minutes of annealing up to 50µm and the total average grain size was measured by the linear intercept method around 79µm (30µm in the beginning).

The average grain size was measured by an image processing program around 74µm shown in Figure 25(c).

Whereas in the recrystallized 50% cold-rolled specimen, the total average grain size was measured by the linear intercept method around 64µm (6µm in the beginning), and by the image processing program the average grain size was measured 59µm can be seen in Figure 25(d).

At a temperature of 1200°C, the abnormal grain growth of some grains was observed in both specimens and it can be seen in Figure 25(e) and (f).

The average grain size of the as-received condition was increased up to 86µm after 60 minutes of heating and measured by the linear intercept method and by image processing program, the total average grain size of the as-received plate was measured 81µm as shown in Figure 25(e).

Thus, the average grain size of recrystallized 50% cold-rolled specimen was counted 84µm by the linear intercept method and the average grain size was measured by the image processing program around 81µm can be seen in Figure 25(f).

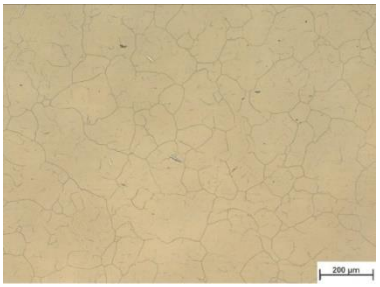

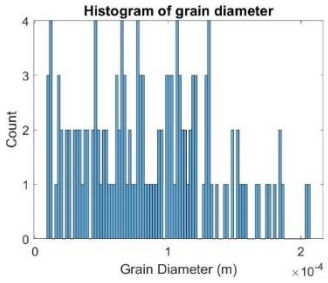

25 (c). LOM image of the as-received plate heat-treated at 1100°C – 60 min, the average austenite grain size was measured at 64µm.

The histogram shows the distribution of grain size of the as-received plate AISI 304L.

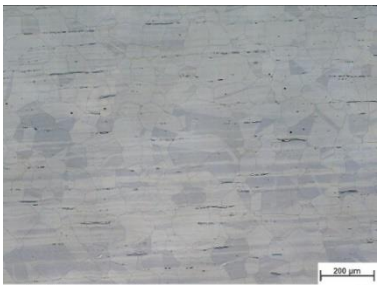

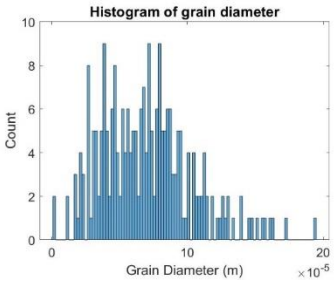

25 (d). LOM image of recrystallized 50% cold-rolled heat-treated at 1100°C – 60 min, the average grain size was measured 59µm.

The histogram shows the distribution of grain size of recrystallized 50% cold-rolled AISI 304L.

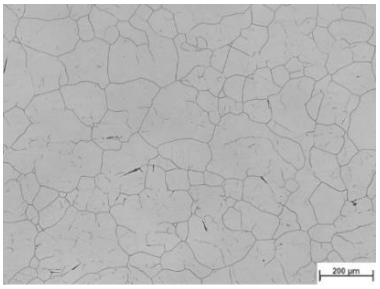

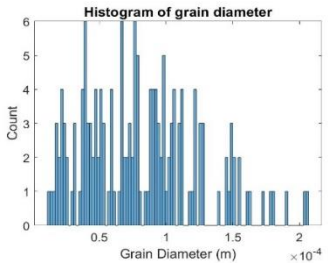

25 (e). LOM image of as-received plate heat-treated at 1200°C – 60 min, the average grain size was measured 84µm.

The histogram shows the distribution of grain size of the as-received plate AISI 304L.

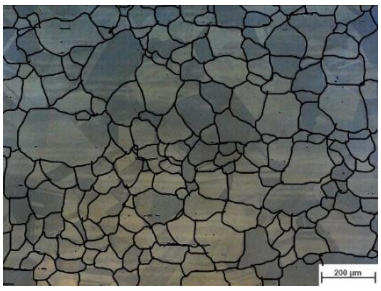

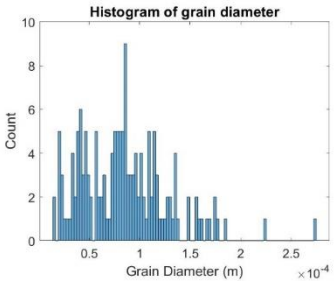

25 (f). LOM image of recrystallized 50% cold-rolled heat-treated at 1200°C – 60 min, the average grain size was measured 81µm.

The histogram shows the distribution of grain size of recrystallized 50% cold-rolled AISI 304L.

Figure 25. *The grain size distribution by image processing programme and linear intercept method at different temperature and holding times (figure a to f).*

The trend of grain growth in recrystallized 50% cold-rolled specimen at a temperature of 1200°C with different time frames see in Figure 26.

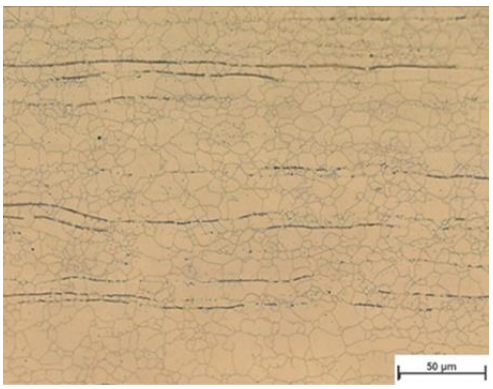

Recrystallized (6µm Grain size)

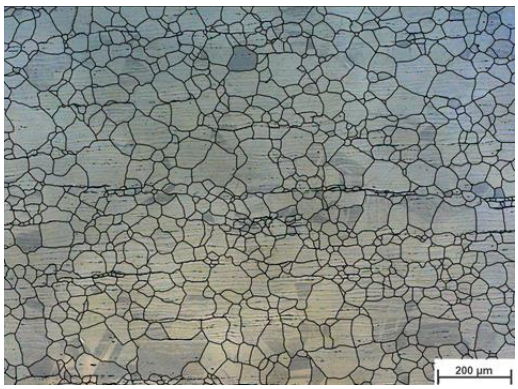

1200°C – 5 min

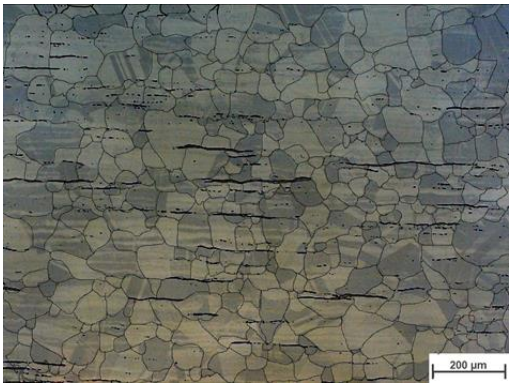

1200°C – 10 min

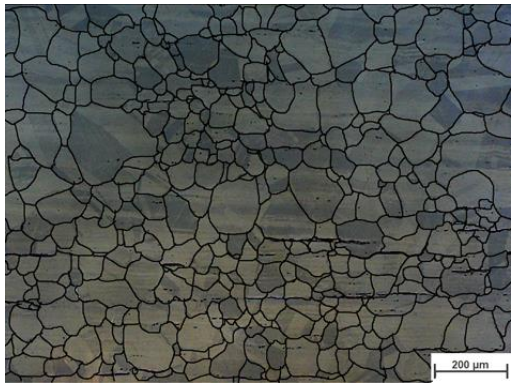

1200°C – 15 min

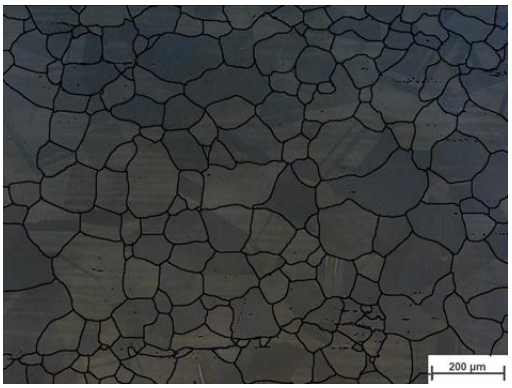

1200°C – 30 min

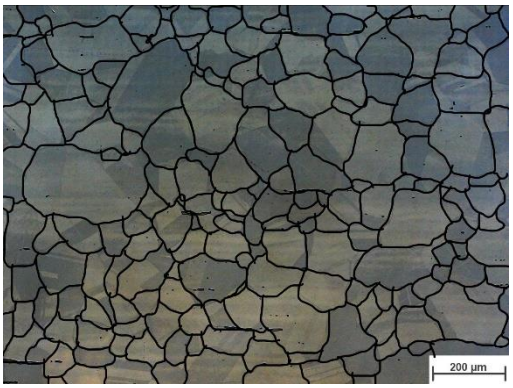

1200°C – 60 min

***Figure 26**. The trend of grain growth in recrystallized 50% cold-rolled specimen at a temperature of 1200°C.*

The Figure 27 and Figure 28 shows the grain growth in the as-received plate and recrystallized 800°C – 60 min 50% cold-rolled at various temperature. At a temperature of 1100°C, the grain growth is a fast process in the beginning in both specimens but by increasing the time of annealing, the grain growth slows down. At a temperature of 1200°C, the grain growth was observed a fast process from the initial to the final heating time (5 min to 60 min) in both specimens.

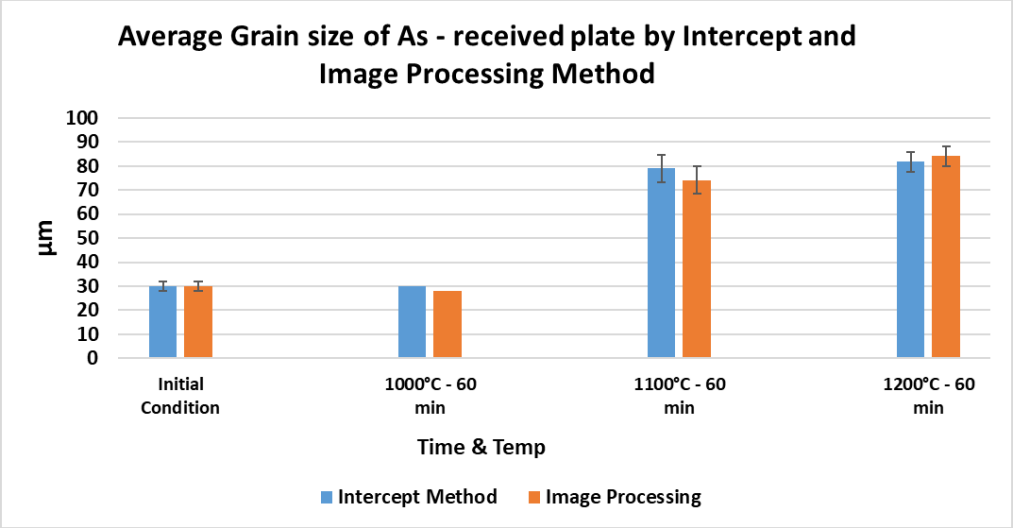

Figure 27. *Shows comparison of average grain size measurement by the linear intercept and image processing program of the as-received plate at various temperature and time.*

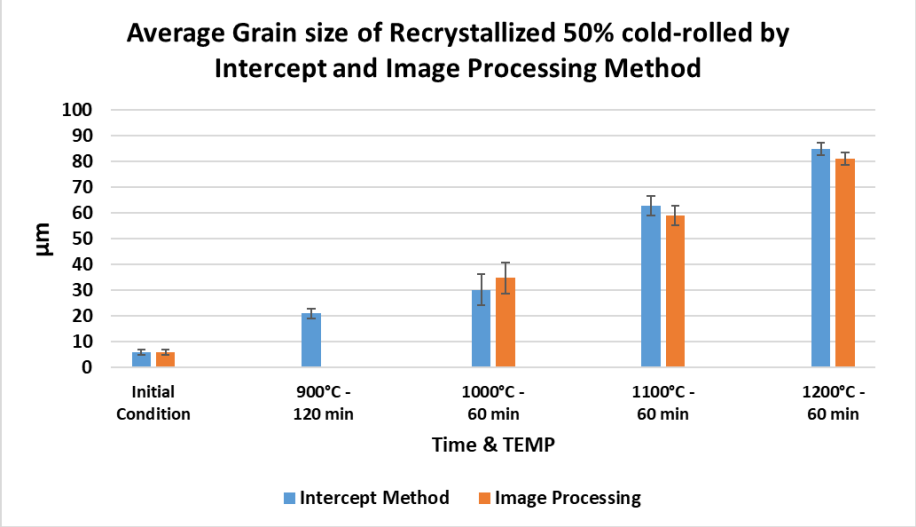

Figure 28. *Shows comparison of average grain size measurement by the linear intercept and image processing program of the recrystallized 50% cold-rolled specimen at various temperature and time.*

5.5.4 Development of Grain size

The error bars in the micrographs show the standard deviation from the mean value. In each sample there are plenty of grains, the mean value is the mean grain diameter of all of them. The deviation is calculated according to the difference between the mean value and size of each grain. Figure 29 shows the grain diameter as a function of heat treatment time at 1200°C along with the processed LOM pictures of the heat-treated samples. As shown in Figure 29, the grain diameter increases rapidly in the early stages of heat treatment and reaches around 81µm after 60 minutes.

Figure 30 shows the result of the same heat treatment applied to samples with an initial grain diameter of 28µm. The grain growth at the beginning is fast and it gets slower by increasing the time of the heat treatment and reaches 84µm after 60 minutes.

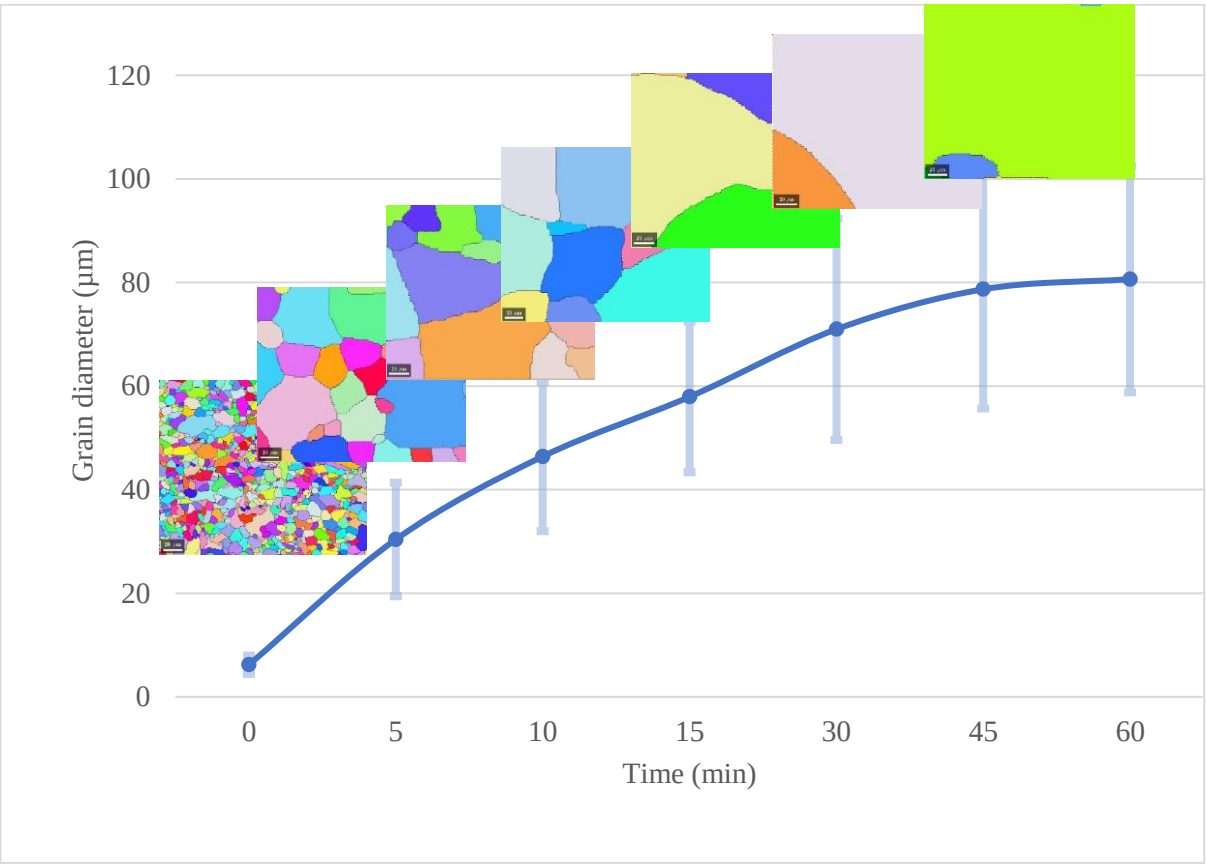

Figure 29. *Grain diameter evolution during isothermal heat treatment of the sample recrystallized 50% cold-rolled with an initial grain diameter of 6µm at 1200°C.*

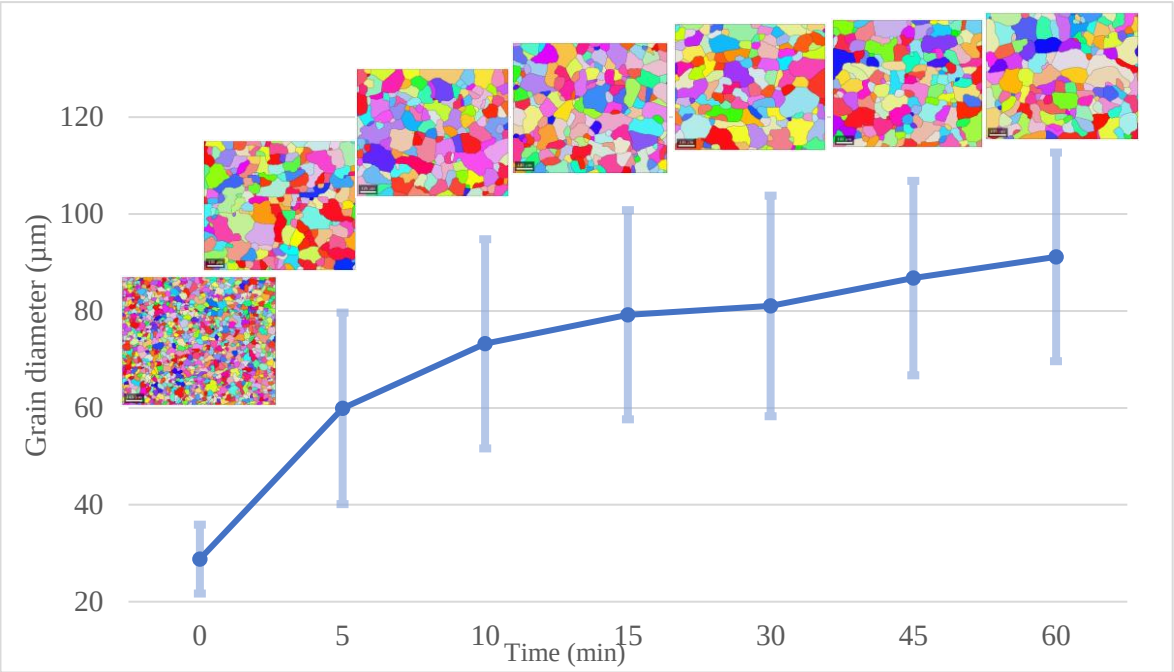

Figure 30. *Grain diameter evolution during isothermal heat treatment of the sample as-received condition with an initial grain diameter of 28µm at 1200°C.*

Figure 31 shows the grain evolution at 1100°C together with the processed LOM pictures of the heat-treated samples with an initial grain size of 6µm which increases up to 60µm after 60 minutes at 1100°C.

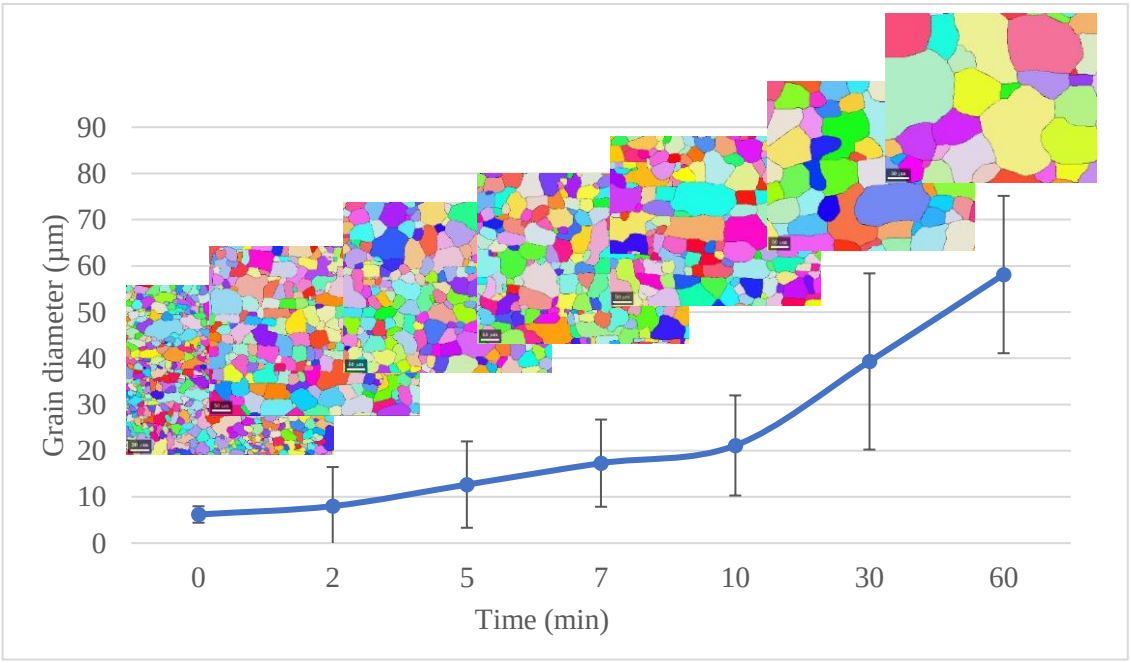

Figure 31. *Grain diameter evolution during isothermal heat treatment of the sample recrystallized 50% cold-rolled with an initial grain diameter of 6µm at 1100°C.*

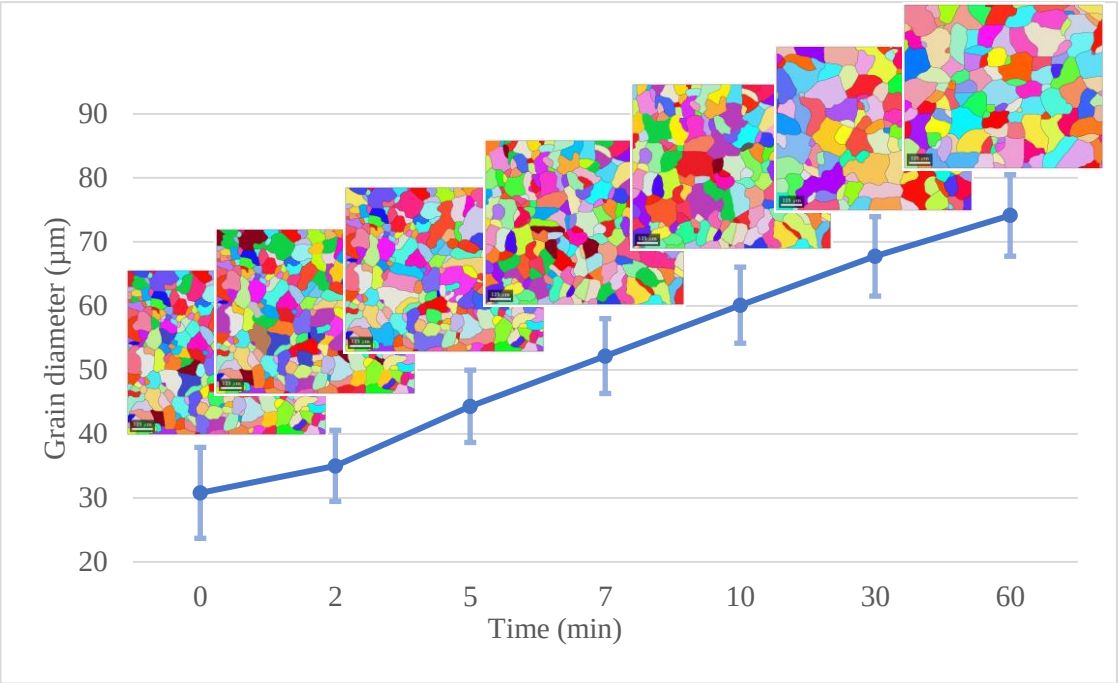

Figure 32. *Grain diameter evolution during isothermal heat treatment of the sample as-received condition with an initial grain diameter of 30µm at 1100°C.*

Figure 32 depicts the grain diameter changes by heat treatment at 1100°C. The grain growth at 1100°C is slower than that observed at 1200°C shown in Figure 30.

The mean grain diameter after 60 minutes of heat treatment is around 74µm while the grain diameter was around 30µm in the beginning.

Figure 33 and Figure 34, shows the grain diameter evolution during the isothermal heat treatment at 1000°C for samples with the initial grain diameter of 6µm and 28µm respectively.

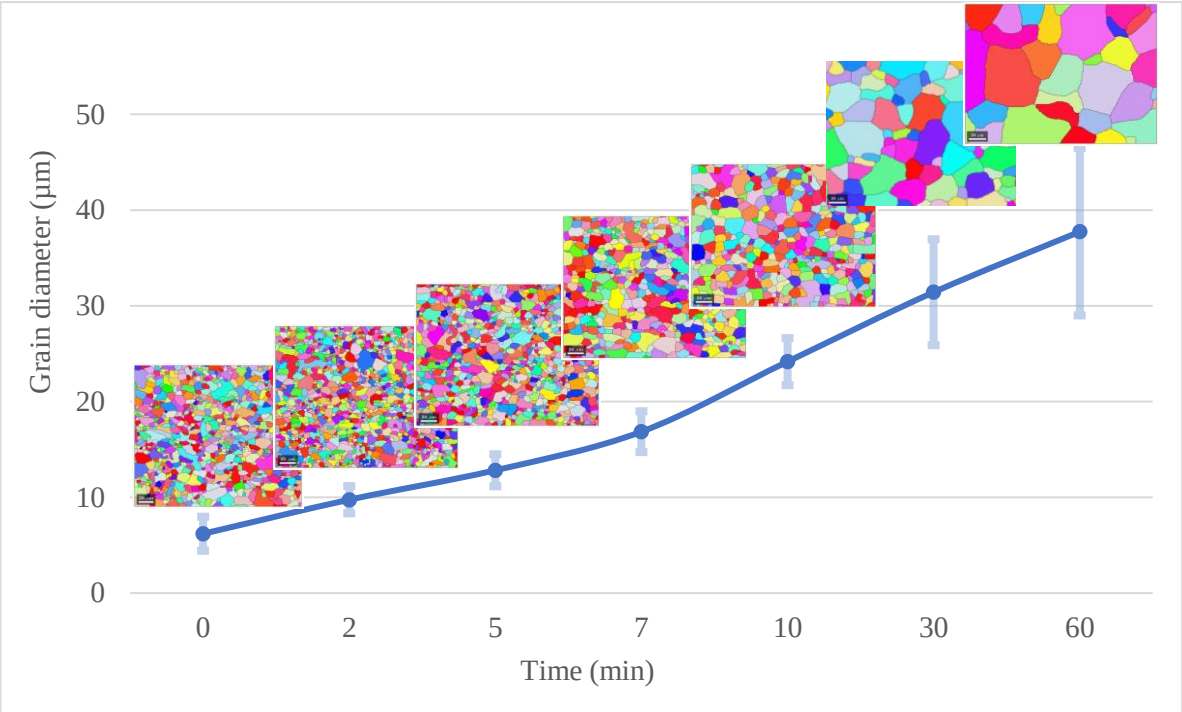

Figure 33. *Grain diameter evolution during isothermal heat treatment of the sample recrystallized 50% cold-rolled with an initial grain diameter of 6µm at 1000°C.*

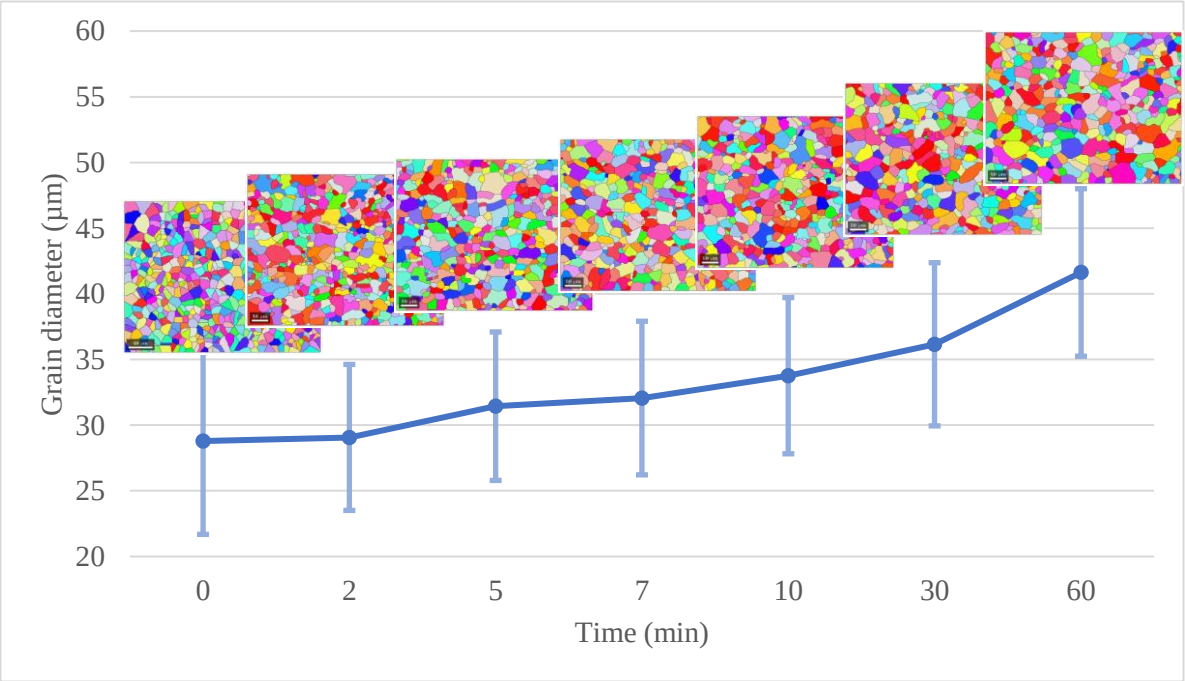

Figure 34. *Grain diameter evolution during isothermal heat treatment of the sample as-received condition with an initial grain diameter of 28µm at 1000°C.*

5.6 Vickers Hardness Test

Three hardness Vickers measurements were conducted for each specimen at the borders and the middle of each mounted sample. The Vickers hardness response of the samples in the initial condition is shown in Figure 35.

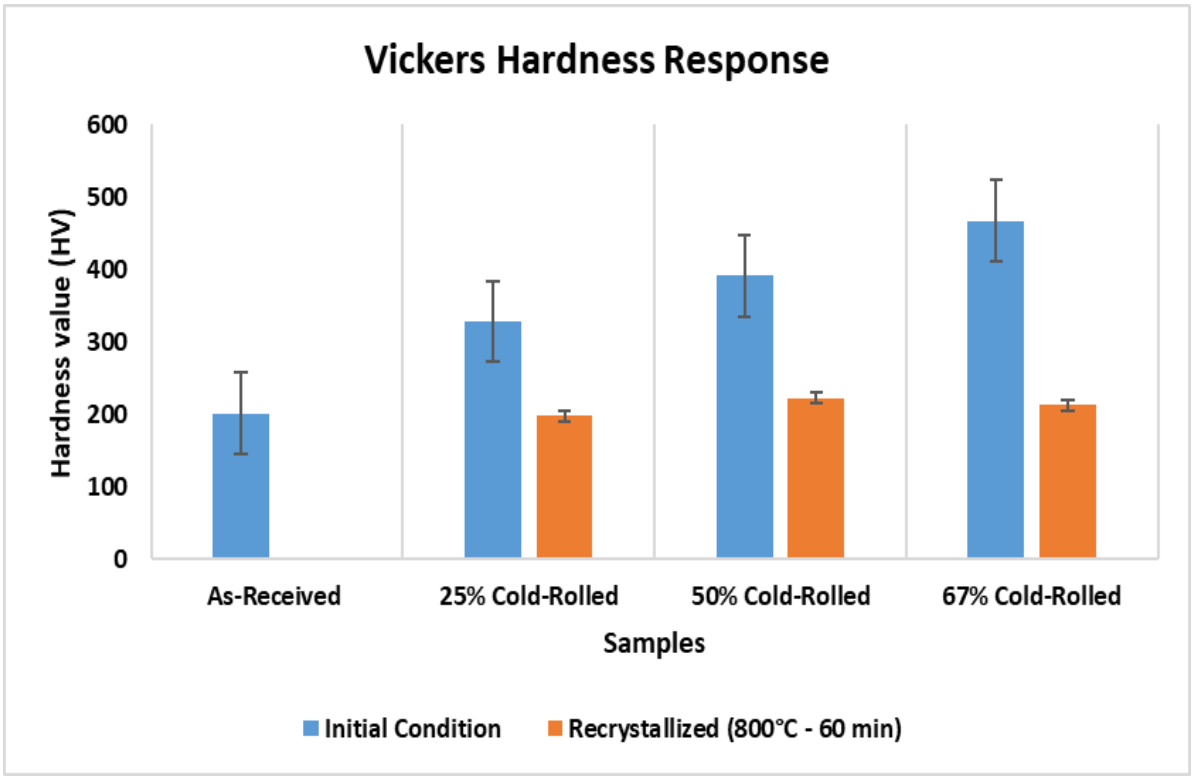

Figure 35. *Comparison of Vickers hardness results between the specimens in the initial condition and recrystallized at 800°C – 60 min (6µm).*

The cold-rolled specimens contain a high value of hardness in the initial condition due to the presence of deformation-induced martensite (DIM) by cold rolling. After various reversion treatments, the value of hardness decreases in the cold-rolled specimens and improving the mechanical properties such as tensile strength, yield strength and toughness.

The recrystallized specimens have more or less the same hardness values as in the as-received plate in the initial condition as shown in Figure 36.

The comparison of hardness values of grain growth specimens including the as – received plate (initial grain size 30µm) and recrystallized 800°C – 60min 50% cold-rolled (initial grain size 6µm) as shown in Figure 36. The average grain size is inversely proportional to the hardness value.

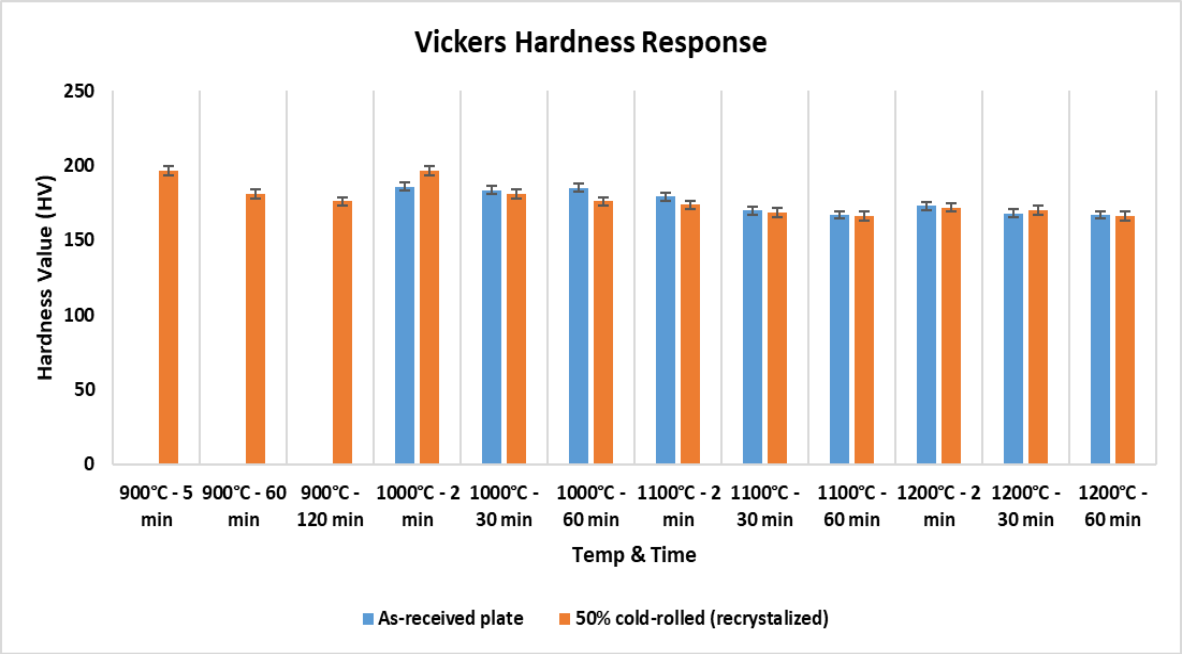

Figure 36. *Comparison of Vickers hardness value between the as-received plate (initial grain size 30µm) and 50% cold-rolled recrystallized at 800°C – 60 min (initial grain size 6µm) after various grain growth heat treatment.*

6 Summary

The behaviour of cold-rolled deformed metastable austenitic stainless steel 304L was investigated through various heat treatments.

- To determine the kinetics of reversion transformation of deformation-induced martensite (DIM).
- The impact of time and temperature on the occurrence of recrystallization in the different cold-rolled deformed specimens such as 25%, 50% and 67%.
- The effect of heating rate and time on the austenite grain growth after recrystallization and as – received condition.

The cold-rolled deformed specimens contain deformation-induced martensite (DIM) and DIM consist of a ferromagnetic (α´- martensite) and paragenetic (ε-martensite) phase.

The specimens were analysed using the magnetic induction device Ferritscope to obtain the value of magnetic phases (δ - ferrite and α´- martensite). At least 60 to 100 readings were taken in each case from the different point areas (borders and middle), and different planes such as a normal, rolling and transverse plane.

The microstructural studies of AISI 304L were conducted with the help of light optical (LOM), Scanning electron microscope (SEM), Electron backscatter diffraction (EBSD) and X-ray diffraction (XRD). The XRD test has been conducted to confirm the existing phases in the cold-rolled deformed specimen.

The reversion annealing of DIM was performed in this study in a temperature range of 600°C to 800°C with different time frames.

The as-received plate with an average grain size of 30µm in the initial condition and recrystallized 800°C – 60 min 50% cold-rolled with average grain size 6µm were chosen for austenite grain growth heat treatment with a temperature range of 900°C to 1200°C with different holding times.

6.1 Conclusion

The calibrated device Ferritscope confirmed, that the as-received plate contains approximately 3% δ-ferrite in the initial condition due to solidification. The cold-rolled specimens contain additionally the magnetic phase α´-martensite. The amount of α´-martensite increase due to the increase of cold rolling deformation. Therefore 67% of cold-rolled specimen contained more α´- martensite than 25% cold-rolled. The result of x-ray diffraction (XRD) showed some ε –martensite in the 25% cold-rolled deformed AISI 304L in the initial condition.

After reversion annealing at 600°C, the light optical microscope (LOM) result did not show significant evidence of reversion of deformation-induced martensite (DIM) while Ferritscope gave evidence of decreasing of magnetic phases at this temperature. At a temperature of 700°C – 180 min, Ferritscope and LOM results gave strong evidence of reversion of α´-martensite but ε –martensite remained stable in 25% and 50% cold-rolled specimen whereas 67% cold-rolled became completely recrystallized at this temperature and time. At the same temperature 700°C with a longer annealing time of 240 min, the electron backscatter diffraction (EBSD) and LOM image processing phase fraction results confirmed the reversion of ε –martensite to the parent austenite phase. The reversion process of DIM was observed very slow at a temperature range of 600°C to 700°C in 25% and 50% cold-rolled specimens, and at 700°C - 180 min very tiny recrystallized strain-free austenite grains were formed in the deformed region of 50% cold-rolled specimen. The reversion of DIM was observed to be a fast process at a temperature of 800°C, after 60 minutes of annealing the 25% and 50% cold-rolled specimens became fully recrystallized with an average grain size of 6µm. Figure 37 gives the detailed results of reversion of DIM at different temperature and times in 25%, 50% and 67% cold-rolled specimens.

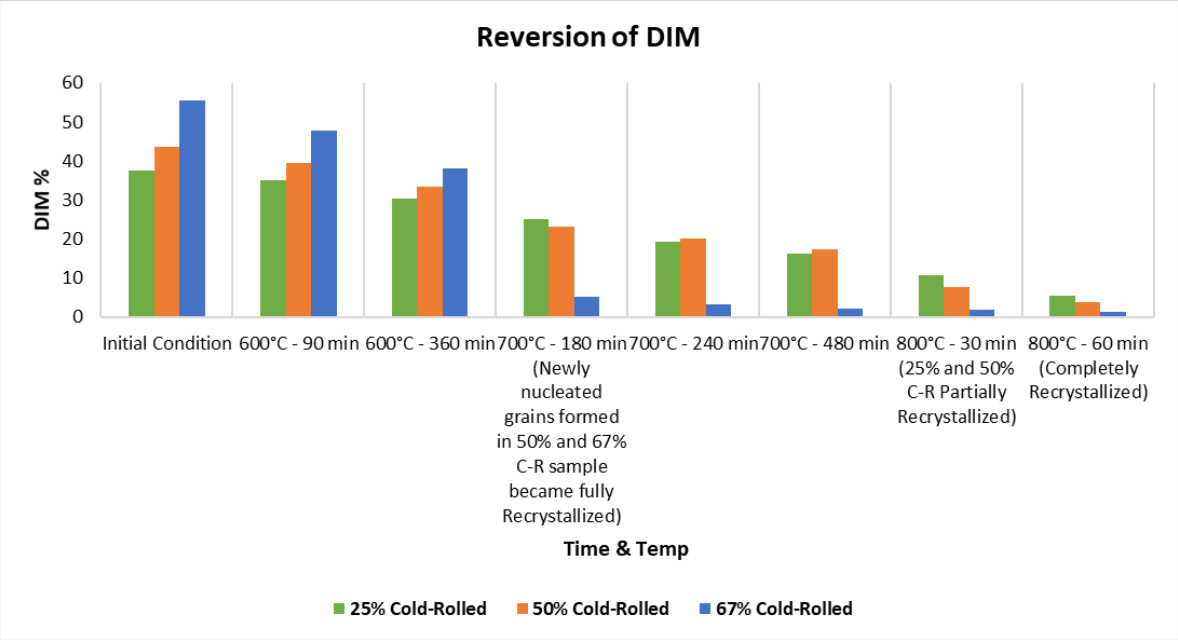

Figure 37. *Shows the reversion of deformation-induced martensite (DIM) at different temperatures and time in 25%, 50% and 67% cold-Rolled (C-R) specimens.*

The austenite grain growth was observed very slow process in recrystallized 50% cold-rolled specimen at a temperature of 900°C and 1000°C, while in as-received specimen austenite grain growth was not observed and average grain size remained stable at 30µm. At a temperature of 1100°C, the grain growth was experienced as a fast process in the beginning but with a long annealing time, the grain growth slows down. The average grain size of as-received was measured 79µm and recrystallized 50% cold-rolled was measured 64µm after 60 minutes of annealing at 1100°C. The austenite grain growth was observed as a fast process from the beginning of annealing in both specimens at a temperature of 1200°C. The average grain size was measured in as-received condition after 60 minutes of annealing time at 1200°C 86µm (30µm was in the initial condition), and the average grain size of recrystallized 50% cold-rolled was measured 81µm (6µm was at the beginning of annealing).

Figure 38, shows the tendency of grain growth in the as-received plate (initial grain size 28µm) at a temperature range of 1000°C to 1200°C with different holding times from (2 min to 60 min). The average grain size was measured by an image processing program. Figure 39, shows the tendency of grain growth in the 50% cold-rolled

recrystallized at 800°C – 60 min (initial grain size 6µm) at a temperature range of 900°C to 1200°C with different holding times from (2 min to 60 min). The average grain size was measured by an image processing program.

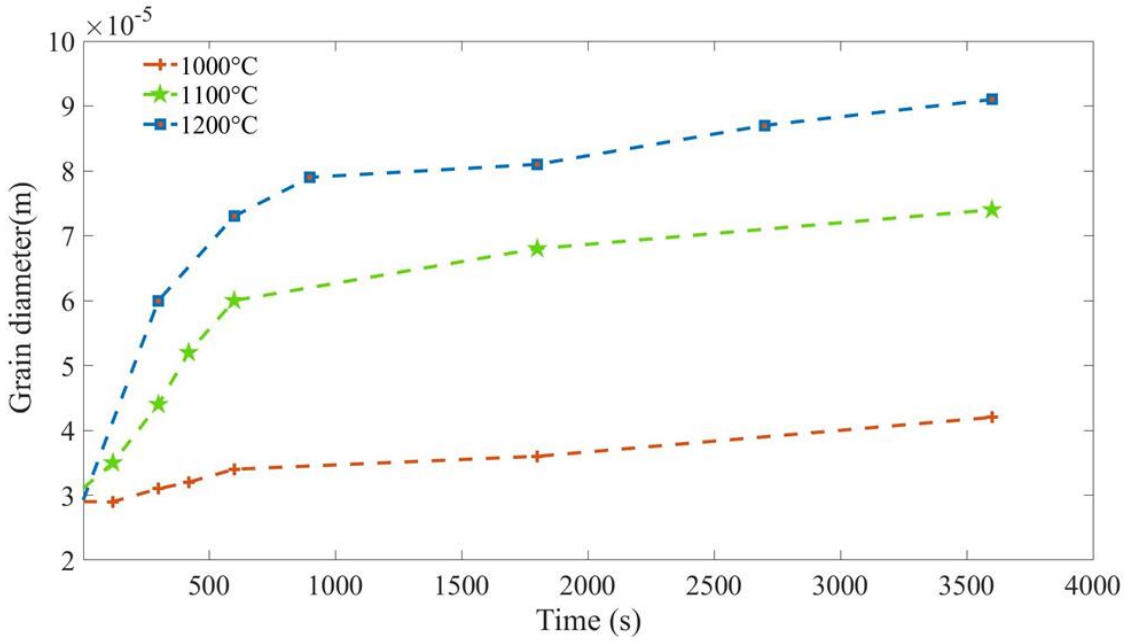

Figure 38. *The tendency of grain growth in the as-received plate was measured by an image processing program at the temperature range of 1000°C to 1200°C at different holding times from (2 min to 60 min).*

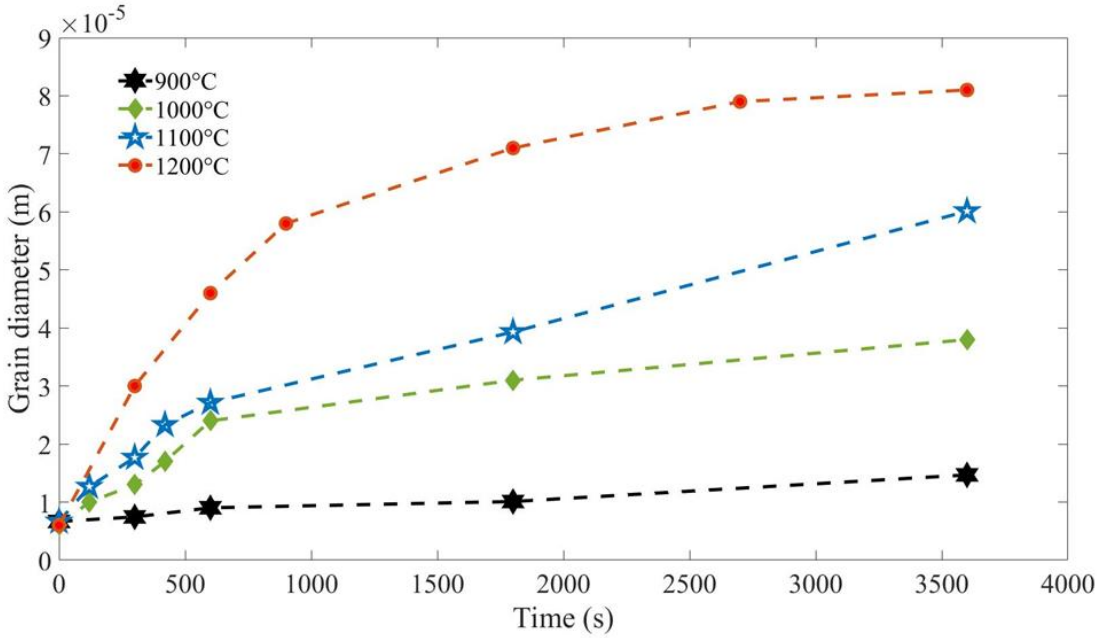

Figure 39. *The tendency of grain growth in the sample 50% cold-rolled recrystallized at 800°C – 60 min (6µm) was measured by an image processing program at the temperature range of 900°C to 1200°C at different holding times from (2 min to 60 min).*

6.2 Outlook

In order to measure the magnetic phases (α´-martensite and δ – ferrite) in the cold-rolled deformed austenitic stainless steels (ASSs), the magnetic induction device Ferritscope is considered a reliable measuring method. The device should be calibrated before employed to the specimens, and to maintain the accuracy in the result at least 40 to 80 readings have to be taken from different areas of the specimen.

Due to resemblance in the texture of deformation-induced martensite (DIM) phases α´and ε- martensite, the light optical microscope (LOM) does not distinguish the two phases. Therefore, electron backscatter diffraction (EBSD) and x-ray diffraction are reliable techniques to evaluate the DIM phases in the plastically deformed material.

The presence of ε – martensite in the plastically deformed ASSs still debatable, due to cold deformation and the existence of high residual stresses it is very difficult to identify the actual amount of ε – martensite by EBSD and XRD test.

To measure the average grain size the linear intercept method is considered time-consuming and needs to count a minimum of 100 to 150 intersects point to meet the accuracy in the final result. While an image processing program is less time consuming providing the detailed results of each grain diameter and average grain size within a few minutes. The image processing program recognises each grain as a single object.

7 Bibliography

[1] Outokumpu, Handbook of Stainless Steel, (2013) 1–29. http://www.outokumpu.com/sitecollectiondocuments/outokumpu-stainless-steel-handbook.pdf.

[2] The Stainless Steel Family – An Overview | Campbell Tip of the Month, (n.d.). http://www.jmcampbell.com/tip-of-the-month/2013/10/the-stainless-steel-family-an-overview/ (accessed October 28, 2020).

[3] R. Nilsson, Experimental Methodologies for Analyzing Austenite Recrystallization in Martensitic Tool Steels, (2015). urn:nbn:se:kth:diva-176091.

[4] M. Shirdel, H. Mirzadeh, M.H. Parsa, Nano/ultrafine grained austenitic stainless steel through the formation and reversion of deformation-induced martensite: Mechanisms, microstructures, mechanical properties, and TRIP effect, Mater. Charact. 103 (2015) 150–161. https://doi.org/10.1016/j.matchar.2015.03.031.

[5] A.F. Padilha, R.L. Plaut, P.R. Rios, Annealing of Cold-Worked Austenitic Stainless Steels, ISIJ Int. Vol.43 (20 (2007) 91406.

[6] M. Odnobokova, A. Belyakov, N. Enikeev, D.A. Molodov, R. Kaibyshev, Annealing behavior of a 304L stainless steel processed by large strain cold and warm rolling, Mater. Sci. Eng. A. 689 (2017) 370–383. https://doi.org/10.1016/j.msea.2017.02.073.

[7] A. Järvenpää, M. Jaskari, A. Kisko, P. Karjalainen, Processing and properties of reversion-treated austenitic stainless steels, Metals (Basel). 10 (2020). https://doi.org/10.3390/met10020281.

[8] K. Tomimura, S. Takaki, Y. Tokunaga, Reversion Mechanism from Deformation Induced Martensite to Austenite in Metastable Austenitic Stainless Steels, ISIJ Int. 31 (1991) 1431–1437. https://doi.org/10.2355/isijinternational.31.1431.

[9] A. Kisko, Microstructure and properties of Reversion Treated Low-Ni High-Mn Austenitic Stainless Steels, university of OULU, 2016.

[10] M.R.B. A.Dehghan-Manshadi, Recrystallization and Grain Growth IV, Mater. Sci. Forum. 715–716 (2012). https://doi.org/10.1201/9780429265587-18.

[11] M. Vasudevan, P. Palanichamy, Characterization of microstructural changes during annealing of cold worked austenitic stainless steel using ultrasonic velocity measurements and correlation with mechanical properties, J. Mater. Eng. Perform. 11 (2002) 169–179. https://doi.org/10.1361/105994902770344231.

[12] Y. Jin, M. Bernacki, G.S. Rohrer, A.D. Rollett, B. Lin, N. Bozzolo, Formation of annealing twins during recrystallization and grain growth in 304L austenitic

stainless steel, Mater. Sci. Forum. 753 (2013) 113–116. https://doi.org/10.4028/www.scientific.net/MSF.753.113.

[13] K.H. Lo, C.H. Shek, J.K.L. Lai, Recent developments in stainless steels, Mater. Sci. Eng. R Reports. 65 (2009) 39–104. https://doi.org/10.1016/j.mser.2009.03.001.

[14] H.M. Cobb, Steel Products Manual: Stainless Steels, The Iron & Steel Society, Warrendale, Pennsylvania, 1999.

[15] A. Aletdinov, S. Mironov, G.F. Korznikova, T. Konkova, R.G. Zaripova, M.M. Myshlyaev, S.L. Semiatin, Martensite-to-Austenite Reversion and Recrystallization in Cryogenically-Rolled Type 321 Metastable Austenitic Steel, Metall. Mater. Trans. A Phys. Metall. Mater. Sci. 50 (2019) 1346–1357. https://doi.org/10.1007/s11661-018-5070-9.

[16] S. Park, Measurement of Acoustic Nonlinearity in Cold-Rolled and Heat-treated 304 Austenitic Stainless Steel using Nonlinear Ultrasound, (2019) 1–56.

[17] J. Liu, Deformation Induced Martensitic Transformation In 304 Stainless Steels, (2016) 1–79.

[18] P. Lambert, Sustainability of metals and alloys in construction, Woodhead Publishing Limited, 2009. https://doi.org/10.1533/9781845695842.148.

[19] M.B. Cortie, History and development ot ferritic stainless steels, J. S. Afr. Inst. Min. Met. 93 (1993) 165–176.

[20] J.M. Alves, L.P. Brandão, A. Dos Santos Paula, Mechanically induced martensitic transformation of hot rolled and annealed 304L austenitic stainless steel at room and cryogenic temperatures, Mater. Res. 22 (2019) 6–10. https://doi.org/10.1590/1980-5373-MR-2019-0150.

[21] D. Maréchal, Linkage between mechanical properties and phase transformations in a 301LN austenitic stainless steel, (2011) 228. https://open.library.ubc.ca/media/stream/pdf/24/1.0071814/1.

[22] M. Naghizadeh, H. Mirzadeh, Modeling the kinetics of deformation-induced martensitic transformation in AISI 316 metastable austenitic stainless steel, Vacuum. 157 (2018) 243–248. https://doi.org/10.1016/j.vacuum.2018.08.066.

[23] R. Naraghi, A. Borgenstam, Martensitic Transformation in Austenitic Stainless Steels Reza Naraghi, (2016).

[24] P.K. Mallick, Strain induced martensite and its reversion in 304 stainless steel, (2017) 169.

[25] F. Haeßner, R.L. Plaut, A.F. Padilha, ric Measurements, 43 (2003) 1472–1474.

[26] E. Dryzek, M. Sarnek, M. Wróbel, Reverse transformation of deformation-induced martensite in austenitic stainless steel studied by positron annihilation,

J. Mater. Sci. 49 (2014) 8449–8458. https://doi.org/10.1007/s10853-014-8555-y.

[27] R. F.J. Humphreys, M. Hatherly Annealing, Recrystallization and Related Annealing Phenomena, Second, Elsevier, 1995. https://doi.org/10.1016/C2009-0-07986-0.

[28] B. Radhakrishnan, G.B. Sarma, T. Zacharia, Modeling the kinetics and microstructural evolution during static recrystallization - Monte Carlo simulation of recrystallization, Acta Mater. 46 (1998) 4415–4433. https://doi.org/10.1016/S1359-6454(98)00077-9.

[29] H. Tripathy, S. Vidhyashree, C. Sudha, S. Raju, Kinetics of static recrystallization and strain induced martensite formation in low carbon austenitic steels using impulse excitation technique, Mater. Today Proc. 27 (2019) 1962–1966. https://doi.org/10.1016/j.matpr.2019.09.037.

[30] C.R. Rehrl, The microstructural break down : the effect of, (2011).

[31] R.L. Goetz, V. Seetharaman, Static recrystallization kinetics with homogeneous and heterogeneous nucleation using a cellular automata model, Metall. Mater. Trans. A Phys. Metall. Mater. Sci. 29 (1998) 2307–2321. https://doi.org/10.1007/s11661-998-0108-z.

[32] K. Huang, Towards the modelling of recrystallization phenomena in multi-pass conditions : application to 304L steel Ke Huang To cite this version : École doctorale n ° 364 : Sciences Fondamentales et Appliquées l ' École nationale supérieure des mines de Paris Spéc, Thesis. (2012).

[33] K. Huang, R.E. Logé, A review of dynamic recrystallization phenomena in metallic materials, Mater. Des. 111 (2016) 548–574. https://doi.org/10.1016/j.matdes.2016.09.012.

[34] T.H.E.R.M.O.M.E.C.H.A.N.I.C.A.L.P.R.O.C.E.S.S.I.N.G. Of, FERRITIC STAINLESS STEEL BY PAUL RICHARDS , B . Sc . (ENG) A Thesis Submitted For The Degree Of Doctor Of Philosophy- University of London John Percy Research Group Department of Metallurgy and Materials Science Royal School of Mines Imperial College of, (1984).

[35] A. Dehghan-Manshadi, M.R. Barnett, P.D. Hodgson, Recrystallization in AISI 304 austenitic stainless steel during and after hot deformation, Mater. Sci. Eng. A. 485 (2008) 664–672. https://doi.org/10.1016/j.msea.2007.08.026.

[36] F. Montheillet, J. Lépinoux, D. Weygand, E. Rauch, Dynamic and static recrystallization, Adv. Eng. Mater. 3 (2001) 587–589. https://doi.org/10.1002/1527-2648(200108)3:8<587::AID-ADEM587>3.0.CO;2-V.

[37] E. Khzouz, Grain Growth Kinetics in Steels, A Major Qualif. Proj. Rep. Submitt. to

Fac. WORCESTER Polytech. Inst. (2011) 5–6. https://www.wpi.edu/Pubs/E-project/Available/E-project-042211-104204/unrestricted/MQP_-_Grain_Growth_Kinetics_in_Steels.pdf.

[38] J. Mizera, J.W. Wyrzykowski, K.J. Kurzydłowski, Description of the kinetics of normal and abnormal grain growth in austenitic stainless steel, Mater. Sci. Eng. 104 (1988) 157–162. https://doi.org/10.1016/0025-5416(88)90417-X.

[39] Y.L. Zhao, J. Shi, W.Q. Cao, M.Q. Wang, G. Xie, Kinetics of austenite grain growth in medium-carbon niobium-bearing steel, J. Zhejiang Univ. Sci. A. 12 (2011) 171–176. https://doi.org/10.1631/jzus.A1000150.

[40] M. Keyvani, Laser Ultrasonic Investigations of Recrystallization and Grain Growth in Cubic Metals, (2018).

[41] A. INTERNATIONAL, Standard Test Methods for Determining Average Grain Size, Astm E112-10. (2010) 1–27. https://doi.org/10.1520/E0112-12.1.4.

[42] Ferrite Content Measurement (Ferritescope Test), (n.d.). http://www.nusatek.com/on-site-material-inspection/ferrite-content-measurement-ferritescope-test.html (accessed November 15, 2020).

[43] A. Putz, M. Althuber, A. Zelić, E.M. Westin, T. Willidal, N. Enzinger, Methods for the measurement of ferrite content in multipass duplex stainless steel welds, Weld. World. 63 (2019) 1075–1086. https://doi.org/10.1007/s40194-019-00721-4.

[44] M. Calmunger, High-Temperature Behaviour of Austenitic Alloys, 2013. https://doi.org/10.3384/lic.diva-98242.

[45] M. Naghizadeh, H. Mirzadeh, Microstructural Evolutions During Annealing of Plastically Deformed AISI 304 Austenitic Stainless Steel: Martensite Reversion, Grain Refinement, Recrystallization, and Grain Growth, Metall. Mater. Trans. A Phys. Metall. Mater. Sci. 47 (2016) 4210–4216. https://doi.org/10.1007/s11661-016-3589-1.

[46] Z. Larouk, H. Bouhalais, Recrystallization behavior of a low carbon steel wire, Phys. Procedia. 2 (2009) 1223–1229. https://doi.org/10.1016/j.phpro.2009.11.085.

[47] P.. H. Dehghan-Manshadi, M.R. Barnett, Deformation and recrystallization of asss.pdf, (n.d.).

[48] Rodrigo Pinto de Siqueira, José Flávio Silveira Feiteira, Dionísio José Rodrigues da Costa, Jefferson Fabrício Cardoso Lins, Investigation of the Grain Growth Evolution in the AISI 304H Austenitic Stainless Steel, J. Mech. Eng. Autom. 6 (2016). https://doi.org/10.17265/2159-5275/2016.02.005.

[49] M. Shirdel, H. Mirzadeh, M. Habibi Parsa, Microstructural evolution during

normal/abnormal grain growth in austenitic stainless steel, Metall. Mater. Trans. A Phys. Metall. Mater. Sci. 45 (2014) 5185–5193. https://doi.org/10.1007/s11661-014-2426-7.

[50] M. Tikhonova, A. Belyakov, R. Kaibyshev, Static grain growth in an austenitic stainless steel subjected to intense plastic straining, Mater. Sci. Forum. 783–786 (2014) 1021–1026. https://doi.org/10.4028/www.scientific.net/msf.783-786.1021.

[51] L. Gavard, F. Montheillet, J. Le Coze, Recrystallization and grain growth in high purity austenitic stainless steels, Scr. Mater. 39 (1998) 1095–1099. https://doi.org/10.1016/S1359-6462(98)00276-0.

8 Appendix

Aqueous nitric acid electrolyte etchant revealed the grain boundaries of AISI 304L.

The 25% cold-rolled specimen, light optical microscope (LOM) images.

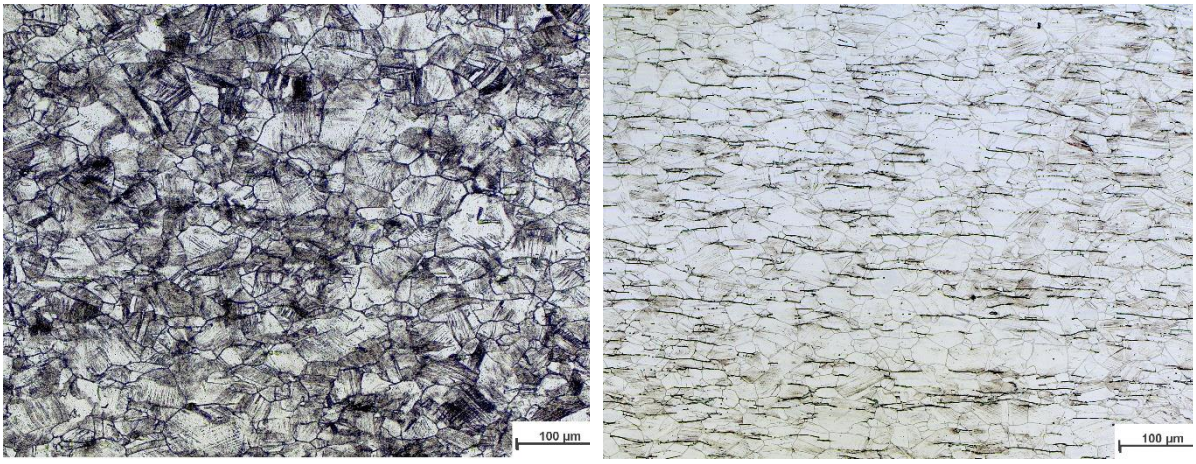

(a) Normal Plane (NP) (b) Transverse Plane (TP)

Figure 40. *Heated treated at (600°C – 90 minutes).*

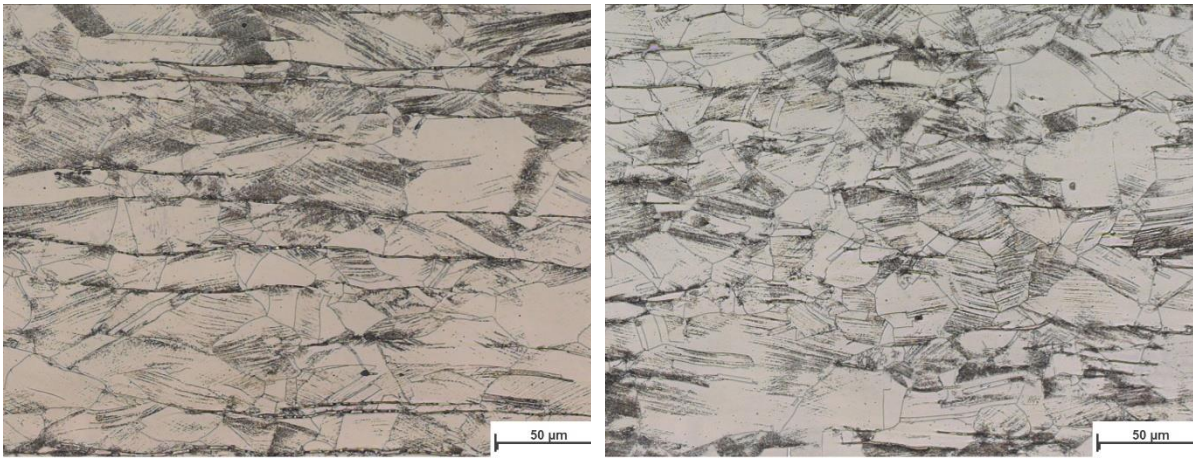

(a) Rolling Plane (RP) (b) Transverse Plane (TP)

Figure 41. *Heated treated at (700°C – 180 minutes).*

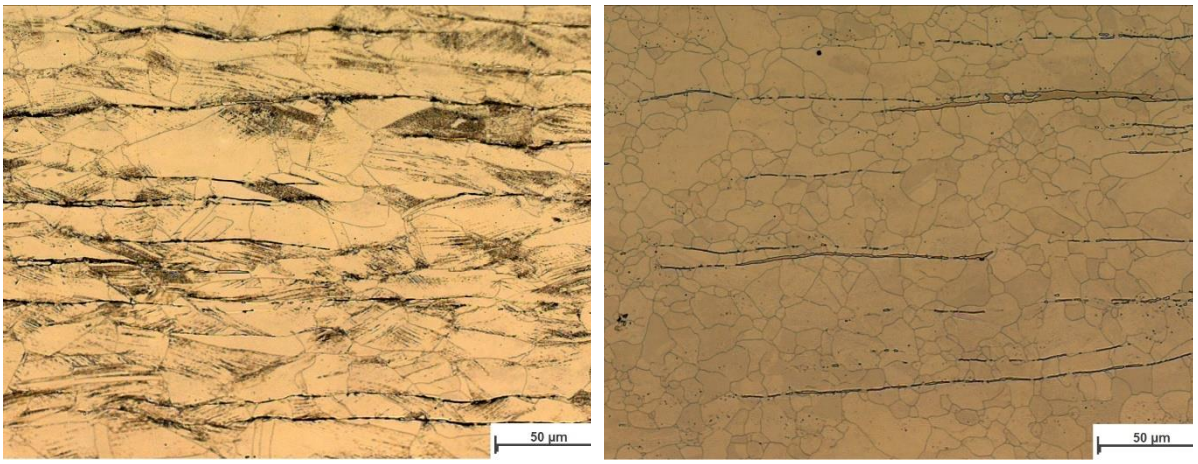

(a) Transverse Plane (TP) (b) Transverse Plane (TP)

Figure 42. *(a) Heat-treated at (700°C – 240 minutes), (b) Heat-treated at (800°C – 90 minutes).*

The 50% cold-rolled specimen. Light optical microscope (LOM) images.

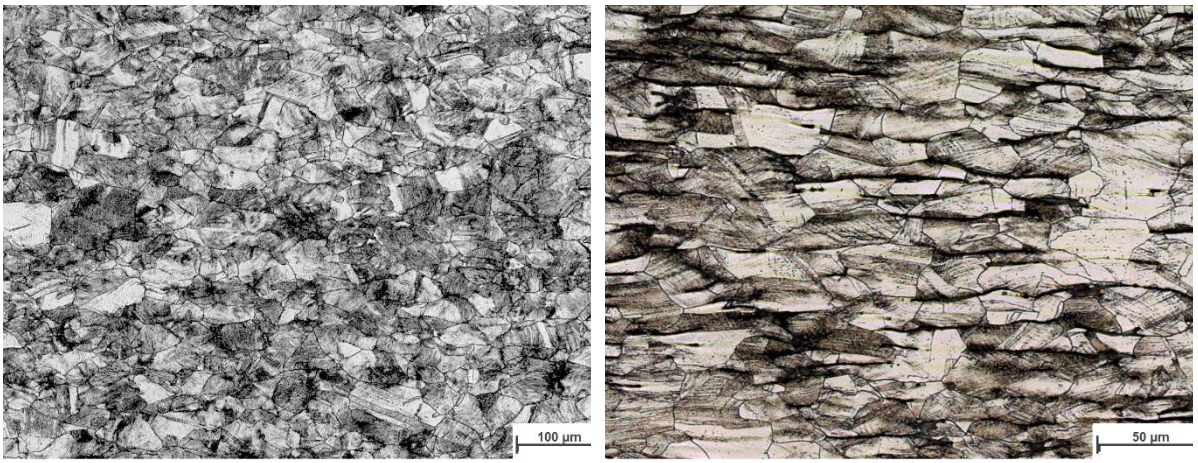

(a) Normal Plane (NP) (b) Transverse Plane (TP)

Figure 43. *Heat-treated at (600°C – 90 minutes).*

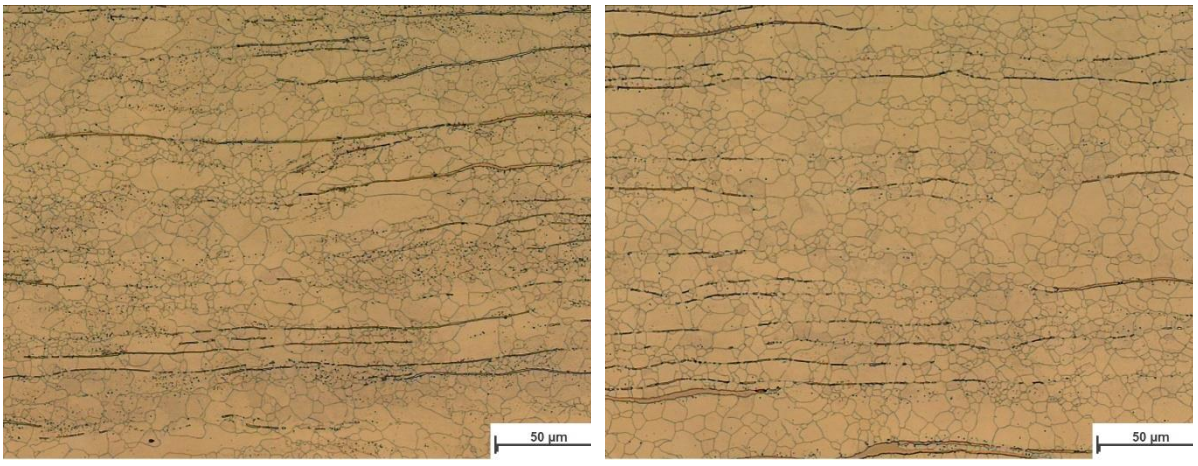

(a) Transverse Plane (TP) (b) Transverse Plane (TP)

Figure 44. *(a) Heat-treated at (800°C – 30 minutes), (b) Heat-treated at (800°C – 90 minutes).*

The 67% cold-rolled specimen. Light optical microscope (LOM) images.

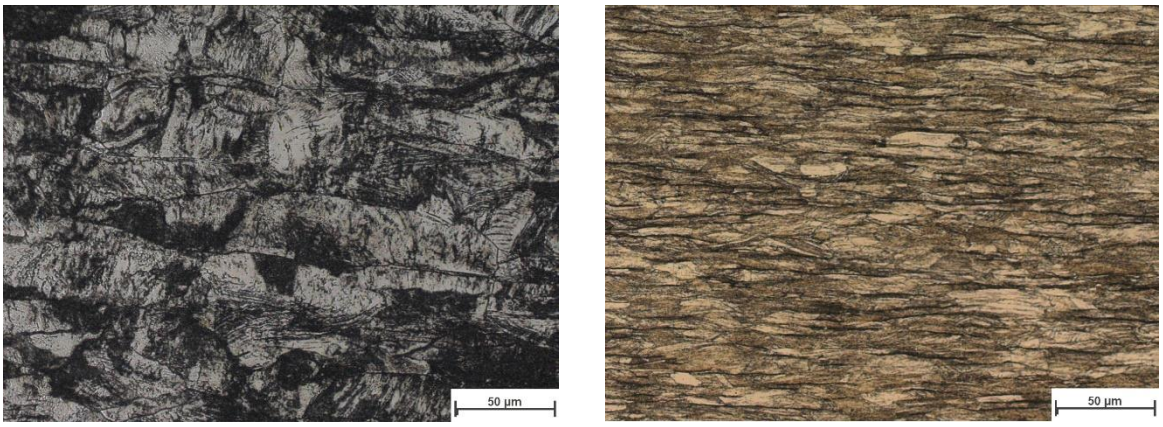

(a) Normal plane (NP) (b) Transvers Plane (TP)

Figure 45. *Heat-treated at (600°C – 90 minutes).*

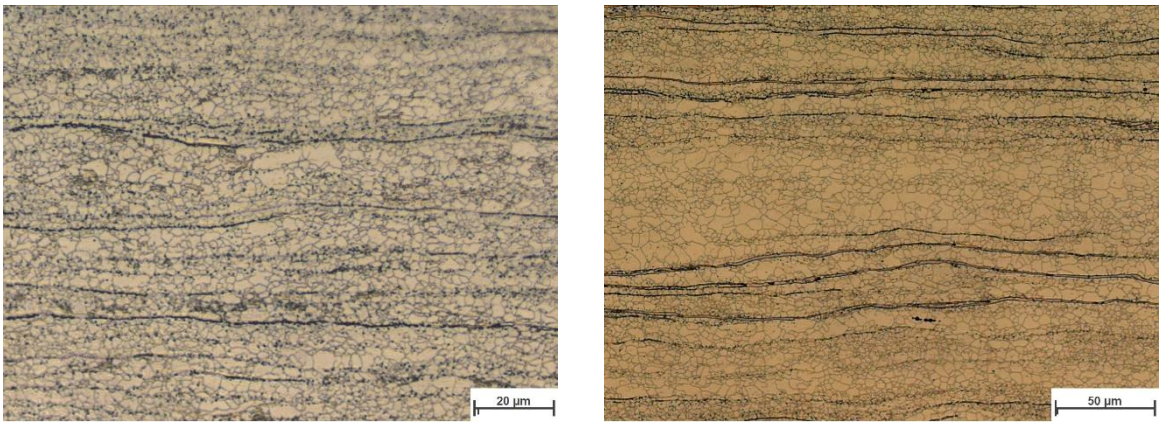

(a) Transverse Plane (TP) (b) Transverse Plane (TP)

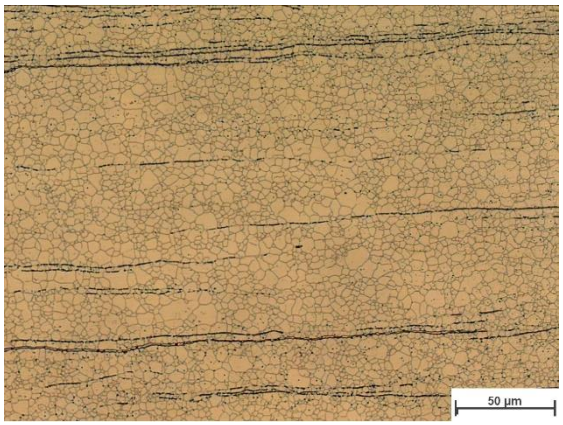

(c) Transverse plane

Figure 46. *(a) Heat-treated at (700°C – 240 minutes), (b) Heat-treated at (800°C – 30 minutes), (c) Heated-treated at (800°C – 90 minutes).*

Beraha tint etchant revealed the deformation-induced martensite content in cold-rolled deformed specimens.

The 25% cold-rolled specimen, light optical microscope (LOM) images.

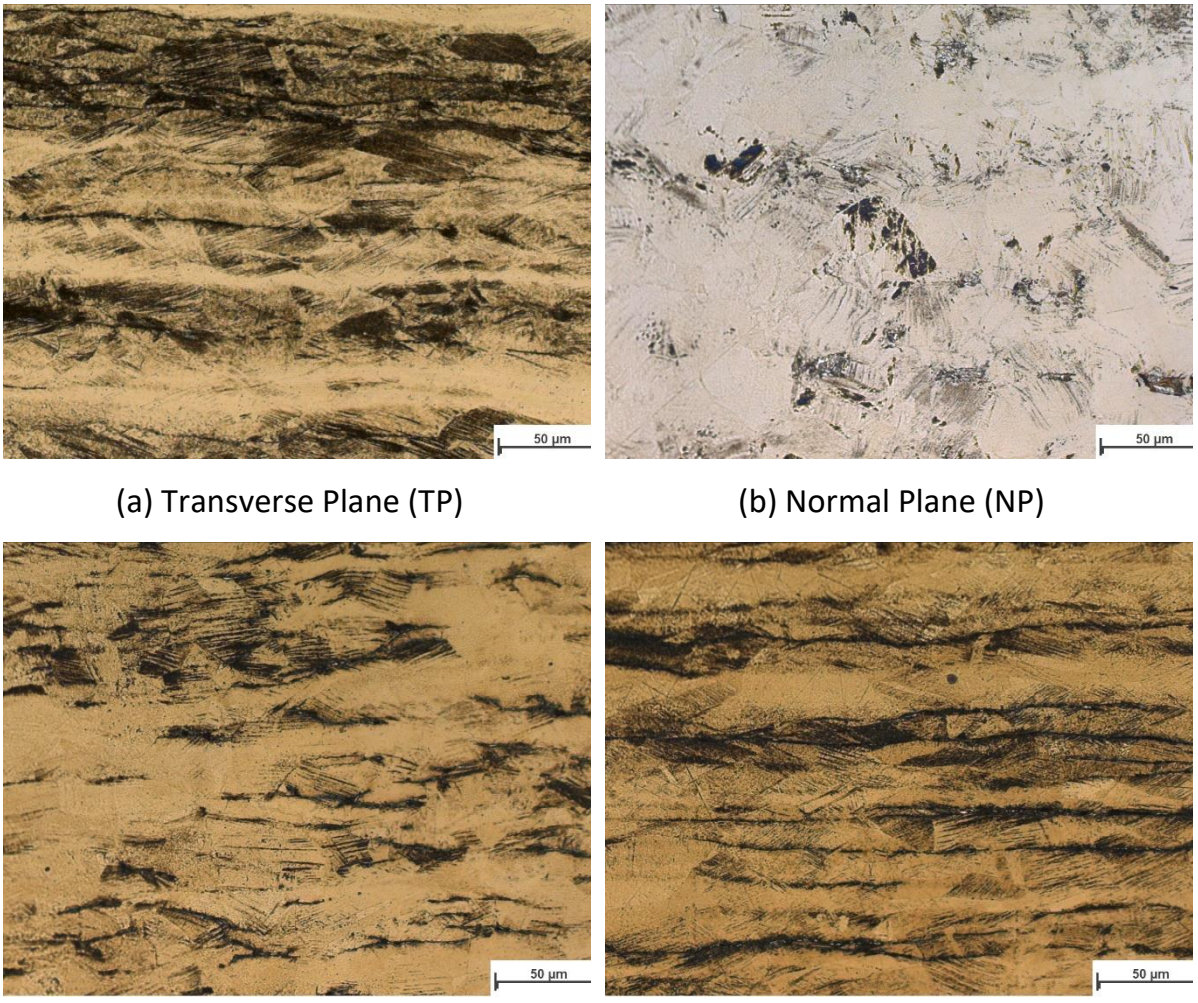

(a) Transverse Plane (TP) (b) Normal Plane (NP)

(c) Rolling Plane (RP) (d) Transverse plane (TP)

Figure 47. *(a) Heat-treated at (700°C – 240 minutes), (b) Heat-treated at (700°C – 480 minutes), (c) Heat-treated at (700°C – 480 minutes), (d) Heat-treated at (700°C – 480 minutes).*

The 50% cold-rolled specimen, light optical microscope (LOM) images.

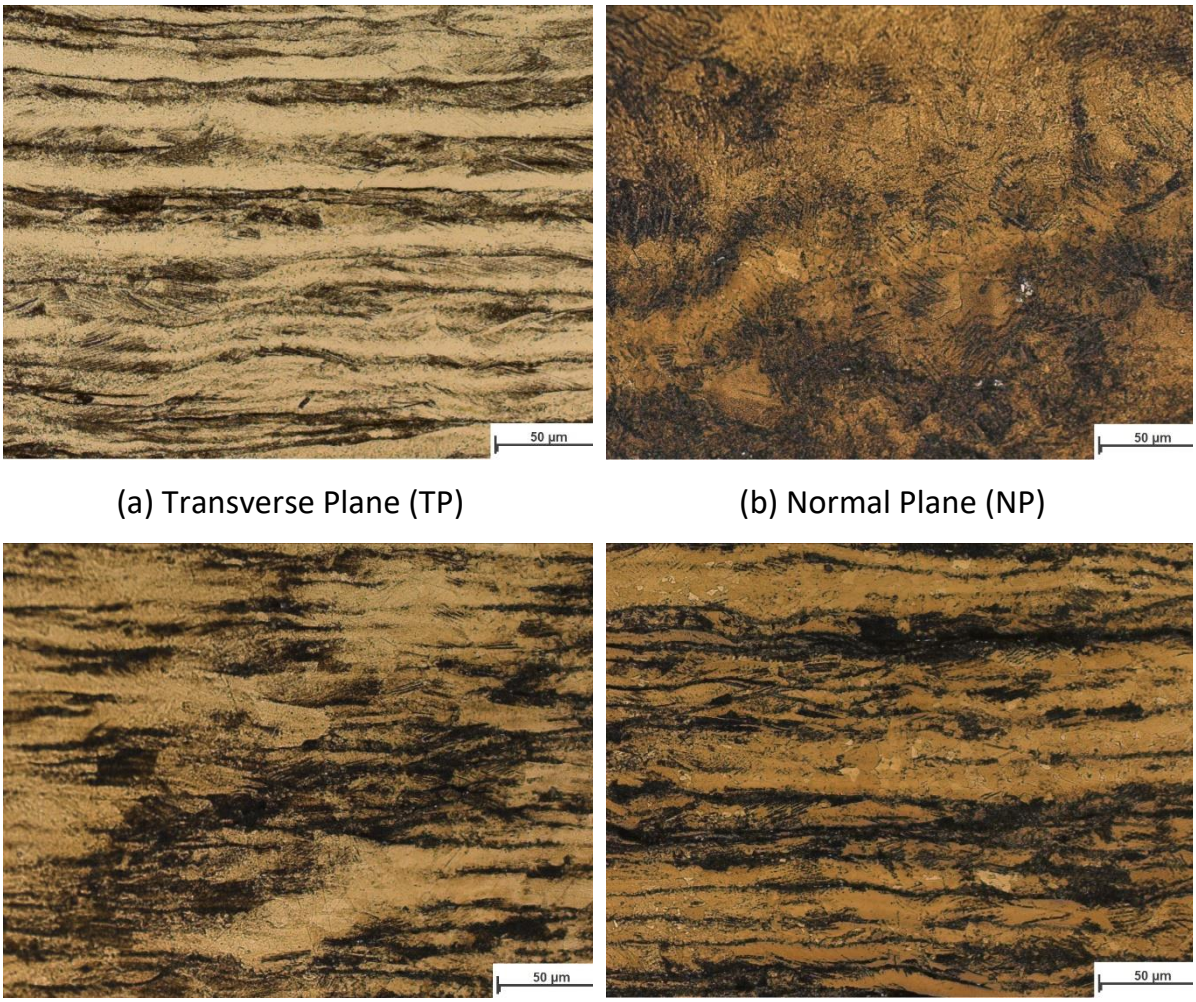

(a) Transverse Plane (TP) (b) Normal Plane (NP)

(c) Rolling Plane (RP) (d) Transverse plane (TP)

***Figure 48**. (a) Heat-treated at (700°C – 240 minutes), (b) Heat-treated at (700°C – 480 minutes), (c) Heated-treated at (700°C – 480 minutes), (d) Heat-treated at (700°C – 480 minutes).*

The 67% cold-rolled specimen, light optical microscope (LOM) images.

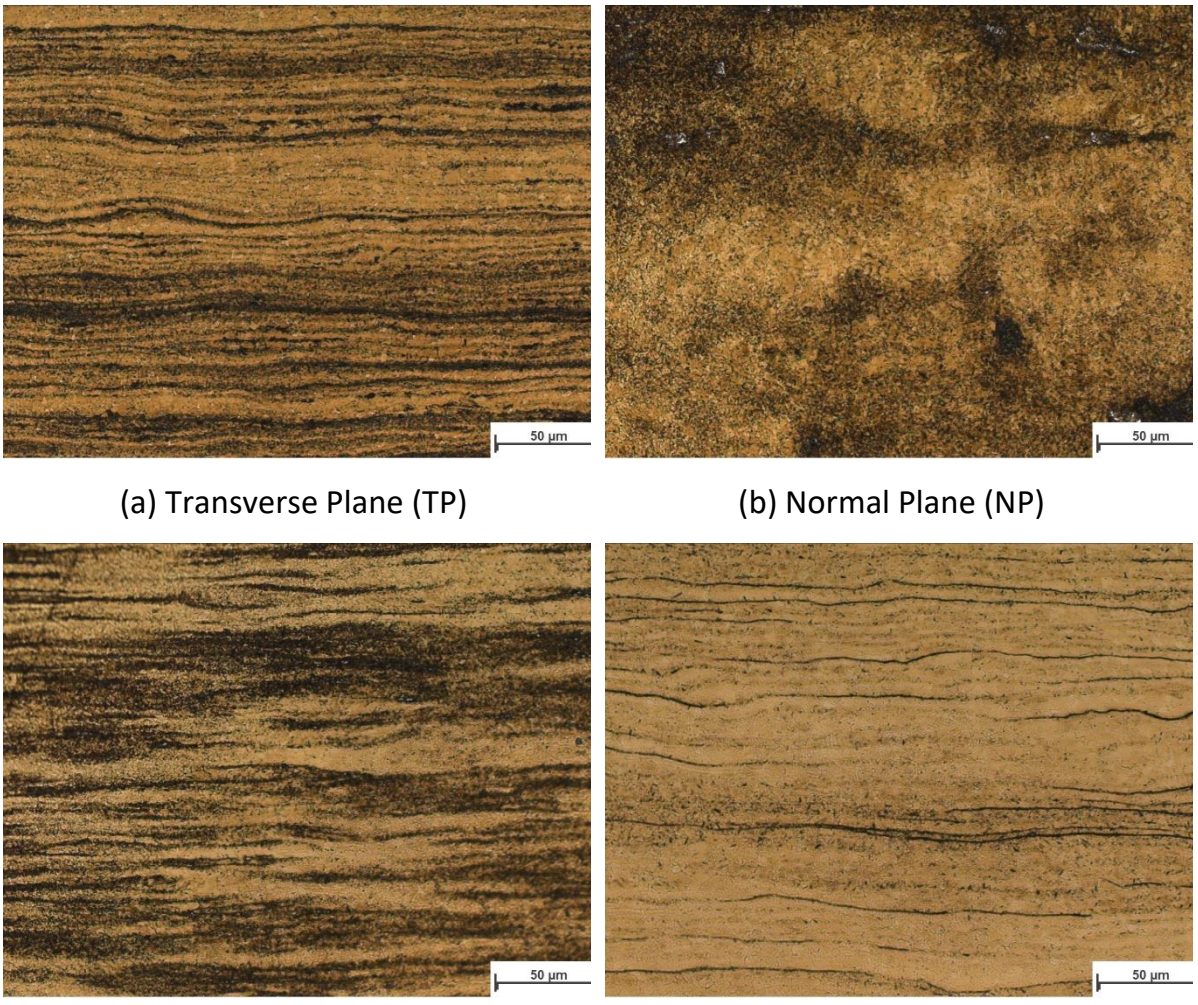

(a) Transverse Plane (TP) (b) Normal Plane (NP)

(c) Transverse plane (TP) (d) Transverse plane (TP)

Figure 49. *(a) Heat-treated at (700°C – 240 minutes), (b) Heat-treated at (700°C – 480 minutes), (c) Heated-treated at (700°C – 480 minutes), (d) Heat-treated at (800°C – 30 minutes).*

Grain growth heat treatments, (Aqueous nitric acid electrolyte etchant).

Recrystallized (800°C – 60 minutes) 50% cold-rolled specimen (average grain size 6 µm in the initial condition).

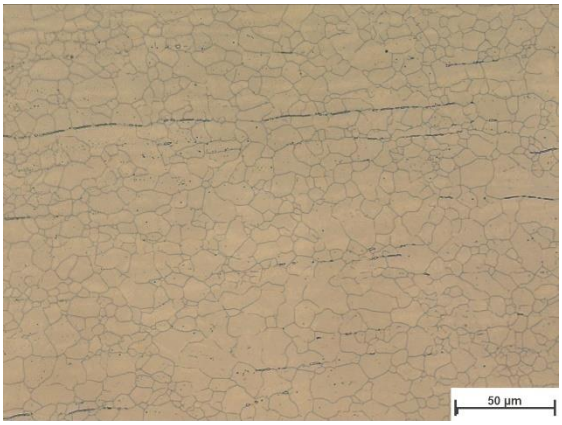

5 min

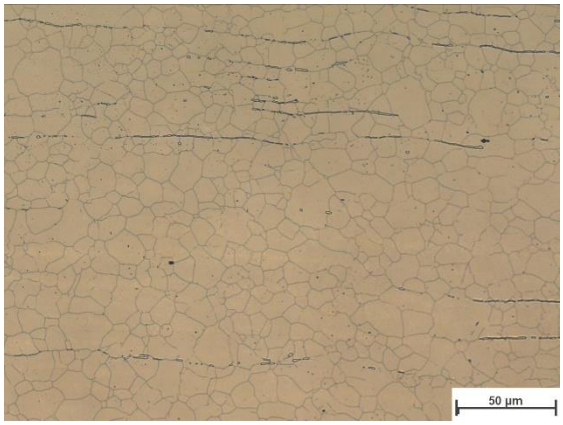

10 min

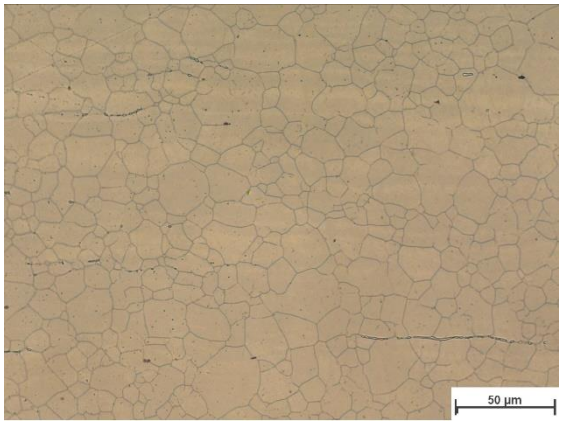

30 min

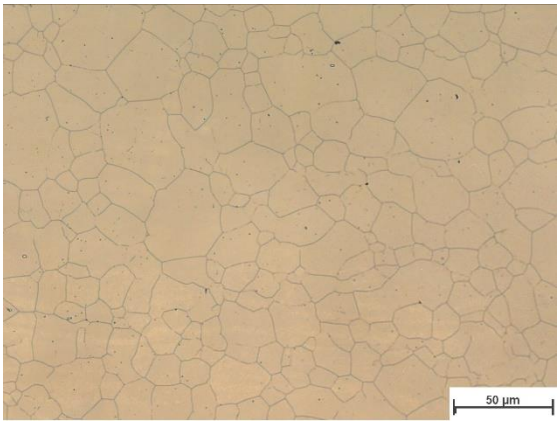

60 min

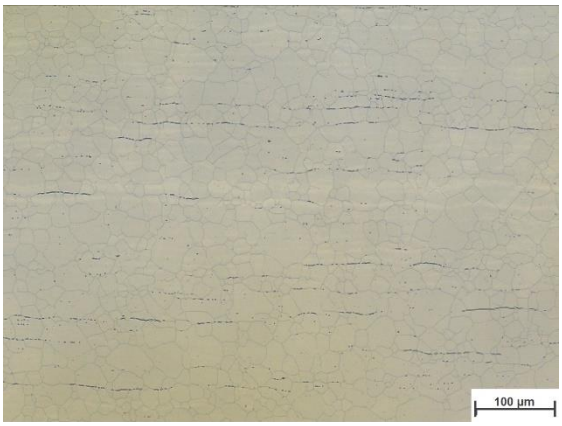

90 min

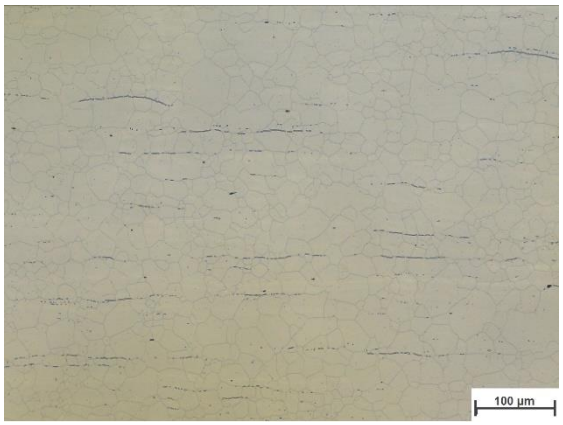

120 min

Figure 50. *The specimen (Transverse Plane) heat-treated at 900°C.*

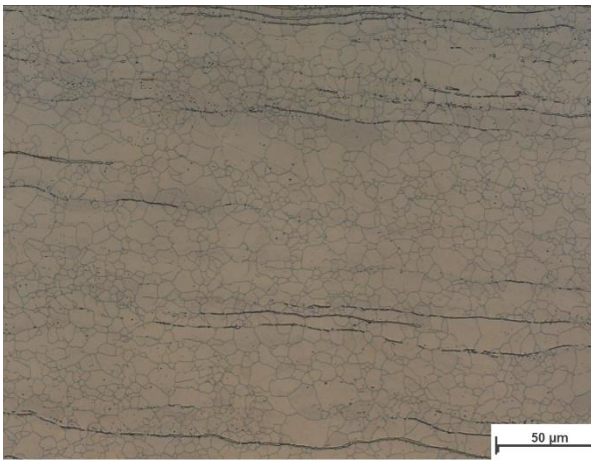

2 min

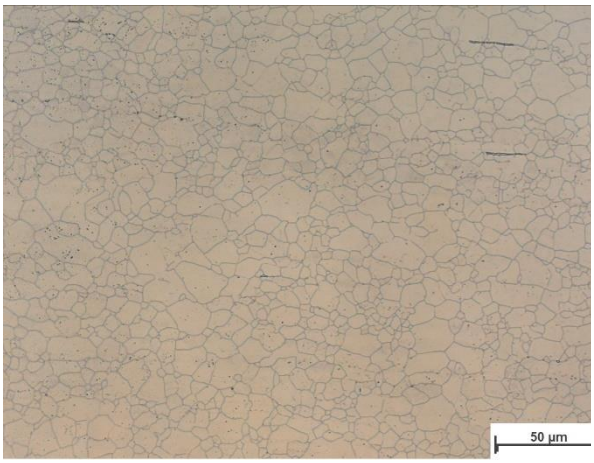

5 min

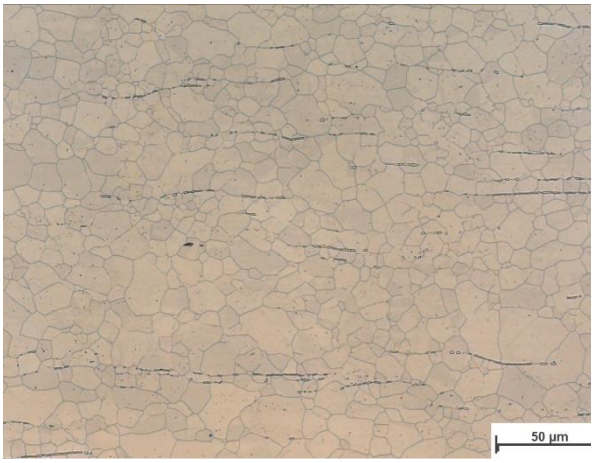

7 min

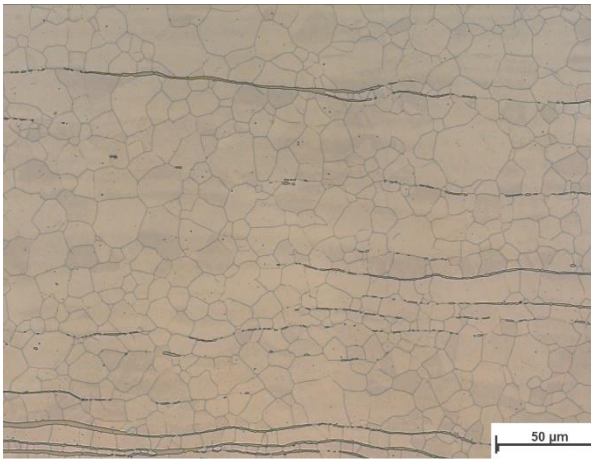

10 min

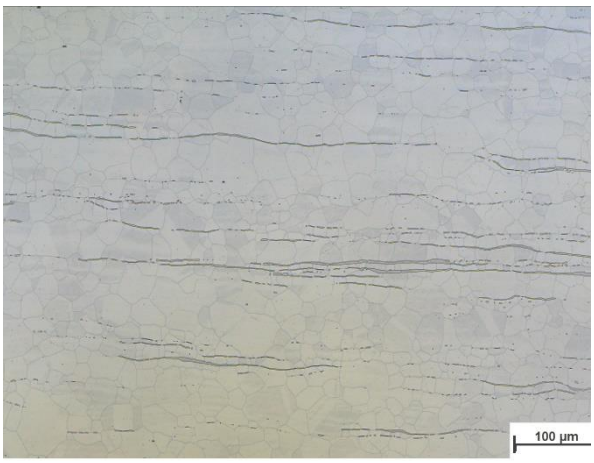

30 min

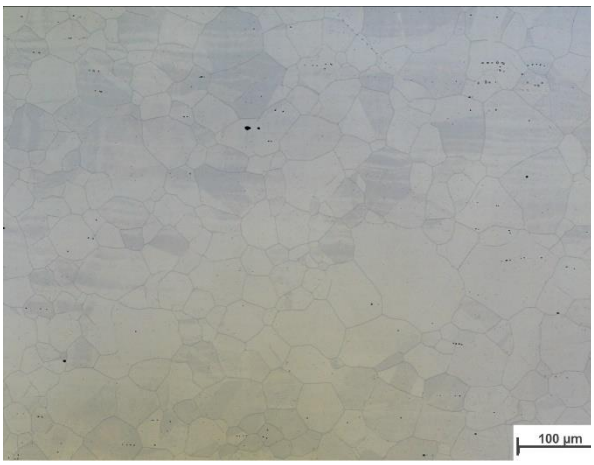

60 min

Figure 51. *The specimen (Transverse Plane) heat-treated at 1000°C.*

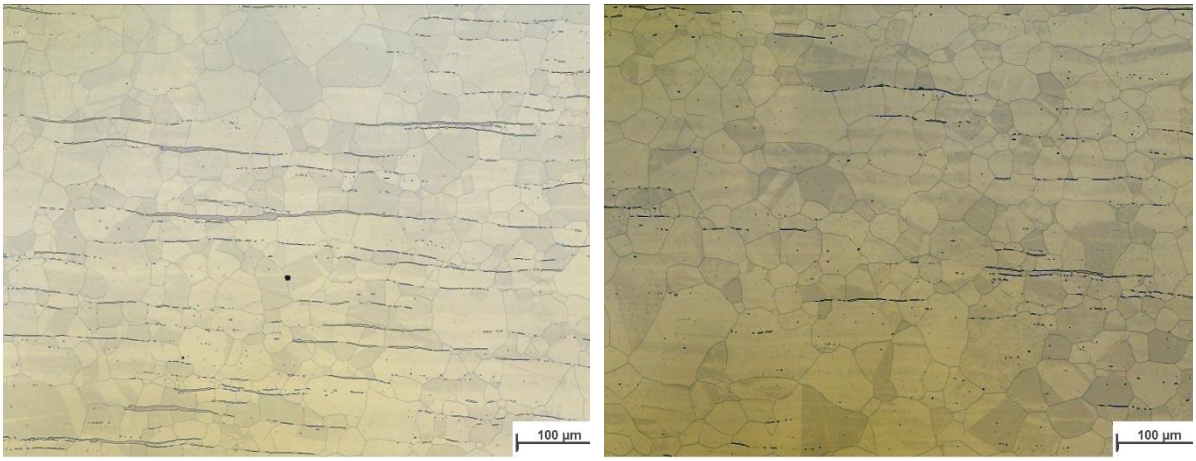

2 min **5 min**

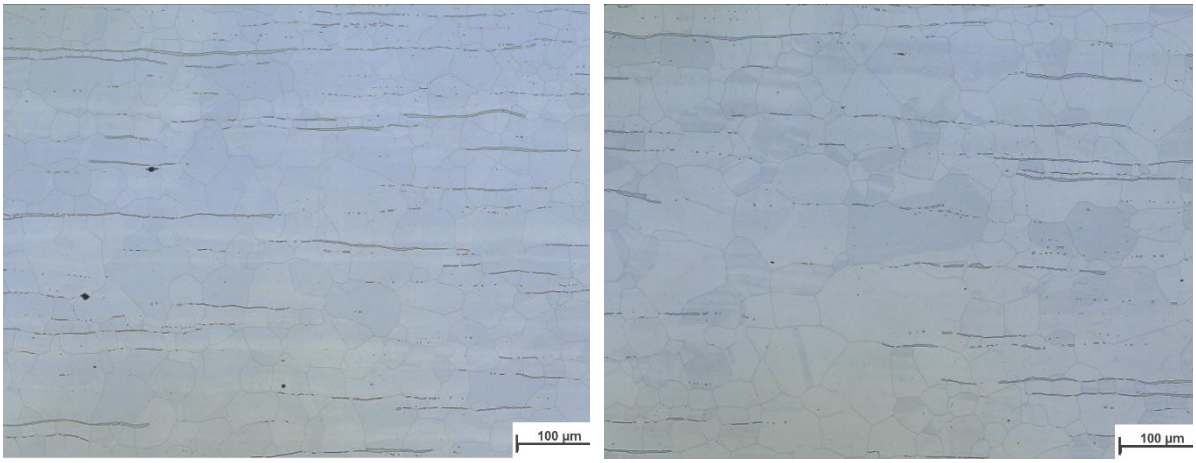

7 min **10 min**

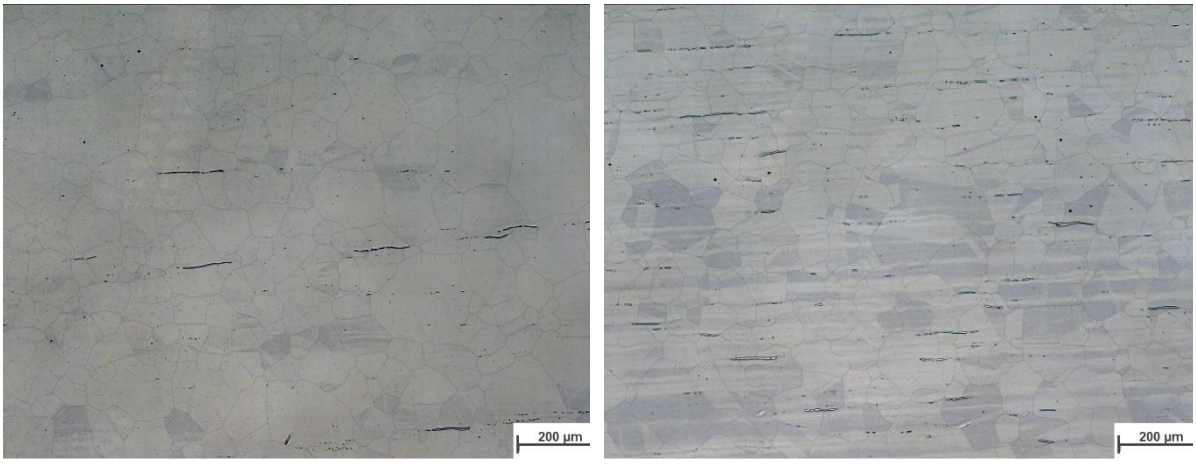

30 min **60 min**

Figure 52. *The specimen (Transverse Plane) heat-treated at 1100°C.*

Grain growth heat treatments, (Aqueous nitric acid electrolyte etchant).

As-received condition (non-rolled) specimen (average grain size 30 µm in the initial condition).

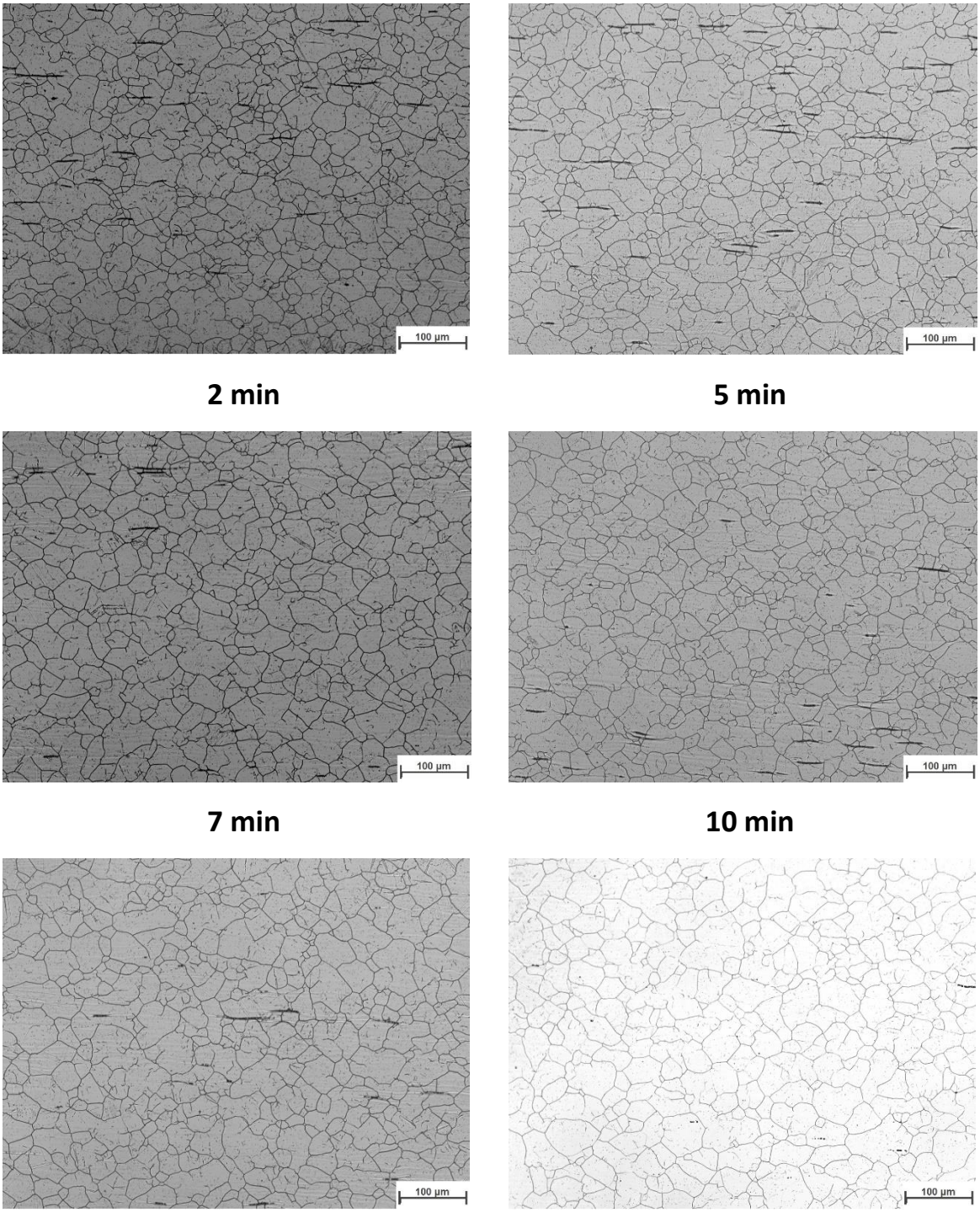

Figure 53. *The specimen (Transverse Plane) heat-treated at 1000°C.*

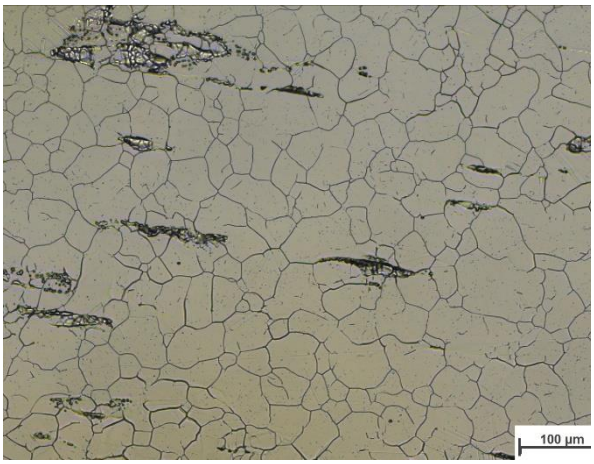

2 min

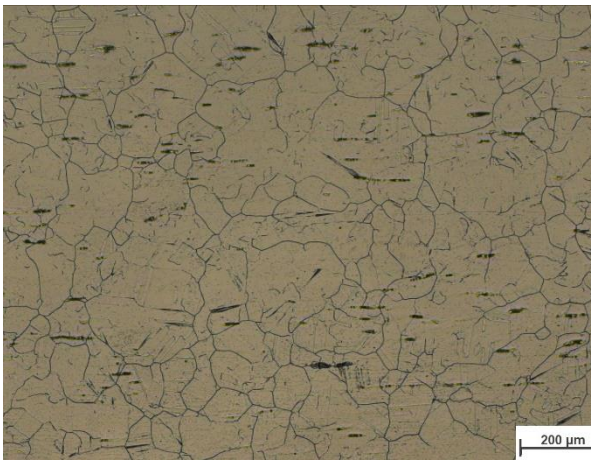

5 min

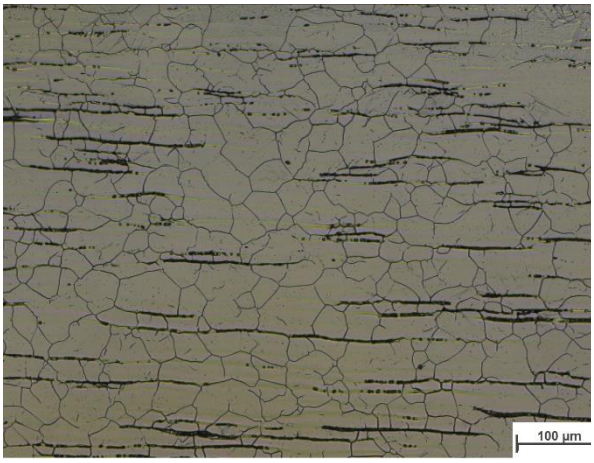

7 min

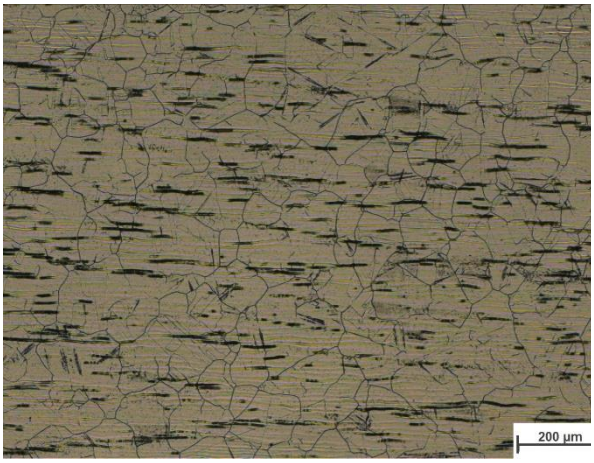

10 min

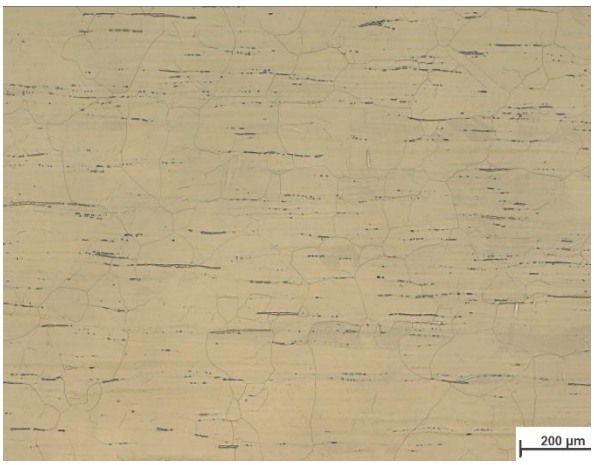

30 min

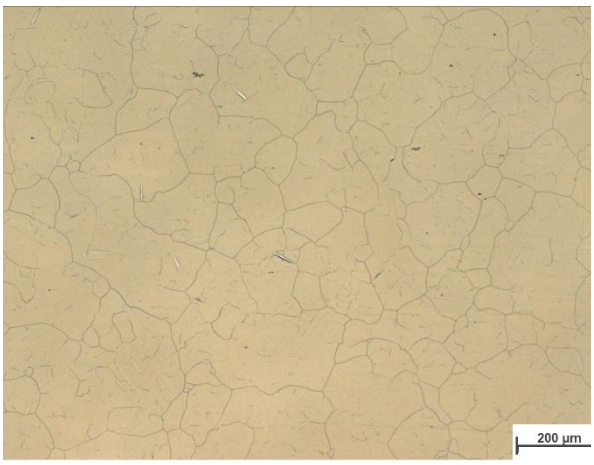

60 min

Figure 54. *The specimen (Transverse Plane) heat-treated at 1100°C.*

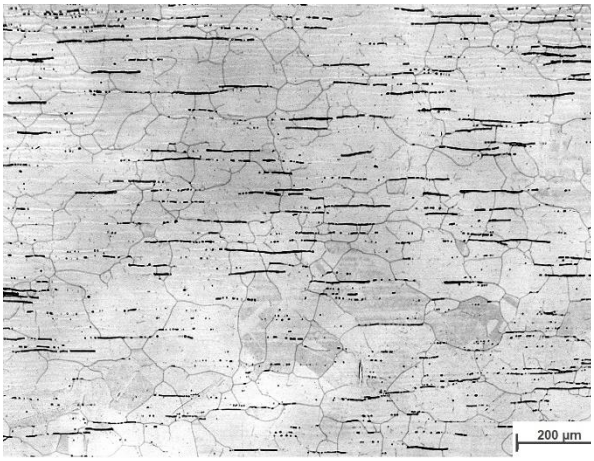

5 min

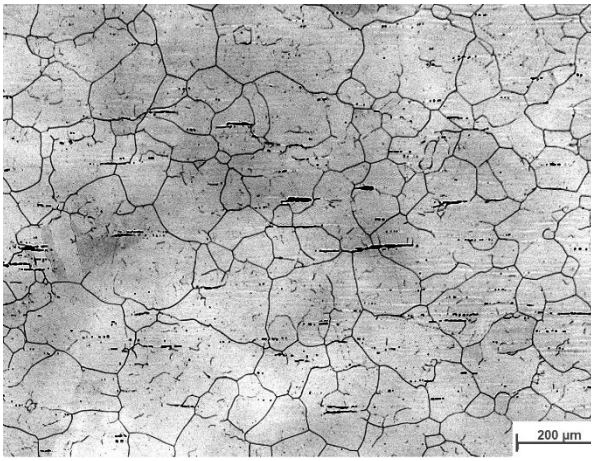

10 min

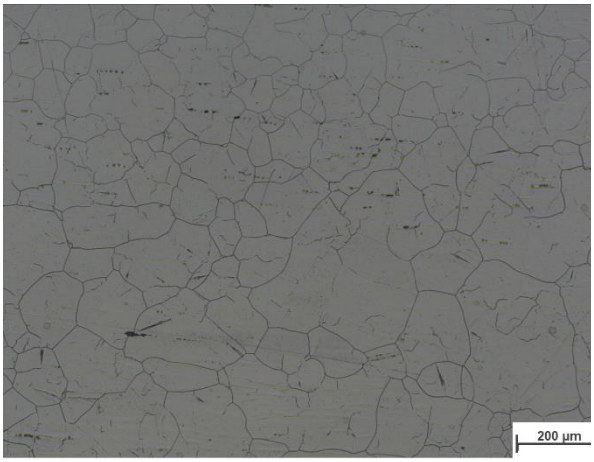

15 min

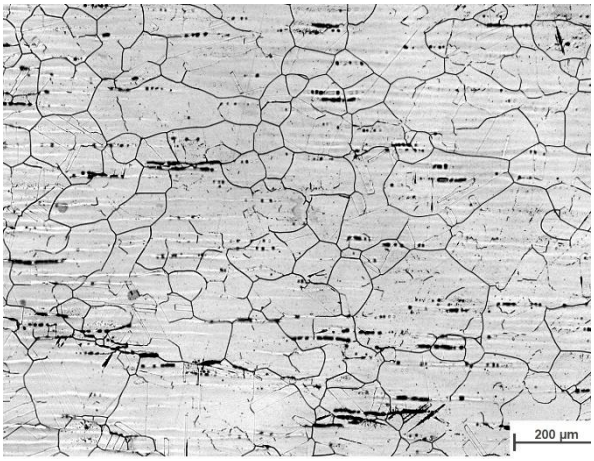

30 min

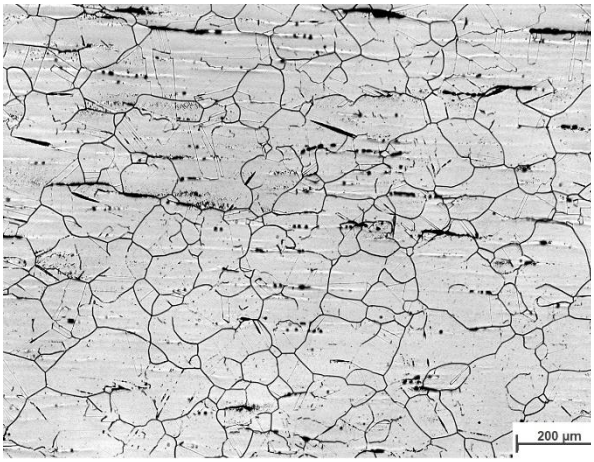

45 min

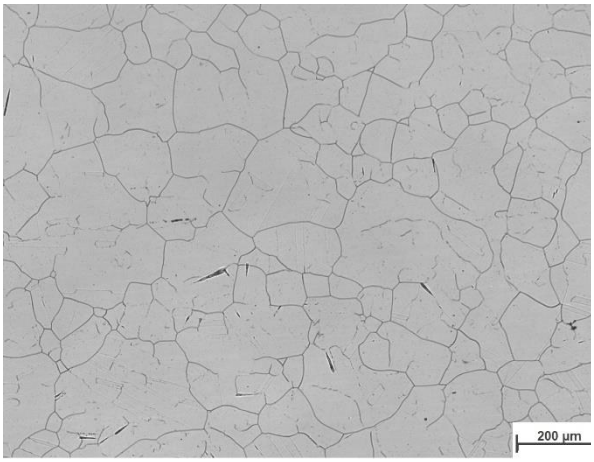

60 min

Figure 55. *The specimen (Transverse Plane) heat-treated at 1200°C.*